THE PROCEEDINGS OF
THE PHYSICAL SOCIETY

Section A

VOL. 64, PART 5 1 May 1951 No. 377 A

Thermal Conductivity of Dense Matter

BY K. S. SINGWI* AND M. K. SUNDARESAN†
* Department of Mathematical Physics, University of Birmingham
† Department of Physics, University of Delhi

Communicated by R. E. Peierls; MS. received 16th October 1950

ABSTRACT. The thermal conductivity of degenerate matter is calculated taking account of the effect of relativistic mechanics. The result is put in a form suitable for astrophysical calculations. The two limiting cases of non-relativistic degeneracy and extreme relativistic degeneracy are discussed.

§ 1. INTRODUCTION

THAT the energy transport in a white dwarf star is mainly due to thermal conduction by electrons was first pointed out by Kothari (1932). In white dwarfs in which the density is not very high ($\rho < 10^6$ gm/cm^3) the free electrons constitute a non-relativistic degenerate gas, for the thermal conductivity of which appropriate expressions have been derived by Marshak (1940) and Mestel (1950). On the other hand, in massive white dwarfs in which the central density is equal to or greater than 10^6 gm/cm^3 relativistic degeneracy sets in, and it is, therefore, of importance to calculate the thermal conductivity of relativistic degenerate matter. Such an expression for the thermal conductivity would be of astrophysical value in determining accurately the temperature and density distribution in the core of a dense white dwarf, the precise knowledge of which is essential for investigating the mechanism of energy generation in such a star. For this reason, and for the sake of completeness, we have in this paper derived a general expression for the thermal conductivity of degenerate matter in terms of the non-dimensional parameter x,

$$x = \frac{h}{mc}\left(\frac{3n}{4\pi g}\right)^{1/3},$$

where n denotes the concentration of electrons and other symbols have their usual meaning. The expression is put in a form suitable for astrophysical calculations. Finally, the two limiting cases of the general formula are discussed.

§ 2. THERMODYNAMIC FORMULAE

We give below certain well-known thermodynamic relations which we shall use in the sequel. The number of electrons in a volume V and possessing energy between the range ϵ and $\epsilon + d\epsilon$ is given by

$$N(\epsilon)\,d\epsilon = \frac{4\pi g V}{c^3 h^3}\,\frac{(\epsilon^2 + 2\epsilon mc^2)^{1/2}(\epsilon + mc^2)}{1 + \exp[(\epsilon - \xi)/kT]}\,d\epsilon,$$

where ξ is the Gibbs free energy per particle, $\boldsymbol{h}$ Planck's constant, $\boldsymbol{m}$ the mass of the electron, g its weight factor ($g=2$) and $\boldsymbol{c}$ the velocity of light. The total number N of electrons in the assembly is

$$N=\frac{4\pi g V}{\boldsymbol{c}^3\boldsymbol{h}^3}\int_0^\infty(\epsilon^2+2\epsilon\boldsymbol{mc}^2)^{1/2}(\epsilon+\boldsymbol{mc}^2)\,\frac{d\epsilon}{1+\exp[(\epsilon-\xi)/\boldsymbol{k}T]}. \quad \ldots\ldots(1)$$

At the absolute zero of temperature, i.e. in a completely degenerate case, (1) becomes

$$N\frac{(\boldsymbol{ch})^3}{4\pi g V}=\int_0^{\xi_0}(\epsilon^2+2\epsilon\boldsymbol{mc}^2)^{1/2}(\epsilon+\boldsymbol{mc}^2)\,d\epsilon=\tfrac{1}{3}(\xi_0{}^2+2\boldsymbol{mc}^2\xi_0)^{3/2},$$

where ξ_0 is the maximum energy corresponding to the top of the Fermi distribution, or

$$\xi_0=\boldsymbol{mc}^2[(1+x^2)^{1/2}-1], \quad \ldots\ldots(2)$$

where we have put

$$x=\frac{\boldsymbol{h}}{\boldsymbol{mc}}\left(\frac{3n}{4\pi g}\right)^{1/3}. \quad \ldots\ldots(3)$$

(2) can be put in the form

$$\left.\begin{aligned}\xi_0+\boldsymbol{mc}^2&=\boldsymbol{mc}^2(1+x^2)^{1/2} && \ldots\ldots(4a)\\ \text{or}\quad (\xi_0{}^2+2\boldsymbol{mc}^2\xi_0)^{1/2}&=\boldsymbol{mc}^2x. && \ldots\ldots(4b)\end{aligned}\right\}$$

The completely non-relativistic case is characterized by $\xi_0/\boldsymbol{mc}^2\to 0$, i.e. $x\to 0$; and the completely relativistic case by $\xi_0/\boldsymbol{mc}^2\to\infty$, i.e. $x\to\infty$.

From (4) we have

$$\xi_0=\tfrac{1}{2}\boldsymbol{mc}^2x^2,\quad x\to 0,\ \ldots\ldots(5a);\qquad \xi_0=\boldsymbol{mc}^2x,\quad x\to\infty \quad \ldots\ldots(5b)$$

At any finite temperature (1) can be evaluated by using the Sommerfeld lemma. It can then be shown that

$$\xi=\xi_0\left\{1-\frac{\pi^2}{6}\left(\frac{\boldsymbol{k}T}{\xi_0}\right)^2\frac{(1+2x^2)[(1+x^2)^{1/2}-1]}{x^2(1+x^2)^{1/2}}+\mathrm{O}\left(\frac{\boldsymbol{k}T}{\xi_0}\right)^4\right\}, \quad \ldots\ldots(6)$$

ξ denotes the Gibbs free energy at temperature T (Kothari and Singh 1942).

For $x\to 0$ (6) reduces to

$$\xi=\xi_0\left\{1-\frac{\pi^2}{12}\left(\frac{\boldsymbol{k}T}{\xi_0}\right)^2+\mathrm{O}\left(\frac{\boldsymbol{k}T}{\xi_0}\right)^4\right\}, \quad \ldots\ldots(7)$$

where ξ_0 is given by (5 a), and for $x\to\infty$, (6) reduces to

$$\xi=\xi_0\left\{1-\frac{\pi^2}{3}\left(\frac{\boldsymbol{k}T}{\xi_0}\right)^2+\mathrm{O}\left(\frac{\boldsymbol{k}T}{\xi_0}\right)^4\right\}, \quad \ldots\ldots(8)$$

where ξ_0 is given by (5b).

The electron concentration n, and therefore x, and the material density ρ in a white dwarf are related by

$$\rho=\frac{8\pi\boldsymbol{m}^3\boldsymbol{c}^3}{3\boldsymbol{h}^3}\mu_e Hx^3=Bx^3 \quad \ldots\ldots(9)$$

(Chandrasekhar 1938), where μ_e is the mean molecular weight per free electron (μ_e is generally 2), H the mass of the hydrogen atom and

$$B=\frac{8\pi\boldsymbol{m}^3\boldsymbol{c}^3}{3\boldsymbol{h}^3}\mu_e H=9{\cdot}82\times 10^5\,\mu_e.$$

From (9) we see that if $\mu_e=2$, x is nearly equal to unity for $\rho=10^6$ gm/cm^3. Hence relativistic effects become important for densities of this order and greater.

§ 3. CALCULATION OF THERMAL CONDUCTIVITY

The method of calculation in this section is analogous to the treatment of the same problem in the theory of metals. We shall therefore omit the details. The Boltzmann equation is

$$v_x \frac{\partial f}{dx} + \mathbf{e}F \frac{\partial f}{\partial p_x} = -\left(\frac{\partial f}{\partial t}\right)_{\text{coll}}, \qquad \ldots\ldots(10)$$

f being the perturbed distribution function, which we may write as

$$f = f_0 + v_x \chi(v) = f_0 - \tau\left(\frac{\partial f}{\partial t}\right)_{\text{coll}} \qquad \ldots\ldots(11)$$

to the first order of approximation. τ is the collision time, and the unperturbed distribution function f_0 is

$$f_0 = [1 + \exp\{(\epsilon - \xi)/\mathbf{k}T\}]^{-1}. \qquad \ldots\ldots(12)$$

Making use of (11) and (12), we have for the first-order solution of f

$$f = f_0 + v_x \frac{\partial f_0}{\partial \epsilon}\left\{\mathbf{e}F - \left(\frac{\partial \xi}{\partial T} + \frac{\epsilon - \xi}{T}\right)\frac{\partial T}{\partial x}\right\}\tau. \qquad \ldots\ldots(13)$$

From the theory of collisions

$$\left(\frac{\partial f}{\partial t}\right)_{\text{coll}} = \int (v_x' - v_x)\chi(v) P(v, v')\, dS', \qquad \ldots\ldots(14)$$

where the probability of collision $P(v, v')$ for the transition of the electron from the state v to the state v' is given by

$$P(v, v') = N_{\mathrm{A}} v \sigma(\theta, v). \qquad \ldots\ldots(15)$$

N_{A} gives the number of scattering centres per unit volume, and the collision cross section $\sigma(\theta, v)$ is given by

$$\sigma(\theta, v) = \frac{Z^2\mathbf{e}^4}{4\mathbf{m}^2 v^4 \sin^4 \frac{1}{2}\theta}\left(1 - \frac{v^2}{\mathbf{c}^2}\right)\left(1 - \frac{v^2}{\mathbf{c}^2}\sin^2 \tfrac{1}{2}\theta\right) \qquad \ldots\ldots(16)$$

(Mott and Massey 1949), assuming only the elastic scattering.

Using the above value of σ, we have for the collision time the expression

$$\begin{aligned} \frac{1}{\tau(v)} &= -N_{\mathrm{A}} \frac{Z^2\mathbf{e}^4}{\mathbf{m}^2 v^3}\left(1 - \frac{v^2}{\mathbf{c}^2}\right)\frac{1}{v_x}\int_0^{2\pi} d\phi \int_{\theta_0}^{\pi} \frac{v_x(\cos\theta - 1)}{(1 - \cos\theta)^2}\left\{1 - \frac{v^2}{2\mathbf{c}^2}(1 - \cos\theta)\right\}\sin\theta\, d\theta \\ &= N_{\mathrm{A}} \frac{Z^2\mathbf{e}^4}{\mathbf{m}^2 v^3}\left(1 - \frac{v^2}{\mathbf{c}^2}\right)\left\{2\pi \log\left(\frac{2}{1 - \cos\theta_0}\right) - \pi\frac{v^2}{\mathbf{c}^2}(1 + \cos\theta_0)\right\} \\ &\simeq N_{\mathrm{A}} \frac{Z^2\mathbf{e}^4}{\mathbf{m}^2 v^3}\left(1 - \frac{v^2}{\mathbf{c}^2}\right) 2\pi \log\frac{2}{1 - \cos\theta_0}, \end{aligned} \qquad \ldots\ldots(17)$$

where the lower limit θ_0 denotes the minimum scattering angle due to the finite radius of the atom and is given by $\theta_0 \simeq \bar{\lambda}/a$. The mean wavelength of the electron is given by $\bar{\lambda} = \hbar/\bar{p}$, $\bar{p}$ being the average electron momentum. We use here the mean value of the electron momentum because in the following calculation we take the factor $\log[2/(1 - \cos\theta_0)]$ out of the integration sign. This, however, will not introduce much error because of the logarithmic dependence of the factor on p. The radius a of the atom is given by

$$a \simeq \left(\frac{3Z}{4\pi n}\right)^{1/3} = \frac{\mathbf{h}}{\mathbf{mc}}\left(\frac{9Z}{32\pi^2}\right)^{1/3}\frac{1}{x}.$$

Substituting the value of $\tau(v)$ from (17) in (13), we have

$$f = f_0 + \frac{\mathbf{m}^2 v^3}{\pi N_{\mathrm{A}} Z^2 \mathbf{e}^4 I(1 - v^2/\mathbf{c}^2)} v_x \frac{\partial f_0}{\partial \epsilon}\left\{\mathbf{e}F - \left(\frac{\partial \xi}{\partial T} + \frac{\epsilon - \xi}{T}\right)\frac{\partial T}{\partial x}\right\}, \qquad \ldots\ldots(18)$$

where

$$I \equiv 2\log[2/(1 - \cos\theta_0)]. \qquad \ldots\ldots(19)$$

The expressions for the current density j and the energy flow Q are, respectively,

$$j=\int f v_x \frac{d^3\vec{p}}{\boldsymbol{h}^3} \quad \ldots\ldots(20) \qquad \text{and} \qquad Q=\int f v_x \epsilon \frac{d^3\vec{p}}{\boldsymbol{h}^3}. \quad \ldots\ldots(21)$$

In equilibrium $j=0$. Substituting the value of f from (18) in (20), and making use of the relativistic relation between p and ϵ, we have, for equilibrium,

$$0=\int_0^\infty \frac{(\epsilon^2+2\epsilon \boldsymbol{mc}^2)^3}{(\epsilon+\boldsymbol{mc}^2)^2}\frac{\partial f_0}{\partial\epsilon}\left\{\boldsymbol{e}F'-\frac{\epsilon-\xi}{T}\frac{\partial T}{\partial x}\right\}d\epsilon, \quad \ldots\ldots(22)$$

where we have put $\boldsymbol{e}F'\equiv \boldsymbol{e}F-\partial\xi/\partial x$.

The integrals in (22) and others in the sequel can be put in the form

$$\int_0^\infty \frac{d}{d\epsilon}\{\phi(\epsilon)\}\frac{d\epsilon}{1+\exp[(\epsilon-\xi)/\boldsymbol{k}T]}.$$

An asymptotic series expansion for the above integral when $\phi(\epsilon)$ is sufficiently regular and vanishes for $\epsilon=0$ was first given by Sommerfeld. Subject to an error of the order of $\exp(-\xi/\boldsymbol{k}T)$, an expansion appropriate for the case $\xi/\boldsymbol{k}T\gg 1$, i.e. the degenerate case, is

$$\int_0^\infty \frac{d}{d\epsilon}\{\phi(\epsilon)\}\frac{d\epsilon}{1+\exp[(\epsilon-\xi)/\boldsymbol{k}T]}=\{\phi(\epsilon)+2c_2(\boldsymbol{k}T)^2\phi''(\epsilon)+2c_4(\boldsymbol{k}T)^4\phi''''(\epsilon)+\ldots\}_{\epsilon=\xi}$$

where the coefficients c_2 and c_4 are $c_2=\pi^2/12$, $c_4=7\pi^4/720$. Taylor's expansion gives

$$\begin{aligned}\phi(\xi)&=\phi(\xi_0)+(\xi-\xi_0)\phi'(\xi_0)+\tfrac{1}{2}(\xi-\xi_0)^2\phi''(\xi_0)+\ldots\\ \phi''(\xi)&=\phi''(\xi_0)+(\xi-\xi_0)\phi'''(\xi_0)+\ldots\\ \phi''''(\xi)&=\phi''''(\xi_0)+\ldots\end{aligned}$$

Evaluating the integrals in (22) with the help of the Sommerfeld lemma, and making use of Taylor's expansion and the relations (4) and (6), we have, after a straightforward but tedious calculation,

$$\boldsymbol{e}F'=8c_2(\boldsymbol{k}T)^2\frac{1}{T}\left(\frac{\partial T}{\partial x}\right)\frac{(2x^2+3)}{x^2(1+x^2)^{1/2}}\left[1-\left(\frac{\boldsymbol{k}T}{\boldsymbol{mc}^2}\right)^2\{L_1(x)-L_2(x)\}+\mathrm{O}\left\{\frac{\boldsymbol{k}T}{\boldsymbol{mc}^2}\right\}^4\right],$$

where $\ldots\ldots(23)$

$$L_1(x)=\frac{6c_2(1+2x^2)(2x^4+5x^2+4)}{x^4(2x^2+3)(1+x^2)}-\frac{c_4}{c_2}\frac{2(x^6+36x^4+36x^2+24)}{x^4(2x^2+3)(1+x^2)} \quad \ldots\ldots(24)$$

and

$$L_2(x)=-4c_2\frac{2x^4+7x^2+9}{x^4(1+x^2)}. \quad \ldots\ldots(25)$$

Substituting for f in (21) from (18), we have

$$Q=\frac{4g}{3Z^2\boldsymbol{e}^4\boldsymbol{c}^2\boldsymbol{h}^3N_{\mathrm{A}}I}\int_0^\infty \frac{\epsilon(\epsilon^2+2\epsilon\boldsymbol{mc}^2)^3}{(\epsilon+\boldsymbol{mc}^2)^2}\frac{\partial f_0}{\partial\epsilon}\left\{\boldsymbol{e}F'-\frac{(\epsilon-\xi)}{T}\frac{\partial T}{\partial x}\right\}d\epsilon. \quad \ldots\ldots(26)$$

On evaluating the integrals in (26), as before, we have

$$\begin{aligned}Q=\frac{4g}{3Z^2\boldsymbol{e}^4\boldsymbol{c}^2\boldsymbol{h}^3N_{\mathrm{A}}I}&\left[-\boldsymbol{e}F'\frac{(\boldsymbol{mc}^2)^4x^6\xi_0}{(1+x^2)}\left\{1+\left(\frac{\boldsymbol{k}T}{\boldsymbol{mc}^2}\right)^2L_3(x)+\mathrm{O}\left(\frac{\boldsymbol{k}T}{\boldsymbol{mc}^2}\right)^4\right\}\right.\\ &\left.+\frac{1}{T}\left(\frac{\partial T}{\partial x}\right)4c_2(\boldsymbol{k}T)^2\frac{(\boldsymbol{mc}^2)^4x^6}{(1+x^2)}\left\{1\pm M(x)+\left(\frac{\boldsymbol{k}T}{\boldsymbol{mc}^2}\right)^2L_4(x)+\mathrm{O}\left(\frac{\boldsymbol{k}T}{\boldsymbol{mc}^2}\right)^4\right\}\right],\end{aligned}$$

$\ldots\ldots(27)$

where

$$L_3(x)=2c_2\left\{\frac{4x^6+14x^4+18x^2}{x^6(1+x^2)}+\frac{11x^4+6x^6}{(1+x^2)^{1/2}x^6}\left(\frac{\boldsymbol{mc}^2}{\xi_0}\right)\right\}, \qquad \ldots\ldots(28)$$

$$\begin{aligned}L_4(x)=\Bigg\{&-8c_2\frac{(1+2x^2)(2x^2+3)}{x^4(1+x^2)}-6c_2\left(\frac{\xi_0}{\boldsymbol{mc}^2}\right)\frac{(1+2x^2)(4x^4+10x^2+8)}{x^6(1+x^2)^{3/2}}\\&+2\frac{c_4}{c_2}\frac{(36x^4+90x^2+72)}{x^4(1+x^2)}+4\frac{c_4}{c_2}\left(\frac{\xi_0}{\boldsymbol{mc}^2}\right)\frac{(x^6+36x^4+36x^2+24)}{x^6(1+x^2)^{3/2}}\Bigg\}\end{aligned} \qquad \ldots\ldots(29)$$

and

$$M(x)=2\left(\frac{\xi_0}{\boldsymbol{mc}^2}\right)\frac{2x^2+3}{x^2(1+x^2)^{1/2}}. \qquad \ldots\ldots(30)$$

Substituting the value of $\boldsymbol{e}F'$ from (23) in (27) and retaining terms of the order of $(\boldsymbol{k}T/\boldsymbol{mc}^2)^2$, we obtain

$$\begin{aligned}Q=\frac{4g}{3Z^2\boldsymbol{e}^4\boldsymbol{c}^2\boldsymbol{h}^3N_{\mathrm{A}}I}\left(-\frac{\partial T}{\partial x}\right)\Bigg[&8c_2\boldsymbol{k}^2T(\boldsymbol{mc}^2)^4\left(\frac{\xi_0}{\boldsymbol{mc}^2}\right)\frac{x^4(2x^2+3)}{(1+x^2)^{3/2}}\\&\times\left\{1+\left(\frac{\boldsymbol{k}T}{\boldsymbol{mc}^2}\right)^2\{L_3(x)-L_1(x)+L_2(x)\}\right\}\\&-4c_2\boldsymbol{k}^2T(\boldsymbol{mc}^2)^4\frac{x^6}{(1+x^2)}\left\{1+M(x)+\left(\frac{\boldsymbol{k}T}{\boldsymbol{mc}^2}\right)^2L_4(x)\right\}\Bigg].\end{aligned} \qquad \ldots\ldots(31)$$

From the definition of thermal conductivity,

$$Q=-\lambda dT/dx, \qquad \ldots\ldots(32)$$

we have, on comparing (31) and (32),

$$\begin{aligned}\lambda=\frac{4g}{3Z^2\boldsymbol{e}^4\boldsymbol{c}^2\boldsymbol{h}^3N_{\mathrm{A}}I}\Bigg[&8c_2\boldsymbol{k}^2T(\boldsymbol{mc}^2)^4\left(\frac{\xi_0}{\boldsymbol{mc}^2}\right)\frac{x^4(2x^2+3)}{(1+x^2)^{3/2}}\\&\times\left\{1+\left(\frac{\boldsymbol{k}T}{\boldsymbol{mc}^2}\right)^2\{L_3(x)-L_1(x)+L_2(x)\}\right\}\\&-4c_2\boldsymbol{k}^2T(\boldsymbol{mc}^2)^4\frac{x^6}{(1+x^2)}\left\{1+M(x)+\left(\frac{\boldsymbol{k}T}{\boldsymbol{mc}^2}\right)^2L_4(x)\right\}\Bigg].\end{aligned} \qquad \ldots\ldots(33)$$

§ 4. THE LIMITING CASES

We shall now consider the two limiting cases of (33): (i) non-relativistic degenerate, and (ii) extreme relativistic degenerate. For the intermediate case, (33) gives the value of thermal conductivity.

Case (i). *Non-relativistic degenerate, i.e.* $x\rightarrow 0$.

$$\underset{x\to 0}{L_1(x)}=\frac{24c_2}{3x^4}-\frac{c_4}{c_2}\frac{16}{x^4}=-\frac{3\pi^2}{10}\left(\frac{\boldsymbol{mc}^2}{\xi_0}\right)^2. \qquad \ldots\ldots(34)$$

$$\underset{x\to 0}{L_2(x)}=-\frac{36c_2}{x^4}=-\frac{3\pi^2}{4}\left(\frac{\boldsymbol{mc}^2}{\xi_0}\right)^2. \qquad \ldots\ldots(35)$$

$$\underset{x\to 0}{L_3(x)}=2c_2\left\{\frac{18}{x^4}+\frac{11}{x^2}\left(\frac{\boldsymbol{mc}^2}{\xi_0}\right)\right\}=\frac{5\pi^2}{3}\left(\frac{\boldsymbol{mc}^2}{\xi_0}\right)^2. \qquad \ldots\ldots(36)$$

$$\begin{aligned}\underset{x\to 0}{L_4(x)}&=\left\{-24\frac{c_2}{x^4}-48c_2\left(\frac{\xi_0}{\boldsymbol{mc}^2}\right)\frac{1}{x^6}+144\frac{c_2}{c_4}\frac{1}{x^4}+96\frac{c_4}{c_2}\left(\frac{\xi_0}{\boldsymbol{mc}^2}\right)\frac{1}{x^6}\right\}\\&=\frac{23}{5}\pi^2\left(\frac{\boldsymbol{mc}^2}{\xi_0}\right)^2.\end{aligned} \qquad \ldots\ldots(37)$$

$$\underset{x\to 0}{M(x)}=6\left(\frac{\xi_0}{\boldsymbol{mc}^2}\right)\frac{1}{x^2}=3. \qquad \ldots\ldots(38)$$

ξ_0 is given by (5 *a*).

Substituting the above values of the functions L and M in (33), we have in the limit $x \to 0$

$$\lambda = \frac{16 g \pi^2 \boldsymbol{k}^2 T \boldsymbol{m} \xi_0^3}{9 Z^2 \boldsymbol{e}^4 \boldsymbol{h}^3 N_A \log[2/(1-\cos\theta_0)]} \left\{1 + \frac{19}{20}\pi^2 \left(\frac{\boldsymbol{k}T}{\xi_0}\right)^2\right\}, \qquad \ldots\ldots(39)$$

which is the same as given by Mestel (1950). Marshak's result (1940) contains a numerical error in the correction term, as has been pointed out by Mestel. (39) is the correct expression for λ in the non-relativistic degenerate case, correct to the order $(\boldsymbol{k}T/\xi_0)^2$.

Case (ii). *Extreme relativistic, i.e.* $x \to \infty$.

$$\underset{x\to\infty}{L_1(x)} = \frac{12c_2}{x^2} - \frac{c_4}{c_2}\frac{1}{x^2} = \frac{53\pi^2}{60}\left(\frac{\boldsymbol{mc}^2}{\xi_0}\right)^2. \qquad \ldots\ldots(40)$$

$$\underset{x\to\infty}{L_2(x)} = -8c_2\frac{1}{x^2} = -\frac{2\pi^2}{3}\left(\frac{\boldsymbol{mc}^2}{\xi_0}\right)^2. \qquad \ldots\ldots(41)$$

$$\underset{x\to\infty}{L_3(x)} = 2c_2\left\{\frac{4}{x^2} + \frac{6}{x}\frac{\boldsymbol{mc}^2}{\xi_0}\right\} = \frac{5\pi^2}{3}\left(\frac{\boldsymbol{mc}^2}{\xi_0}\right)^2. \qquad \ldots\ldots(42)$$

$$\begin{aligned}\underset{x\to\infty}{L_4(x)} &= \left\{-32c_2\frac{1}{x^2} - 48c_2\left(\frac{\xi_0}{\boldsymbol{mc}^2}\right)\frac{1}{x^3} + 72\frac{c_4}{c_2}\frac{1}{x^2} + 4\frac{c_4}{c_2}\left(\frac{\xi_0}{\boldsymbol{mc}^2}\right)\frac{1}{x^3}\right\} \\ &= \frac{11}{5}\pi^2\left(\frac{\boldsymbol{mc}^2}{\xi_0}\right)^2. \qquad \ldots\ldots(43)\end{aligned}$$

$$\underset{x\to\infty}{M(x)} = 4\left(\frac{\xi_0}{\boldsymbol{mc}^2}\right)\frac{1}{x} = 4. \qquad \ldots\ldots(44)$$

ξ_0 is given by (5 *b*).

Using the above values of the functions L and M in (33), we have in the limit $x \to \infty$

$$\lambda = \frac{4\pi^2 \boldsymbol{k}^2 T \xi_0^4}{9 Z^2 \boldsymbol{e}^4 \boldsymbol{c}^2 \boldsymbol{h}^3 N_A \log[2/(1-\cos\theta_0)]} \left\{1 + \frac{26}{15}\pi^2 \left(\frac{\boldsymbol{k}T}{\xi_0}\right)^2\right\}. \qquad \ldots\ldots(45)$$

In the extremely degenerate case, i.e. when the temperature term in the braces is negligible, we have

$$\lambda = \frac{4\pi^2 \boldsymbol{k}^2 T \xi_0^4}{9 Z^2 \boldsymbol{e}^4 \boldsymbol{c}^2 \boldsymbol{h}^3 N_A \log[2/(1-\cos\theta_0)]}. \qquad \ldots\ldots(46)^*$$

ACKNOWLEDGMENTS

Our thanks are due to Professor R. E. Peierls for discussions and for his kind interest in this work. One of us (K.S.S.) would like to thank the British Council for the award of a scholarship.

REFERENCES

Chandrasekhar, S., 1938, *Introduction to the Study of Stellar Structure* (University of Chicago Press), p. 413.

Kothari, D. S., 1932, *Mon. Not. R. Astr. Soc.*, **93,** 61.

Kothari, D. S., and Singh, B. N., 1942, *Proc. Roy. Soc.* A, **180,** 414.

Lee, T. D., 1950, *Astrophys. J.*, **111,** 625.

Marshak, R. E., 1940, *Ann. N.Y. Acad. Sci.*, **41,** 49.

Mestel, L., 1950, *Proc. Camb. Phil. Soc.*, **46,** 331.

Mott, N. F., and Massey, H. S. W., 1949, *The Theory of Atomic Collisions* (Oxford: University Press), p. 80.

* When the above investigation was almost complete our attention was drawn to a paper by Lee (1950) on hydrogen content and energy-productive mechanism of white dwarfs, in the appendix of which the author has considered the case $x \to \infty$, and has derived the expression (46). His expression agrees with ours. Our main aim in this paper has, however, been to derive the general expression (33), which is true for all values of x. As a matter of fact, in the known massive white dwarfs such as Sirius B or the central star of the crab nebula, it is intermediate values of x which are of importance.

The Saturation Magneto-Resistance of Ferromagnetic Alloys

By R. PARKER
Department of Physics, University of Nottingham

Communicated by L. F. Bates; *MS. received 4th August* 1950, *and in amended form 29th December* 1950

ABSTRACT. It is suggested that the magneto-resistance coefficient of a ferromagnetic alloy is composed of two terms, one associated with the temperature-dependent, the other with the temperature-independent contribution to the electrical resistivity. An equation based on this hypothesis is in good agreement with the experimental results for silicon–iron alloys. The validity of the equation for other alloys is discussed.

§ 1. INTRODUCTION

In general when a ferromagnetic material, initially demagnetized, is placed in a magnetic field H an appreciable change in its electrical resistivity ρ occurs. The observed variation of ρ with applied field strength may be divided into two ranges: firstly, the range at higher values of H where changes in the spontaneous magnetization J_s take place, and secondly, a more complex change in the region of technical magnetization. Consideration in the present communication will be confined to changes of resistance in the latter range and, where necessary, correction will be made to the experimental results quoted to eliminate the change in ρ due to a change in the value of J_s.

Two magneto-resistance coefficients are usually defined: (*a*) the longitudinal magneto-resistance coefficient $(\Delta\rho/\rho)_{\parallel}$ and (*b*) the transverse coefficient $(\Delta\rho/\rho)_{\perp}$, which denote respectively the relative change in ρ due to the application of a magnetic field along and perpendicular to the direction of the current flow. There are no simple relations between the magneto-resistance and the applied field or the intensity of magnetization of a specimen. The work of McKeehan (1930) and Englert (1932) on strained materials showed that the magneto-resistance coefficients are functions of the domain vector orientation only, and do not depend upon whether a given orientation is produced by the application of a magnetic field or by an elastic stress. For this reason the difference of the two magneto-resistance coefficients at technical saturation $(\Delta\rho/\rho)_{\parallel\,\mathrm{sat}}-(\Delta\rho/\rho)_{\perp\,\mathrm{sat}}$ is a constant for a given material and is independent of the state of strain of a particular specimen. From measurements on nickel at different temperatures Gerlach (1932) showed that $(\Delta\rho/\rho)_{\parallel\,\mathrm{sat}}$ and $(\Delta\rho/\rho)_{\perp\,\mathrm{sat}}$ are directly proportional to the value of J^2.

The results of measurements of magneto-resistance for single crystals of iron and nickel (Kaya 1927, Döring 1938, Shirakawa 1940) indicate that the magneto-resistance coefficients are functions of crystal direction. The measured values for polycrystalline iron and nickel are in agreement with the value of the magneto-resistance coefficient calculated assuming the polycrystalline specimen to consist of a large aggregate of randomly orientated single crystallites.

In the present state of development of the theory of electrical conduction in metals it is not possible to account for the phenomena of magneto-resistance briefly outlined above. However, guided by this theory, it is possible, making certain plausible assumptions, to explain a number of experimental results obtained with the alloys of iron and silicon. In §2 these assumptions will be discussed and from them an equation will be derived for the saturation value of the magneto-resistance coefficient of a particular type of alloy in terms of temperature and composition. The application of this equation to the case of silicon–iron alloys will be given in §3 and certain deductions compared with the experimental results of Shirakawa (1939) and Parker (1950).

§ 2. A SUGGESTED MECHANISM OF MAGNETO-RESISTANCE PROCESSES

According to the quantum theory the electrical resistance of a metal is supposed to be due to the scattering of the electron waves by aperiodicities in the ionic lattice. Such aperiodicities arise, firstly, from thermal vibrations of the lattice points, and secondly, from the presence of impurity atoms or dislocations in the lattice. In this way the resistance may be considered to have two components, one of which increases approximately linearly with temperature, the other being temperature-independent (Matthiessen's rule). The theory suggests an explanation for the experimental result that for sufficiently small quantities of added impurity the resistance increases linearly with the concentration of impurity at a given temperature (Mott and Jones 1936).

If this analysis holds for a polycrystalline silicon–iron alloy of a sufficiently small silicon content then the resistivity is given by $\rho = \rho_F + \rho_s$ where ρ_F and ρ_s are the temperature dependent and independent contributions respectively. Hence, if N_F and N_s are the numbers of atoms per cm³ of iron and silicon present respectively,

$$\rho = N_F\sigma_F + N_s\sigma_s \qquad \ldots\ldots(1)$$

where σ_F and σ_s are measures of the efficiency of scattering of conduction electrons (averaged over all crystal directions) by thermal vibrations and by aperiodicities in the lattice due to the presence of the silicon atoms. Equation (1) is simplified in that it neglects the contribution to the resistance due to the thermal vibrations of the silicon atoms. In order to account for the magneto-resistance effects let us postulate (*a*) that the values of σ_F and σ_s depend on the angle α between the spontaneous magnetization vector and an arbitrary crystal direction. Guided by Gerlach's results on nickel (§1) it will further be assumed (*b*) that the changes of σ_F and ρ_s are directly proportional to J_s^2 for a given value of α.

Let Δ denote the changes when a specimen is brought from the demagnetized state to technical saturation, so that $\Delta\rho_F = N_F\Delta\sigma_F$, $\Delta\rho_s = N_s\Delta\sigma_s$, and $\Delta\rho = \Delta\rho_F + \Delta\rho_s$; then, by definition $\Delta\rho/\rho = (N_s\Delta\sigma_s + N_F\Delta\sigma_F)/(N_s\sigma_s + N_F\sigma_F)$ so that

$$\Delta\sigma_s/\sigma_s = \Delta\rho_s/\rho_s = \Delta\rho/\rho + \rho_F/\rho_s(\Delta\rho/\rho - \Delta\rho_F/\rho_F). \qquad \ldots\ldots(2)$$

Writing $\rho_F = \rho_0(1 + \beta t)$, where ρ_0 is the value of ρ_F at 0° c., t the temperature, on the centigrade scale, of the specimen and β the mean temperature coefficient of ρ_F, and writing $\Delta\rho/\rho$, $\Delta\rho_F/\rho_F$ and $\Delta\rho_s/\rho_s$ as functions of J_s we obtain from (2)

$$\Delta\rho_s/\rho_s(J_s) + \Delta\rho_F/\rho_F(J_s) \times \rho_0(1+\beta t)/\rho_s = \Delta\rho/\rho(J_s)[1 + \rho_0(1+\beta t)]/\rho_s$$

and $$\Delta\rho/\rho(J_s) = [\Delta\rho_s/\rho_s(J_s) + \rho_0(1+\beta t)/\rho_s \times \Delta\rho_F/\rho_F(J_s)]/[1 + \rho_0(1+\beta t)/\rho_s]. \qquad \ldots(3)$$

If our hypothesis is correct, (3) should describe the saturation magneto-resistance of silicon–iron alloys as a function of temperature and of silicon content. All quantities on the right-hand side of (3), with the exception of $\Delta\rho_s/\rho_s$, can be obtained from independent experimental results. The value of $\Delta\rho_s/\rho_s$ for a given value of J_s can be determined from measurements on one silicon–iron alloy at a given temperature and the use of equation (2). With the aid of assumption (*b*) above the value $\Delta\rho_s/\rho_s$ for different values of J_s can be calculated if J_s is a known function of the temperature T.

§ 3. COMPARISON WITH EXPERIMENTAL RESULTS

Now, the assumption has been made that $\Delta\rho/\rho$ of iron has the same dependence on J_s as that of nickel. If $(\Delta\rho/\rho)_\infty$ and J_∞ represent the technical saturation magneto-resistance and magnetization at the absolute zero of temperature, respectively, Gerlach's relation is expressed in the fact that

$$\Delta\rho/\rho = (\Delta\rho/\rho)_\infty J_s^2/J_\infty^2. \qquad \ldots\ldots(4)$$

The values of J_s^2/J_∞^2 at various temperatures may be taken in the case of iron from Potter's (1934) results. The results of Shirakawa's (1939, 1940) measurements of $(\Delta\rho/\rho)_{\parallel\,\mathrm{sat}}$ on two different specimens of iron are recorded in Figure 1. The agreement at $-195°$ c. is poor, probably due to the appreciable temperature independent contribution to the resistivity. This may be looked upon as a general feature of low temperature results, except in materials of the highest purity. At higher temperatures the results are consistent with Gerlach's hypothesis, but do not provide a quantitative check owing to the considerable probable error.* However a casual inspection of Shirakawa's curves shws thato alloys of Fe–Si and Fe–Ni do not even qualitatively obey equation (4).

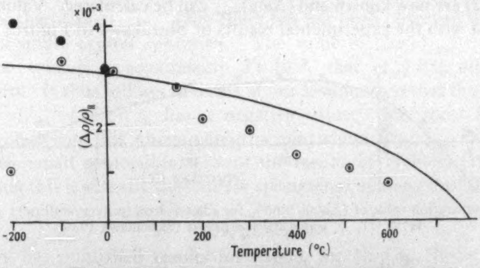

Figure 1. The longitudinal saturation magneto-resistance for iron.
○ Shirakawa 1939. ● Shirakawa 1940.
The best curve compatible with equation (4) is drawn through the points.

The experimental results of $(\Delta\rho/\rho)_{\parallel\mathrm{sat}}$ for iron containing 0–9·5% silicon (Shirakawa 1939) will now be discussed. This alloy system has been chosen for the following reason. For up to 10% of silicon the contribution of the iron atoms to the spontaneous magnetization is not affected. Up to 9·5% silicon there is no change in crystal structure and no formation of a superlattice below the Curie temperature θ. The linear increase in ρ with silicon concentration is conveniently large (owing to the great difference in atomic number of the two elements), and has been measured with considerable accuracy by Gumlich (1913) and Yensen (1924). In the subsequent calculation the mean of their results will be used and this will be assumed to be independent of temperature.

* An impurity of 0·5%, as revealed by one analysis would be expected to influence $(\Delta\rho/\rho)_{\parallel\,\mathrm{sat}}$ even at $-95°$ c. to some extent. Above 150° c. the magneto-crystalline energy is so small that a difference in the initial domain orientation of the specimen cannot be ruled out: for this reason the appropriate data of $(\Delta\rho/\rho)_{\parallel\,\mathrm{sat}} - (\Delta\rho/\rho)_{\perp\,\mathrm{sat}}$ would have been of greater value.

According to our hypothesis $(\Delta\sigma_s/\sigma_s)_\infty$, the value of $\Delta\sigma_s/\sigma_s$ at the absolute zero of temperature, is an atomic property of the alloy, and $(\Delta\rho_s/\rho_s)_\infty$ should therefore be independent of composition. The latter value will now be calculated from (2) and (4) for alloys containing 0·66, 1·66, 5·18 and 9·43% silicon from Shirakawa's experimental results at room temperature. The value of $\rho_0(1+\beta t)$ used here is the mean quoted by Cleaves and Thompson (1935). $\Delta\rho_F/\rho_F(J_s)$ is taken from the calculated curve shown in Figure 1 and a correction is applied for the silicon content by subtracting the contribution to $\Delta\rho_F$ of the iron atoms displaced by silicon. The value of J_s^2/J_∞^2 for each alloy is calculated by assuming the validity of the law of (magnetic) corresponding states. It will be seen from the Table that although $(\Delta\rho/\rho)_{\parallel\,\text{sat}}$ varies from $+1{\cdot}0\times10^{-3}$ to $-0{\cdot}9\times10^{-3}$, $(\Delta\rho_s/\rho_s)_\infty$ remains constant within experimental error, the average value being $-1{\cdot}34\times10^{-3}$.

Si (%)	0·66	1·66	5·18	9·43
$(\Delta\rho/\rho)_{\parallel\,\text{sat}}\times10^3$ at room temperature	+1·00	+0·14	−0·74	−0·90
$(\Delta\rho_s/\rho_s)_{\parallel\,\text{sat}}\times10^3$ at room temperature	−1·21	−1·26	−1·35	−1·24
θ (° K.)	1040	1030	1010	910
$(\Delta\rho_s/\rho_s)_\infty$	−1·26	−1·32	−1·41	−1·34

A similar confirmation is also found at other temperatures as may be demonstrated in the following way. With the aid of equation (4) $(\Delta\rho_s/\rho_s)_{\parallel\,\text{sat}}$ can now be found as a function of temperature. All quantities on the right-hand side of equation (3) are now known and $(\Delta\rho/\rho)_{\parallel\,\text{sat.}}$ can be calculated. Values so obtained are compared with the experimental results of Shirakawa in Figures 2, 3, 4 and 5.

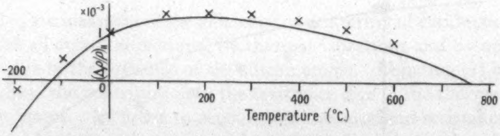

Figure 2. The saturation value of $(\Delta\rho/\rho)_\parallel$ 0·66% for silicon–iron (polycrystalline): curve calculated from (3); × experimental points (Shirakawa 1939).

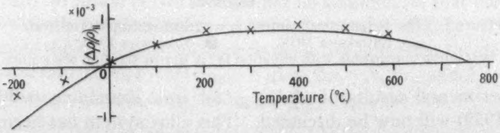

Figure 3. Results similar to Figure 2 for 1·66% silicon–iron (polycrystalline).

It will be seen that the agreement obtained at all temperatures is within the limits of the experimental errors in the determinations of the quantities used in (3).

Further qualitative confirmation of the above hypothesis is provided by experimental work recently carried out by the author. The magneto-resistance of a single crystal containing 2·8% silicon was measured along a [110] direction and it was observed that $(\Delta\rho/\rho)_\parallel$ has a most unusual minimum value in the region where only rotations from the [100] and [010] into the [110] direction take place. It was found that Döring's assumption $\Delta\rho/\rho=F(\alpha^2,\alpha^4)$ was not valid. A plausible explanation of the form of the observed variation may, however, be given as follows. From the polycrystalline curve it can be estimated that in 2·8% silicon–iron at room temperature ρ_F and ρ_s contribute to $\Delta\rho/\rho$ to comparable extents. We assume that the two processes have simple but different variations with α. In the early part of the magnetization curve the variation of σ_s with α makes the larger contribution to $(\Delta\rho/\rho)_{\parallel}$ of the alloy, but as saturation is approached $\Delta\sigma_F$ becomes the dominant term.

Another unusual feature receives a simple explanation. A given crystal (1·8% Si) cut along a [100] direction was found to have $(\Delta\rho/\rho)_{\parallel\,\mathrm{sat}}$ numerically more negative than $(\Delta\rho/\rho)_{\perp\,\mathrm{sat}}$. This effect has not been observed with any pure iron or nickel single crystal specimen. The value of $(\Delta\rho/\rho)_{\parallel\,\mathrm{sat}}-(\Delta\rho/\rho)_{\perp\,\mathrm{sat}}$ for polycrystalline iron is approximately 3×10^{-3}, that of 1·8% silicon–iron is practically zero. It thus follows in terms of our assumptions that the contribution of ρ_s to $(\Delta\rho/\rho)_{\parallel\,\mathrm{sat}}-(\Delta\rho/\rho)_{\perp\,\mathrm{sat}}$ has a negative value. The most likely crystal direction for observing this phenomenon is one where $(\Delta\rho/\rho)_{\parallel\,\mathrm{sat}}-(\Delta\rho/\rho)_{\perp\,\mathrm{sat}}$ for pure iron is as small as possible. From the results of Webster (1926, 1927) it can be seen that this is actually the case for specimens cut along the [100] direction.

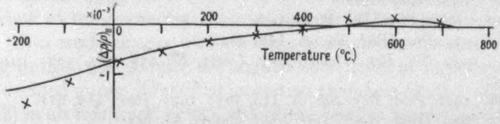

Figure 4. **Results similar to Figure 2 for 5·18% silicon–iron (polycrystalline).**

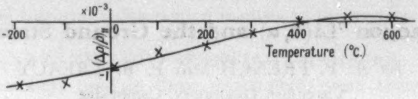

Figure 5. **Results similar to Figure 2 for 9·43% silicon–iron (polycrystalline).**

§4. CONCLUSION

Shirakawa has published results for $(\Delta\rho/\rho)_{\parallel}$ for Ni–Co, Ni–Fe, Fe–Co and Ni–Cu. The analysis of the present paper cannot readily be applied to these results. In the case of the first three alloy systems further assumptions must be made, to allow for the variation of Bohr magneton number with composition. In the case of Ni–Cu alloys it is difficult to separate the contributions to ρ of the thermal vibrations of the nickel lattice and of the copper solid solution (Mott 1936) at various temperatures. Equation (3) has been found to give the results so far reported to within the expected accuracy.

No theoretical justification for the variation of scattering cross section area of ions (for conduction electrons) with magnetization direction has yet been given. It is thought significant, however, that it should be proportional to J_s^2, since, except near the Curie temperature, this is a measure of the 3d electron spin alignment inside ferromagnetic domains.

ACKNOWLEDGMENTS

The author wishes to express his thanks to Professor L. F. Bates for his interest in this work and to Dr. R. Street for a number of valuable suggestions.

REFERENCES

CLEAVES, H. E., and THOMPSON, J. G., 1935, *The Metal Iron* (New York : McGraw-Hill).
DÖRING, W., 1938, *Ann. Phys., Lpz.*, **32,** 259.
ENGLERT, E., 1932, *Ann. Phys., Lpz.*, **14,** 589.
GERLACH, W., 1932, *Ann. Phys., Lpz.*, **12,** 849, and *Phys. Z.*, **33,** 953.
GUMLICH, E., 1913, *Ferrum*, **10,** 33.
KAYA, S., 1927, *Sci. Rep. Tohoku Imp. Univ.*, **17,** 1027.
MCKEEHAN, L. W., 1930, *Phys. Rev.*, **36,** 948.
MOTT, N. F., 1936, *Proc. Roy. Soc.* A, **156,** 368.
MOTT, N. F., and JONES, H., 1936, *The Theory of the Properties of Metals and Alloys* (Oxford : University Press).
PARKER, R., 1950, *Proc. Phys. Soc.* B, **63,** 996.
POTTER, H. H., 1934, *Proc. Roy. Soc.* A, **146,** 362.
SHIRAKAWA, Y., 1939, *Sci. Rep. Tohoku Imp. Univ.*, **27,** 255, 484, 532; 1940, *Ibid.*, **29,** 132, 152.
WEBSTER, L. W., 1926, *Proc. Roy. Soc.* A, **113,** 167; 1927, *Ibid.*, **114,** 611.
YENSEN, T. D., 1924, *Trans. Amer. Inst. Elect. Engrs.*, **43,** 145.

The Reaction ^{7}Li(d, α) and the Ground State of ^{5}He

BY A. P. FRENCH AND P. B. TREACY
Cavendish Laboratory, Cambridge

Communicated by E. S. Shire; *MS. received* 11*th October* 1950, *and in amended form* 27*th December* 1950

ABSTRACT. A differential ionization chamber with electron collection has been designed for the study of α-particle spectra. Two chambers of this type have been used to investigate α–α coincidences in the reaction ^{7}Li(d, α n)^{4}He. The results confirm that this process takes place, and the observed angular correlation of successive α-particles lends some support to the view that the virtual ground state of ^{5}He is $P_{3/2}$.

§ 1. INTRODUCTION

THE spectrum of α-particles from bombardment of Li with deuterons was first studied in detail by Williams *et al.* (1937). These workers found a fairly definite group of α-particles at the upper end of a continuous distribution. The results were taken to show that the following two reactions could occur:

$$^7\text{Li}+{}^2\text{D}\rightarrow{}^8\text{Be}^*+{}^1\text{n} \quad \ldots\ldots\ldots\ldots\ldots \quad \text{A}$$

$$\searrow {}^5\text{He}+{}^4\text{He} \quad \ldots\ldots\ldots\ldots\ldots \quad \text{B}$$

Reaction A could produce a continuous distribution of the kind observed, whereas the ^{4}He formed in reaction B would appear as a group of definite energy. The absence of a group due to ^{5}He implied that it had a very short lifetime; the α-particles from its decay in flight would then contribute to the continuous energy distribution.

From the energy release in reaction B it was inferred that the ^{5}He liberates about 0·9 MEV. energy in breaking up into an α-particle and a neutron. Staub and Stephens (1939) subsequently found that the cross section for scattering of neutrons in ^{4}He had a peak at about 1·0 MEV. neutron energy, and suggested that the same state of ^{5}He was involved. There was, however, some evidence for doublet structure in the scattering cross section (Staub and Tatel 1940), and other scattering experiments (Barschall and Kanner 1940, Hall and Koontz 1947) have supported the view that two levels of ^{5}He are involved. The energy interval between two such states is still in doubt (Goldstein 1950), although the most recent collected data on total cross sections (Adair 1950) seem to suggest that it may be large.

Apart from the early experiments of Williams *et al.* (1937) all studies of ^{5}He have been made in scattering experiments, and it was thought that some further work on the α-particles from ^{7}Li + D might be of interest. The types of experiment decided upon were: (i) a study of the α-particle group from reaction B, which in view of the scattering experiments might be expected to show some structure; (ii) a study of α–α coincidences, to establish that reaction B in fact occurs and, in this case, to infer the angular correlation of successive α-particles.

It was decided to use differential ionization chambers (Rutherford *et al.* 1930, Lewis 1942) in all this work. Such chambers, besides having good resolution in range, are rather well suited to selecting particles of a given energy within a continuous distribution. Because the type of chamber used in these experiments had certain novel features, a description is given in the next section.

§ 2. THE DIFFERENTIAL CHAMBERS

The two chambers used in these experiments were essentially similar in design. The prime need, especially for the coincidence work, was to obtain fast pulses, so it was decided to make use of electron collection in argon. A diagram of one chamber is shown in Figure 1. The three brass rings A, B, C are mounted on a brass frame and are insulated from it by means of polystyrene washers. The complete assembly can be removed from the body of the chamber. The rings A and B carry wire grids and form the high voltage electrodes (at +120 v. and −120 v. respectively). The collector ring C carries a gold foil on each side. The diameter of ring A is smaller than that of B or C, so as to define the solid angle of acceptance for α-particles. The α-particles enter the chamber through a mica window W after traversing an air absorption cell of variable

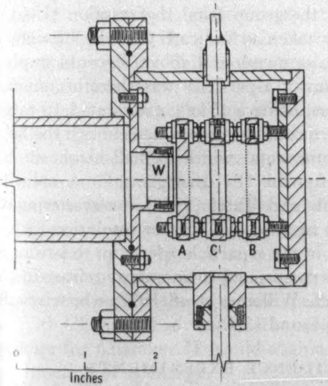

Figure 1. Differential chamber.

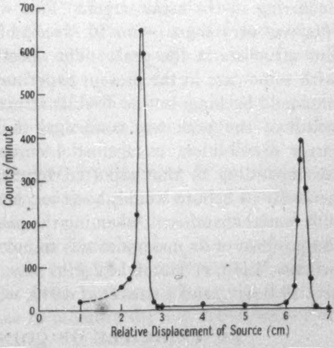

Figure 2. Calibration curve with a source of Th C+C′.

pressure. The window is mounted to withstand pressure in both directions. The whole chamber is filled to 20 cm. Hg pressure with argon containing 3% CO_2. Under these conditions the spacings AC and CB are adjusted so that the path lengths from which electrons are collected are 2·1 and 1·8 mm. air equivalent in the front and back parts of the chamber respectively. These values are chosen to suppress pulses of the wrong sign due to particles travelling somewhat further than those being detected. The gold foils and the gas between them at C represent an air equivalent of 2 mm. This stopping power was introduced so as to increase the differential pulse heights without worsening the resolution of the chamber. These details of design were based on a curve given by Stetter and Jentschke (1935) for specific ionization by a single α-particle.

A pre-amplifier supplied by D.C. was mounted on the chamber. The integrating and differentiating time constant settings in the main amplifier were 10 μsec., and under normal working conditions the signal-to-noise ratio for the largest differential pulses was about 3 or 4. Quite apart from amplifier noise, there is of course a continuous distribution of differential pulse sizes unless the α-particle spectrum is narrower than the resolution width of the chamber.

Figure 2 shows the result of a test of the chamber using ThC + C′ α-particles. In this experiment the air absorption cell was dispensed with, and the source was moved with respect to the chamber. It can be seen that the width at half-maximum of each group is about 2·5 mm. All calibrations during the experiments on lithium were made with sources of thorium-active deposit.

§ 3. EXPERIMENTS WITH A SINGLE CHAMBER

The work of Williams *et al.* (1937) showed that the group of α-particles attributed to reaction B was wider than the group from the reaction ^{6}Li(d, α) occurring in the same target. This was taken to indicate that the lifetime of ^{5}He was very short ($\sim 6 \times 10^{-20}$ sec.) but, as mentioned above, it could imply a fine structure in the peak. The spectrum of α-particles was therefore studied with some care in the present experiments, using a 15 kev. evaporated Li target on a gold backing, but no doublet structure could be detected, although the large width of the peak was confirmed (6·0 mm. total width at half-height on the range distribution, as against 4·9 mm. for the ^{6}Li(d, α) group). A splitting corresponding to that reported by Staub and Tatel (1940) for scattering of neutrons in helium would, however, have been on the limit of resolution for the differential chamber. Assuming the peak in the α-particle spectrum to be single, the position of its maximum was found to correspond to an energy release in the process ^{7}Li(d, α)^{5}He of 14·2 ± 0·1 MeV. (cf. Williams *et al.* 1937, whose results give 14·0 MeV., and Lattes *et al.* 1947, who found 13·4 MeV.).

§ 4. PRINCIPLE OF COINCIDENCE EXPERIMENTS

According to known mass values (Bethe 1947, Rosenfeld 1948) the total energy release in the disintegration $^7\mathrm{Li} + {}^2\mathrm{D} \rightarrow {}^4\mathrm{He} + {}^4\mathrm{He} + {}^1\mathrm{n}$ is 15·10 ± 0·08 MeV. If the peak in the α-particle spectrum from ^{7}Li + D is in fact due to formation of ^{5}He, with a reaction energy of 14·2 MeV., the subsequent break-up of ^{5}He must occur with an energy release of about 0·9 MeV. One can then write the two stages of break-up from the compound nucleus $^9\mathrm{Be}^*$ in the following way:

$$^9\mathrm{Be}^* \rightarrow \alpha_1 + {}^5\mathrm{He} + 14{\cdot}2\ \mathrm{MeV}.$$
$$^5\mathrm{He} \rightarrow \alpha_2 + {}^1\mathrm{n} + 0{\cdot}9\ \mathrm{MeV}.$$

If the ^{5}He breaks up instantaneously, the secondary α-particle α_2 emerges within a cone of semi-angle about 10° whose axis is the initial direction of motion of the recoiling ^{5}He. This axis can be specified by observing in coincidence with α_2 the primary α-particle α_1 moving in a given direction. It is, moreover, possible to infer the angular distribution of break-up of the ^{5}He if one measures the energy distribution of the α_2. This can be readily seen by reference to Figure 3. The ^{5}He is assumed to be moving with velocity V (represented by OA) at 180° to α_1 in a frame of reference in which the ^{9}Be* is at rest. The break-up of ^{5}He then imparts to α_2 a velocity v (represented by AB) in the direction θ in the centre-of-mass system of the ^{5}He. The resultant observed velocity of α_2 is given by OB. The energy E of α_2 is thus given by $E=\frac{1}{2}m(V^2+v^2+2Vv\cos\theta)$, where m is the α-particle mass.

Now the angular distribution of break-up of the ^{5}He with respect to the direction OA (and referred to a system moving with the ^{5}He nucleus) can be described by a function $f(\theta)$, so that $f(\theta)\,d\Omega$ represents the probability of emission of α_2 into $d\Omega$ at θ. But if $g(E)\,dE$ is the number of particles α_2 in a range of energy dE at E, then by definition (apart from a suitable normalizing factor) $f(\theta)d\Omega=g(E)\,dE$. But $d\Omega=2\pi\sin\theta d\theta$ and $dE=-mVv\sin\theta d\theta$, so that $f(\theta)=\text{const.}\times g(E)$. This is the required relation between angular and energy distribution functions; the result is familiar in connection with studies of recoil nuclei in the elastic scattering of neutrons.

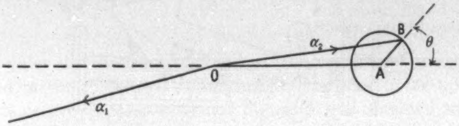

Figure 3. Geometry of coincidence experiment. The circle is the locus of the ends of the velocity vectors for α_2.

The experimental arrangement that suggested itself was to use a narrow-angle chamber to detect the particles α_1, and a wide-angle chamber to accept all particles α_2 corresponding to them. By fitting each chamber with an air absorption cell it was possible to carry out two measurements: (i) Chamber II (to detect α_2) could be set to record particles near the centre of the expected energy distribution in the break-up of ^{5}He. The α–α coincidence rate could then be measured as a function of the range of α-particles detected in Chamber I. This would show whether the peak in the α-particle spectrum is, in fact, due to production of ^{5}He. (ii) With Chamber I set to detect α-particles at the peak, variation of the absorber pressure for Chamber II would enable one to measure the α–α coincidence rate as a function of α_2 energy.

The details and the results of these measurements are given in the next sections.

§ 5. EXPERIMENTAL DETAILS

Figure 4 shows the arrangement used in the coincidence experiment. A thin layer of Li_2O on Al foil was bombarded with a narrow beam of 0·93 Mev. deuterons. Chamber I subtended a cone of semi-angle 2° at the target. Alpha-particles entering it had passed through the Al target backing, but the estimated mean angle of multiple scattering was less than 1°. Chamber II subtended a cone of semi-angle 18°. The axes of the chambers were set at 75° and 90° respectively to the deuteron beam, so as to be at 180° to each other in the centre-of-mass system of the compound nucleus ^{9}Be*.

Coincidences were recorded by conventional means, and a measure of the random rate was obtained by a delayed coincidence method (Littauer 1950). The limitation on amplifier bandwidth imposed by the smallness of the differential pulses in the ionization chambers made it necessary to use a rather long resolving time ($\sim 3\,\mu$sec.) in the coincidence unit. Even under these conditions not all true coincidences were recorded, owing to the necessarily continuous distribution of pulse sizes, and no attempt was made to estimate the absolute coincidence rate.

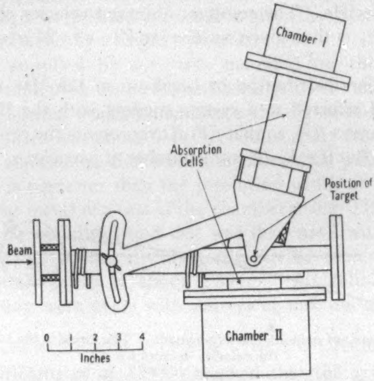

Figure 4. Schematic diagram of coincidence arrangement. Cross hatching denotes sylphon bellows.

The two mica windows between the target and Chamber I were supported only around their circumferences and had a total stopping power of 5·0 cm. air equivalent. The windows leading to Chamber II were mounted on grids in the form of brass plates drilled with small holes. This was necessary because of the small stopping power and large aperture required. To make the transmission of the grids uniform, they were drilled radially towards the centre of the target spot. By placing a thorium C source at the target position it was possible, by using annular screens of various radii, to check the transmission of the windows at different angles to the axis of the chamber.

§ 6. RESULTS

In Figure 5 is shown the coincidence count (for a fixed count in Chamber II) as a function of the energy of those α-particles detected in Chamber I. Chamber II was set to record α-particles of mean energy 4·6 Mev. The single counts in Chamber I are also plotted. It is evident that coincidences are associated with the group previously ascribed to reaction B above. The widths of the peaks are due essentially to target thickness and straggling.

Figure 6 shows the relative numbers of coincidences per Chamber I count for various energies of α-particles in Chamber II when Chamber I was set at the peak of its distribution (8·6 Mev.). The range of α-energies that could be detected by Chamber II by adjustment of absorption cell pressure was from 3·3 MeV. to 6·9 MeV. In view of Figure 5, it appears safe to assume that most coincidences so observed correspond to reaction B rather than to the break-up of ^{8}Be from reaction A. The energy distribution of coincident α-particles cannot well be fitted to the curve of broken outline in Figure 6, which is the form one might expect from a rectangular distribution modified to take account of straggling, chamber resolution and target thickness. This implies that the break-up of ^{5}He is not isotropic in its centre-of-mass system. Figure 6 was obtained with are solving time in the coincidence unit short enough to exclude the detection of protons in coincidence. (Such protons would arise from neutron recoils.) Using a longer resolving time (>4 μsec.), the shape of the curve was modified slightly.

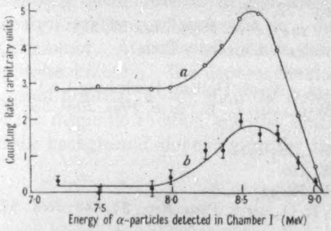

Figure 5. Curve *a*: single counts in Chamber I.
Curve *b*: α–α coincidences.

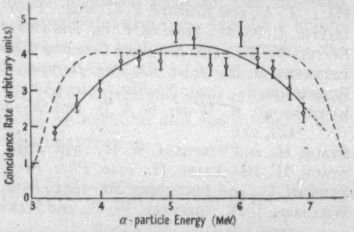

Figure 6. Variation of coincidence rate with energy of α-particles detected in Chamber II.
Full curve: $f(\theta)=1+1{\cdot}2\sin^2\theta$.
Broken outline: isotropic distribution.

§7. DISCUSSION

The energy distribution exhibited in Figure 6 is best fitted by an angular correlation function of the form $f(\theta)=1+A\sin^2\theta$. If the background of true coincidences due to break-up of $^8\mathrm{Be}^*$ is ignored, the value of A is found by a least-squares analysis to be $1{\cdot}2\pm0{\cdot}1$. In making this analysis it is necessary (since θ is defined only in terms of energy) to assume a definite value for the binding energy of ^{5}He. The value used was 0·90 MeV., on the basis of our measurements on the α-particle spectrum. A better value (0·94 MeV.) can be deduced from the most recent measurements on the scattering of neutrons in helium (Hall and Koontz 1947, Bashkin *et al.* 1950, Adair 1950) if one assumes that the total cross section has only one maximum near 1 MeV. and that its position is not displaced by interference between s- and p-waves.

It is clear that our results on the angular correlation are not accurate enough to justify any detailed interpretation. One can however say that a dominant contribution from a $P_{1/2}$ state of ^{5}He seems to be excluded, since in this case the angular distribution would be isotropic. The possibility of an almost pure $P_{3/2}$ state recently advocated by Goldstein (1950) is not inconsistent with the present measurements, although a clear-cut solution to the problem of ^{5}He has yet to be found.

ACKNOWLEDGMENTS

We should like to record our indebtedness to the late Mr. W. Birtwhistle for his expert help during our work on the 1 MV. H.T. set.

This work was made possible for one of us (P. B. T.) through the tenure of an Exhibition of 1851 Overseas Scholarship.

REFERENCES

Adair, R. K., 1950, *Rev. Mod. Phys.*, **22,** 249.

Barschall, H. H., and Kanner, M. H., 1940, *Phys. Rev.*, **58,** 590.

Bashkin, S., Petree, B., Mooring, F. P., and Peterson, R. E., 1950, *Phys. Rev.*, **77,** 748.

Bethe, H. A., 1947, *Elementary Nuclear Theory* (New York : John Wiley).

Goldstein, H., 1950, *Phys. Rev.*, **79,** 740.

Hall, T. A., and Koontz, P. G., 1947, *Phys. Rev.*, **72,** 196.

Lattes, C. M. G., Fowler, P. H., and Cuer, P., 1947, *Proc. Phys. Soc.*, **59,** 883.

Lewis, W. B., 1942, *Electrical Counting* (Cambridge : University Press).

Littauer, R. M., 1950, *Rev. Sci. Instrum.*, **21,** 750.

Rosenfeld, L., 1948, *Nuclear Forces* (Amsterdam : North Holland Publishing Co.).

Rutherford, E., Ward, F. A. B., and Wynn-Williams, C. E., 1930, *Proc. Roy. Soc.* A, **129,** 211.

Staub, H., and Stephens, W. E., 1939, *Phys. Rev.*, **55,** 131.

Staub, H., and Tatel, H., 1940, *Phys. Rev.*, **58,** 820.

Stetter, G., and Jentschke, W., 1935, *Phys. Z.*, **36,** 441.

Williams, J. H., Shepherd, W. G., and Haxby, R. O., 1937, *Phys. Rev.*, **51,** 888; *Ibid.*, **52,** 390.

On the Experimental Determination of the Lifetimes of Atomic Energy States*

By G. STEPHENSON

Imperial College, London

Communicated by R. W. B. Pearse; MS. received 22nd November 1950

ABSTRACT. The lifetimes of certain atomic resonance states have been measured using a magnetic rotation method devised by Weingeroff in 1931. This method possesses the advantage of not requiring an accurate knowledge of the vapour pressure data. The experimental results are compared with theoretical values obtained using the recent Bates–Damgaard Coulomb approximation, and with results based on Hartree and Slater type wave functions. Good agreement is found with the Bates–Damgaard results.

§1. INTRODUCTION

Previous experimental methods for the measurements of the lifetimes of atomic states have been subject to error mainly due to the inaccuracy of vapour pressure data (for references and a general survey of past work see Landolt–Börnstein 1950, Mitchell and Zemansky 1934). A magnetic rotation method devised by Weingeroff (1931) which does not require a knowledge of the vapour pressure data has apparently been overlooked, and forms the basis of the work described here. The lifetimes of the resonance states corresponding to the following transitions have been measured:

$$\text{Na } \lambda\lambda 5890,\ 5896\ \text{A.}\ (3\,^2S_{1/2}-3\,^2P),\quad \text{K } \lambda\lambda 7665,\ 7699\ (4\,^2S_{1/2}-4\,^2P),$$

$$\text{Rb } \lambda\lambda 7800,\ 7946\ \text{A.}\ (5\,^2S_{1/2}-5\,^2P),\quad \text{Tl } \lambda 5350\ (6\,^2P_{3/2}-7\,^2S_{1/2}).$$

§2. THEORETICAL BASIS OF THE METHOD

It is well known that when plane polarized light is passed through an absorbing vapour in a magnetic field parallel to the incident radiation and observed with a crossed analysing nicol, a certain intensity of radiation of frequency ν (say) appears in the field of view. This intensity is known to depend on (*a*) the angle χ_ν through which the plane of polarization is rotated by the magnetic field and (*b*) the absorption coefficient K_ν for the vapour at frequency ν. Weingeroff (1931) observed that when the magnetic field was at some constant value and the analysing nicol rotated in the direction of magnetic rotation, the observed absorption line was first bright on a dark background and then dark on a bright background. A similar effect was noticed when the analyser was rotated in the opposite direction. If ϕ denotes the position of the analyser with reference to the crossed position ($\phi=0$), then the difference between the intensity of light I due to the magnetic rotation and the continuous background and the intensity due to the background alone is given by the usual expression

---

* This paper forms part of the Thesis submitted to the University of London for the degree of Ph.D.

$$I=I_0\int_{-\infty}^{\infty}\{\sin^2(\chi_\nu+\phi)\exp(-K_\nu l)-\sin^2\phi\}d\mu, \qquad \ldots\ldots(2.1)$$

where l is the length of the absorbing column, $\mu=2\pi(\nu-\nu_0)$, ν_0 is the frequency of the absorption line and I_0 is the intensity of the continuous background.

The expression for the rotation of the plane of polarization χ_ν has been derived by Voight (1920) and Kuhn (1926). The theory given by Kuhn leads to the result

$$\chi_\nu=\pm\frac{\mathbf{e}z\rho Hl}{8\mathbf{m}\mathbf{c}^2\mu^2} \qquad \ldots\ldots(2.2)$$

where H is the magnetic field strength in oersted, $\rho=4\pi Nf\mathbf{e}^2/\mathbf{m}$, f is the oscillator strength for the transition, N the number of atoms of absorbing vapour per cm^3 $\mathbf{m}$ the electronic mass and $\mathbf{e}$ the electronic charge.

The z factor is considered in § 3.

The expression for the absorption coefficient K_ν for combined Doppler and natural broadening has been given by Mitchell and Zemansky (1934) and Plaskett (1947). The expression obtained is

$$K_\nu=\frac{\sqrt{\pi}\,\mathbf{e}^2Nf}{\mathbf{m}\mathbf{c}\gamma}\left[\exp(-\omega^2)+\frac{\delta}{\gamma\sqrt{\pi}\omega^2}\right], \qquad \ldots\ldots(2.3)$$

where $\omega=(\nu-\nu_0)/\gamma$, $\gamma=(2\mathbf{k}T/M)^{1/2}\nu_0/\mathbf{c}$ and $\delta=A_{nm}/4\pi$, M is the molecular or atomic weight, T the absolute temperature, $\mathbf{k}$ Boltzmann's constant and A_{nm} the Einstein probability coefficient between states n and m. When the pressure of the absorbing vapour and the length of the absorbing column are great enough to absorb completely the central region of the line (but not great enough to produce Holtsmark broadening) the above expression becomes

$$K_\nu=\rho A_{nm}/4\mathbf{c}\mu^2. \qquad \ldots\ldots(2.4)$$

Substituting the expressions for K_ν and χ_ν given by equations (2.4) and (2.2) in equation (2.1), and making the substitutions $x^2=\mathbf{e}zH\rho l/8\mathbf{m}\mathbf{c}^2\mu^2$, $b=2\mathbf{m}\mathbf{c}A_{nm}/\mathbf{e}zH$ it is found that

$$I=I_0\left(\frac{\mathbf{e}zH\rho l}{8\mathbf{m}\mathbf{c}^2}\right)^{1/2}\int_{-\infty}^{\infty}\left\{\frac{1}{x^2}\sin^2(x^2+\phi)\exp(-bx^2)-\frac{1}{x^2}\sin^2\phi\right\}dx. \qquad \ldots\ldots(2.5)$$

The evaluation of this integral leads to the expression

$$I=\frac{I_0}{4}\left(\frac{\pi l\rho A_{nm}}{2\mathbf{c}}\right)^{1/2}\{(\alpha+1)^{1/2}\cos 2\phi+(\alpha-1)^{1/2}\sin 2\phi-\sqrt{2}\}, \qquad \ldots\ldots(2.6)$$

where $\alpha^2=1+4/b^2$. The position of the analysing nicol (ϕ_0, say) at which the absorption line merges with the continuous background is given by setting $I=0$.

The equation for ϕ_0 then becomes

$$(\alpha+1)^{1/2}\cos 2\phi_0+(\alpha-1)^{1/2}\sin 2\phi_0=\sqrt{2}. \qquad \ldots\ldots(2.7)$$

The value of α, and hence A_{nm}, may readily be obtained from this equation once the value of ϕ_0 has been measured. The graph of ϕ_0 against b is found to consist of two separate parts leading to two different values of ϕ_0 for each value of b corresponding to the two possible directions of rotation. As b tends to zero ϕ_0 tends to $-22\frac{1}{2}°$ and $+67\frac{1}{2}°$; the maximum sensitivity is obtained by working with negative values of ϕ_0.

§ 3. DISCUSSION OF THE z FACTOR

A simple calculation on the basis of the theory given in the last section shows that for a value of $10^8\,\text{sec}^{-1}$ for the transition probability A_{nm} the corresponding magnetic field is of the order of 20–30 oersted. The necessity of working in weak magnetic fields of this order leads to difficulties in the calculation of the z factor which will now be discussed.

It is shown, on the basis of Kuhn's theory, that the z factor for a line possessing no hyperfine structure is given by

$$z=\sum_s \alpha_s\beta_s, \qquad \ldots\ldots(3.1)$$

where α_s is the splitting factor of the sth right- or left-handed circularly polarized component and β_s its relative intensity (where $\sum_s \beta_s=1$). If, however, the line possesses hyperfine structure then Weingeroff showed that, in order to calculate z, it is necessary to sum over all the Zeeman components of the hyperfine components. Mathematically, the new expression for z is

$$z=\sum_i K_i \sum_{s_i} \alpha_{s_i}\beta_{s_i}, \qquad \ldots\ldots(3.2)$$

where i is the number of circularly polarized components in the hyperfine structures and α_{s_i}, β_{s_i} are the splitting factors and relative intensities of the s_ith left- or right-handed Zeeman components of each hyperfine component. The factor K_i is defined as

$$f_i=K_i f, \qquad \ldots\ldots(3.3)$$

where f_i is the oscillator strength of the ith hyperfine component and f the total oscillator strength for the whole transition. The condition $\sum_i K_i=1$ is imposed on K_i, and, as in the simple Kuhn theory, it is also required that $\sum_{s_i}\beta_{s_i}=1$. In the transition from weak to strong fields (where 'strong' implies complete Back–Goudsmit effect of the hyperfine structure) the z factor will vary, due to the change in the Zeeman pattern of the hyperfine structure components. In weak fields of the order of one or two oersted the normal Zeeman splitting of the hyperfine structure takes place, whilst for fields of the order of a few hundred oersted the Back–Goudsmit effect sets in. The calculation of the z factors appropriate to these two cases is a reasonably simple problem, but for intermediate field strengths the calculations are extremely long and involve a great deal of numerical computation. A table giving the z values for some of the more common transitions has been given by Mitchell and Zemansky (1934) for the case of complete Back–Goudsmit effect of the hyperfine structure.

Table 1 gives the z values calculated by the author* for the normal Zeeman splitting of the hyperfine structure ($H \sim 0$) and complete Back–Goudsmit effect of the hyperfine structure ($H \sim 1{,}000$). The nuclear spin is represented by I. An experimental result obtained by Weingeroff showed that the value of z at 30 oersted for the $(3\,{}^2S_{1/2} - 3\,{}^2P_{1/2})$ transition in the sodium atom was 1·27; this is only slightly different from the asymptotic value of 1·33 (see Table 1) corresponding to complete Back–Goudsmit effect of the hyperfine structure and would seem to indicate that even at these low field strengths the Back–Goudsmit effect must have almost completely set in. It is reasonable to assume that the Back–Goudsmit effect occurs to the same degree at approximately the same field strength for all transitions since, unlike the multiplet separations, the hyperfine structure separations are all of the same order of magnitude. On this basis the variation of z from its asymptotic value for all other transitions considered in Table 1 should be less than the variation observed for sodium since the limits of z are closer together. In view of the results it appears justified to use the simple z values appropriate to complete Back–Goudsmit effect of the hyperfine structure for all the transitions considered here without introducing any large error; the lifetimes obtained in this work are calculated on this basis.

Table 1

Transition	I	z ($H \sim 1{,}000$)	z ($H \sim 0$)
${}^2S_{1/2} - {}^2P_{1/2}$	1/2	1·333	0·533
${}^2S_{1/2} - {}^2P_{1/2}$	3/2	1·333	0·528
${}^2S_{1/2} - {}^2P_{3/2}$	3/2	1·166	0·833
${}^2S_{1/2} - {}^2P_{1/2}$	5/2	1·333	0·892

§ 4. EXPERIMENTAL METHODS AND RESULTS

It will be recalled that the theory given in § 2 of this paper required that the central region of the absorption line be completely absorbed. This naturally places a restriction on the minimum length of the absorption tube and the maximum pressure of the absorbing vapour (which at the same time must not be high enough to produce Holtsmark broadening). It has been shown by Mitchell and Zemansky (1934) that if only Doppler and natural broadening are present then the absorption coefficient K_0 at the centre of the line is given by

$$K_0 = \frac{\pi N \boldsymbol{e}^2 f \lambda_0}{\boldsymbol{mc}} \left(\frac{M}{2\pi \boldsymbol{R} T} \right)^{1/2}, \qquad \ldots\ldots(4.1)$$

where λ_0 is the wavelength, $\boldsymbol{R}$ the gas constant and T the absolute temperature. For complete absorption of the central region of the line $K_0 l$ must be large, and it can be shown that when the absorption coefficient takes the form given by equation (2.4) then $K_0 l$ takes values in the range 2000–3000.

Substituting in (4.1) for the constants, it follows that

$$l > 0{\cdot}022\, T \left(\frac{T}{M} \right)^{1/2} \frac{1}{p f \lambda_0}, \qquad \ldots\ldots(4.2)$$

where p is the vapour pressure in mm. Hg and λ_0 the wavelength in Ångströms. In order to be certain that no Holtsmark broadening occurred the maximum vapour pressure was taken as 5×10^{-3} mm. Table 2 gives the values of the minimum lengths of absorbing vapours required to give complete absorption at the centre of the line.

---

* G. Stephenson, Ph.D. Thesis, University of London, 1950.

The vapour pressure data used here are taken from Dushman (1949).

Table 2

Atom	M	λ (Å.)	Assumed f	Assumed p (mm.)	T (°c.)	l (cm.)
Na	23	5896	0·3	5×10^{-3}	265	5·9
K	39	7699	0·3	5×10^{-3}	184	2·7
Rb	85	7947	0·3	5×10^{-3}	156	1·6
Tl	204	5350	0·1	5×10^{-3}	566	4·1

As a further precaution the lengths of the tubes were made considerably longer than the above minimum values. The final experiments were carried out using absorption tubes approximately 16 cm. long. The tubes were made from Pyrex and quartz and the metals distilled in, the tubes being sealed off at a pressure of 10^{-4} mg. Hg.

Critical values of ϕ_0 for which the absorption line merged with the continuous background were obtained visually with a constant deviation spectrometer. For lines occurring in the near red or infra-red it was found convenient to use an infra-red image converter.

After care had been taken to ensure that the magnetic field strength and the temperature were uniform over the whole length of the absorbing column, the following results were obtained. The oscillator strengths or f-values for the transitions are also tabulated.

Table 3

$H = 29{\cdot}6 \pm 0{\cdot}35$ oersted

Atom	T (°c.)	Transition	λ (Å.)	z	Mean ϕ_0	b	$\tau\times10^{-8}$ (sec.)	f-value
Na	260	$^2S_{1/2}-{}^2P_{1/2}$	5896	4/3	15° 05′	0·179	$1{\cdot}61\pm0{\cdot}06$	0·325
Na	260	$^2S_{1/2}-{}^2P_{3/2}$	5890	7/6	14° 39′	0·205	$1{\cdot}61\pm0{\cdot}06$	0·650
K	186	$^2S_{1/2}-{}^2P_{1/2}$	7699	4/3	16° 37′	0·106	$2{\cdot}71\pm0{\cdot}09$	0·330
K	186	$^2S_{1/2}-{}^2P_{3/2}$	7665	7/6	16° 14′	0·122	$2{\cdot}71\pm0{\cdot}09$	0·657
Rb	155	$^2S_{1/2}-{}^2P_{1/2}$	7947	4/3	17° 19′	0·101	$2{\cdot}85\pm0{\cdot}09$	0·335
Rb	155	$^2S_{1/2}-{}^2P_{3/2}$	7800	7/6	17° 02′	0·119	$2{\cdot}78\pm0{\cdot}09$	0·661
Tl	560	$^2P_{3/2}-{}^2S_{1/2}$	5350	7/6	14° 42′	0·202	$1{\cdot}43\pm0{\cdot}05$	0·151

§ 5. THEORETICAL DISCUSSION

Throughout this section it will be convenient to work in atomic units. We define (*a*) the unit of energy as equal to the ionization potential of the hydrogen atom $E = 2\pi^2 \boldsymbol{m}\boldsymbol{e}^4/\boldsymbol{h}^2$, and (*b*) the unit of length as equal to the radius of the first Bohr orbit $a_0 = \boldsymbol{h}^2/4\pi^2\boldsymbol{m}\boldsymbol{e}^2$. The Einstein transition probability coefficient A_{nm} is related to the line strength S_{nm} (in atomic units) by the usual relation (Condon and Shortley 1935)

$$A_{nm} = \frac{64\pi^4 \boldsymbol{e}^2 a_0{}^2 S_{nm}}{3\boldsymbol{h}\lambda_0{}^3 g_n}, \qquad \ldots\ldots(5.1)$$

where g_n is the statistical weight of the upper state n and λ_0 is the wavelength of the radiation in centimetres. It can further be shown that $S_{nm} = P(m)Q(l)\sigma^2$, where $P(m)$ and $Q(l)$ are functions of the quantum numbers involved in the transition and σ^2 is defined by

$$\sigma^2 = \frac{1}{(4l^2-1)}\left|\int rP_n(r)P_m(r)\,dr\right|^2, \qquad \ldots\ldots(5.2)$$

Here l is the greater of the two azimuthal quantum numbers involved in the transition and $P_n(r)$, $P_m(r)$ are the normalized radial wave functions satisfying the reduced Schrödinger equation $P'' + [2V(r) - E - l(l+1)/r^2]P = 0$. It follows directly that the transition probability is given by the expression

$$A_{nm} = \frac{4\boldsymbol{h}^3\nu^3}{3\boldsymbol{m}^2\boldsymbol{e}^2\boldsymbol{c}^3} \frac{P(m)Q(l)\sigma^2}{g_n}. \qquad \ldots\ldots(5.3)$$

The quantities $P(m)$, $Q(l)$ may be readily obtained for any transition from the tables given by Goldberg (1935, 1936), White and Eliasen (1932) and Russell (1936). The corresponding f-values may be obtained from the usual relation

$$f_{nm} = \frac{\boldsymbol{mc}^3}{8\pi^2\boldsymbol{e}^2\nu^2}\left(\frac{g_n}{g_m}\right)A_{nm} \qquad \ldots\ldots(5.4)$$

and the lifetimes from the relation

$$\frac{1}{\tau_n} = \sum_m A_{nm}, \qquad \ldots\ldots(5.5)$$

where the summation extends over all states lower than the nth.

The numerous methods of calculating the appropriate wave functions for the states concerned will not be described here as these appear in most treatises on quantum theory; surveys of the previous work on the calculation of σ^2 using various types of wave functions have been given by Hartree (1948) and Bates and Damgaard (1949).

Calculations of the theoretical values of the lifetimes of the resonance states considered experimentally in this paper have been carried out using both Slater type wave functions and the recent Bates–Damgaard Coulomb field approximation. A further calculation for the rubidium resonance state has been made using Hartree non-exchange self-consistent wave functions. Table 4 gives the values of σ^2 obtained with different wave functions. For comparison the values obtained by other authors using Hartree exchange wave functions are also tabulated (see Bates and Damgaard 1949).

Table 4

		σ^2 (in atomic units)			
Atom	Transition	Exchange	Non-exchange	Bates	Slater
Na	$3\,^2S-3\,^2P$	6·3	—	6·10	7·60
K	$4\,^2S-4\,^2P$	9·0	10·4	8·30	16·6
Rb	$5\,^2S-5\,^2P$	—	13·65	8·82	22·3
Tl	$6\,^2P-7\,^2S$	—	—	0·90	5·2

Table 5 gives the lifetimes of the resonance states obtained using the Bates–Damgaard method, together with the experimental values given in §4 of this paper.

Table 5

Atom	Transition	$\tau \times 10^{-8}$ sec. (theor.)	$\tau \times 10^{-8}$ sec. (exp.)
Na	$3\,^2S_{1/2}-3\,^2P_{1/2}$	1·66	1·61 ± 0·06
	$3\,^2S_{1/2}-3\,^2P_{3/2}$	1·66	1·61 ± 0·06
K	$4\,^2S_{1/2}-4\,^2P_{1/2}$	2·70	2·71 ± 0·09
	$4\,^2S_{1/2}-4\,^2P_{3/2}$	2·70	2·71 ± 0·09
Rb	$5\,^2S_{1/2}-5\,^2P_{1/2}$	2·71	2·85 ± 0·09
	$5\,^2S_{1/2}-5\,^2P_{3/2}$	2·71	2·78 ± 0·09
Tl	$6\,^2P_{3/2}-7\,^2S_{1/2}$	1·74	1·43 ± 0·05

These values are in excellent agreement with experiment, especially for the lighter atoms. The discrepancy for the heavy thallium atom is due to the existence of large exchange forces. It has also been shown by Bates and Damgaard that for p–s transitions (such as the thallium resonance lines) the p–ground state wave function lies too close to the nucleus to allow the field to be taken as Coulombian.

The Bates–Damgaard method, although giving good agreement with experimental results for simple systems, cannot, in general, be expected to give accurate results for heavy complicated atoms. Further experimental results are required before the possible accuracy can be estimated.

It is noticeable that the Hartree exchange wave functions do not appear to be so accurate as the Coulomb approximation for the cases of Na and K. Further, as would be expected, the Slater wave functions lead to useless results, except possibly for atoms lighter than Na.

ACKNOWLEDGMENTS

The author wishes to express his gratitude to Dr. R. W. B. Pearse for his constant interest and advice during the course of the work and to Professor D. R. Hartree for supplying the non-exchange wave functions for the rubidium resonance states. The work was made possible by the award of a Maintenance Grant from the Department of Scientific and Industrial Research.

REFERENCES

Bates, D. R., and Damgaard, A., 1949, *Phil. Trans. Roy. Soc.* A, **242,** 101.

Condon, E. U., and Shortley, G. H., 1935, *Theory of Atomic Spectra* (Cambridge: University Press), p. 98.

Dushman, S., 1949, *Vacuum Technique* (New York: John Wiley), p. 740.

Goldberg, L., 1935, *Astrophys. J.*, **82,** 1; 1936, *Ibid.*, **84,** 11.

Hartree, D. R., 1948, *Rep. Prog. Phys.*, **12** (London: Physical Society), p. 113.

Kuhn, W., 1926, *K. Danske Vidensk. Selks. Mat.-fys. Medd.*, **7,** No. 12.

Landolt–Börnstein, 1950, *Physical Tables*, Vol. 1 (Berlin: Springer-Verlag), p. 260.

Mitchell, A. C. G., and Zemansky, M. W., 1934, *Resonance Radiation and Excited Atoms* (Cambridge: University Press).

Plaskett, H., 1947, *Mon. Not. R. Astr. Soc.*, **107,** 117.

Russell, H. N., 1936, *Astrophys. J.*, **83,** 29.

Voight, W., 1920, *Handb. Elect. Magn. Graetz.*, **4,** 577.

Weingeroff, M., 1931, *Z. Phys.*, **67,** 679.

White, H. E., and Eliasen, A. Y., 1933, *Phys. Rev.*, **44,** 753.

Precise Determination of Lattice Constants by Electron Diffraction and Variations in the Lattice Constants of Very Small Crystallites

By F. W. C. BOSWELL*
Department of Physics, University of Toronto

Communicated by N. F. Mott; *MS. received 8th August* 1950

ABSTRACT. Previous workers have reported that lattice constants determined by electron diffraction differ from the accepted X-ray values. It has been suggested that these differences may be due to a change in lattice constant with crystal size. To examine this question further, the lattice constants of several alkali halides have been determined, by electron diffraction, to a higher accuracy than had previously been attained. The X-ray value of the lattice constant of TlCl was used as a standard reference. The lattice constants of six alkali halides, with crystal sizes greater than 150 A., were found to agree with the X-ray values to within the experimental error of 0·05%. It has been shown that for crystal sizes less than 100 A. the lattice constants of the alkali halides were found to be less than the X-ray values by an amount dependent on crystal size. For a crystal size of about 30 A. the decrease was approximately 0·5%.

Similar determinations on evaporated gold films showed that, for a crystal size of about 20 A., the decrease in the lattice constant was almost 2%. For a crystal size of 40 A., the largest obtained, the lattice constant was 0·2% less than the X-ray value. Evaporated films of silver and bismuth also were found to have lattice constants less than the X-ray values.

It can therefore be concluded that previous reports of an increase of the lattice constants of alkali halides with decreasing crystal sizes are in error. Some of the discrepancies noted by previous workers may have resulted from assigning the X-ray value to the lattice spacing of gold films or gold foil used as a standard reference.

§ 1. INTRODUCTION

During the past twenty years a number of workers have reported discrepancies between values of lattice constants determined by electron diffraction and those determined by X-ray diffraction. Finch and Fordham (1936) determined the lattice constants of twelve alkali halides in terms of gold foil and colloidal graphite standards; they reported values for the lattice constants which were generally higher than the X-ray values, in some cases by as much as 0·6%. However, Boochs (1939) determined the lattice constants of four alkali halides in terms of evaporated gold films and found that the values obtained were in agreement with the X-ray results to within ±0·15%.

Gnan (1934) determined the spacing of NaCl in terms of Bi using films deposited *in vacuo* and found a value for the lattice constant of NaCl which was 0·2% higher than the X-ray value. Pickup (1936) made a similar determination and obtained a result for NaCl which was 0·7% high.

Similar discrepancies have been noted in the case of zinc oxide. Both Finch and Wilman (1934) and Cosslett (1935) have obtained anomalous values for the lattice constants of ZnO determined by electron diffraction in terms of gold. In a more recent report by Chia-Si Lu and Malmberg (1943) it was stated that the lattice constants of ZnO smoke determined by electron diffraction were in agreement with Bunn's X-ray values. However, the lattice constant of the thinned gold foil standard used by these workers was determined by X-ray diffraction and found to be 0·4% less than the accepted spacing.

---

* Now at the Department of Mines and Technical Surveys, Ottawa, Canada.

It does not appear that these discrepancies are due to impurities in the samples, heating of the specimen due to the electron beam or charging up of the photographic plate.

The only other likely explanation, which has been suggested by several workers, is a change in the lattice constant with crystal size for very small crystals. Finch and Fordham (1936) suggested that their results on the alkali halides were evidence that small crystals of these substances had larger lattice constants than the bulk materials. Pickup (1936) suggested that other discrepancies may be due to a similar effect.

The present work was undertaken in order to elucidate some of the discordant results previously noted and to find if there is a detectable change in the lattice constant of very small crystallites. To carry out this work it was first necessary to determine, by electron diffraction, the lattice constants of a number of specimens with relatively large crystal sizes. These results would be compared with the X-ray results. The lattice constants of several of the substances would then be determined for a range of crystal sizes, in order to find whether the lattice constant changed as the crystal size decreased.

§2. EXPERIMENTAL METHODS

Experimentally, the problem of precise comparison of lattice constants by electron diffraction may be divided into three phases: first, the design and operation of a high resolution electron diffraction camera; second, an accurate method for comparing the lattice constants of different specimens; third, the measurement of the patterns obtained.

The High Resolution Electron Diffraction Camera

The resolution in a transmission electron diffraction pattern depends on the specimen, the cross section of the central electron beam at the photographic plate and the stability of the accelerating potential. An electron microscope, built at Toronto in 1944, was adapted for use as a precision electron diffraction camera. The electron microscope is of the conventional electromagnetic type and has been described by Burton and Kohl (1945). Two of the lenses were used to form a demagnified image of the electron source on the photographic plate. The diameter of the final spot at the photographic plate is estimated to be 10 microns. A ray diagram of this set-up is shown in Figure 1. An aperture, which could be centred while the instrument was in operation, was used to limit the cross section of the electron beam at the specimen.

The stabilized power supply of an R.C.A. type E.M.U. electron microscope was used to supply the accelerating potential of about 50 kilovolts. The fluctuations in the high voltage were measured and the greatest variation observed was 1 part in 2,500 over a period of one minute. Generally the voltage was stable to 1 part in 2,500 over a period of several minutes.

Preparation of Specimens

Formvar films about 100 A. thick were prepared in the usual manner and mounted on stainless steel 200-mesh grids $\frac{1}{8}$ inch in diameter. These films were put into a vacuum system and the specimen material was evaporated on to them from a 15 mil tungsten filament at the pressure of 10^{-5} mm. Hg. The filament had been cleaned previously by heating to a white heat *in vacuo*. The temperature of the filament was such that the evaporation took place in two or three minutes. Films of various thicknesses were prepared in each case and those giving the most intense patterns free from background and orientation effects were selected by examination in the diffraction camera. During the transfer of the specimens from the evaporating unit to the diffraction camera, care was taken not to breathe on the films or expose them to water vapour.

The above method worked well for producing alkali halide films with crystal sizes over 100 A. However, due to the fact that the mean crystal size in thin evaporated films of alkali halides increases immediately upon exposure to air, it was necessary to produce the films inside the diffraction camera in order to study the diffraction patterns of very small crystals. An arrangement was made whereby a specimen could be evaporated from a 15 mil tungsten filament situated inside the diffraction camera. The evaporation could be carried out while the diffraction camera was in operation. Thus the first detectable diffraction pattern could be photographed and the evaporation could be stopped at any stage and the patterns recorded as the film thickness and crystal size increased. A typical set of diffraction patterns, obtained during the growth of an NaBr film, is shown in Figure 2 (Plate I)*. The first faint rings indicated a crystal size of about 30 A. As the film grew thicker the diffraction rings grew more intense and sharper. When the film was estimated to be at least 300 A. thick the ring breadth indicated a crystal size of only 60 A. There was a slight indication of orientation in some of the films before exposure to the air. After the alkali halide films had been kept in the air for a short time the crystal size increased to about 150 A. Orientation effects were always quite marked after exposure to the air. An exceptional case was that of LiF which is practically insoluble in water. Films of LiF, kept in air for a period of several months, showed a ring breadth corresponding to a crystal size of only 90 A.

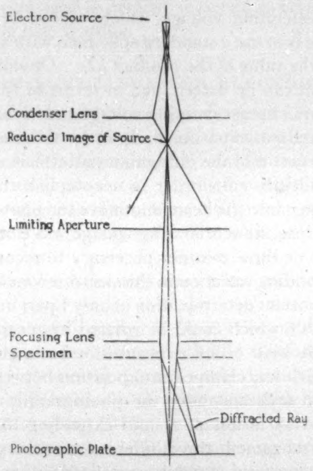

Figure 1. Ray diagram showing the electron–optical system used.

---

* For Plates see end of issue.

Method of Comparing Lattice Constants of Different Specimens

For cubic crystals we may write Bragg's law in the form

$$\frac{\bar{R}}{1+\frac{3}{8}(\bar{R}/L)^2-\frac{13}{128}(\bar{R}/L)^4+\dots}=\frac{\lambda L(h^2+k^2+l^2)^{1/2}}{a}, \qquad \dots\dots(1)$$

where λ is the electron wavelength, L is the camera length, a is the lattice constant of the specimen, h, k, l are the Miller indices corresponding to the diffracted beam, and $\bar{R}$ is the measured radius of the diffraction ring. If we call the expression on the left of equation (1) the 'corrected radius' R we may write

$$R=\frac{\lambda L(h^2+k^2+l^2)^{1/2}}{a}. \qquad \dots\dots(2)$$

The lattice constant a cannot be found absolutely from equation (2) since λ depends on the accelerating voltage which cannot be accurately measured. Thus the usual practice is to use a standard specimen with a known lattice constant in order to determine the value of the product λL. Obviously, the accuracy with which a lattice constant can be determined in terms of that of the standard will depend on the variation in the accelerating voltage and in the camera length during the time required for the two exposures. In order to obtain the highest possible accuracy in the measurement of the diffraction patterns it was necessary to record both patterns independently. In order to accomplish this it was necessary to introduce a new specimen into the beam and move the photographic plate between the two exposures. Since the accelerating voltage was constant to 1 part in 2,500 over the period of two or three minutes necessary to record the two comparison exposures, the corresponding variation in the electron wavelength would introduce an error in the lattice constant determination of only 1 part in 5,000. The specimens were mounted on a table which could be rotated by means of a shaft extending through a Wilson type seal. The exposures were recorded on a 2 × 10-inch photographic plate which was clamped into position between two flat brass plates for each exposure. In order to move the photographic plate, the lower brass plate could be released by means of a shaft extending through a flexible metal bellows. With this arrangement three different specimens could be moved into the beam and eight exposures could be recorded on one photographic plate. The total possible change in the camera length between successive exposures was less than 1 part in 3,000. Thus with a specimen giving a sharp ring pattern the lattice constant could be determined, in terms of the standard, to better than 0·05%.

Determination of the Lattice Constant and the Mean Crystal Size

The ring diameters were measured by means of a Hilger optical comparator with a 2-inch objective and a 7 × eyepiece. By means of a vernier attachment the settings could be read to the nearest micron. No correction was made for the comparator screw, since the lattice constant was determined from the average of eight or ten ring diameters and the slight errors in the screw would average out. From the measured ring radii the corrected radii R were determined. For each R the corresponding (h, k, l) were assigned and the constant $\lambda L/a$ was calculated. Thus an average value of $\lambda L/a$ was obtained for each pattern.

The widths of the rings at half-intensity were measured from the traces of the patterns obtained with a Leeds–Northrup microphotometer connected with a

Speedomax recorder. Now the angular half-width of a diffraction ring is related to the mean crystal size in the specimen by the relation $\beta = 0{\cdot}9\lambda/T$ radians, where β is the angular half-width of a diffraction ring due to the crystal size, T is the length of the crystal perpendicular to the electron beam, and λ is the electron wavelength. Since the length of the camera is 28·5 cm. the linear half-breadth B of a ring at the plate, due to the finite size of the crystal only, is

$$B = 25{\cdot}6\lambda/T \text{ cm.} \qquad \ldots\ldots(3)$$

Taking into account the finite size of the beam at the photographic plate it is

$$B' = B + b, \qquad \ldots\ldots(4)$$

where B' is the observed linear half-width and b is an instrumental factor. For our camera we have estimated the instrumental factor b to be 35 microns. The equations (3) and (4) were used to determine the mean crystal size of the specimen from the measured ring half-widths.

§ 3. A STANDARD SUBSTANCE FOR ELECTRON DIFFRACTION

The conditions which should be met by an acceptable standard substance are as follows: (i) the recorded pattern should consist of several very sharp rings which can be measured with high accuracy, in order that a good average value of the constant involved can be obtained; (ii) the material should be easily prepared in a form suitable for electron diffraction; (iii) when prepared, the diffraction specimen should remain chemically stable and without physical change, such as increase in crystal size, over a period of several days; (iv) the crystal structure and lattice constant must be accurately known and independent of the method of preparation.

These conditions are not all easily met by any one substance. Several workers have used gold as a standard substance, either in the form of an evaporated film or thinly beaten foil. However, there is some doubt as to whether the lattice constant of a very thin gold film is in agreement with the accepted X-ray value (see Chia-Si Lu and Malmberg 1943). In addition, the diffraction rings obtained from a gold film always show considerable broadening due to lattice imperfections. Some workers have obtained sharper patterns by evaporating the metal on to a heated substrate, but this method is inconvenient and the rings obtained are still not of maximum sharpness. Other metals that might be used as a standard behave in a similar way to gold and are hence unsuitable.

Sodium chloride is another material often suggested a standard for electron diffraction. It is quite easy to obtain an excellent diffraction pattern from an evaporated film of NaCl. The disadvantage of this substance is that the film can only be kept in the air for a few hours, before the crystals grow to such a size that they will no longer transmit electrons. The other alkali halides, with the exception of LiF, likewise grow on exposure to air. Lithium fluoride has a tendency to form very small crystallites which cause considerable line broadening.

Zinc oxide, which gives very sharp diffraction rings, has been used as a standard. However, both Finch and Wilman (1934), and Cosslett (1935) found that the lattice constant of ZnO specimens, skimmed from the surface of molten zinc, depended on the age of the specimen. More recently it has been reported by Chia-Si Lu and Malmberg (1943) that the lattice constant of ZnO smoke is in agreement with the X-ray value and independent of the age of the specimen.

In view of these conflicting reports, ZnO cannot yet be regarded to be entirely suitable as a diffraction standard.

Shishacow (1937) suggested the use of 'two-dimensional' crystals of Si_2O_5 as a reference material for electron diffraction. If the crystals are truly two-dimensional, one would suspect that the diffraction pattern would have somewhat diffuse rings. Shishacow gives the lattice constant of the crystals to only 0·3%, which is not accurate enough for precision work.

The length of the basal axis in graphite which determines the (*hk*0) diffractions has been used as a standard reference (Finch and Fordham 1936, Wilman 1940). Since this length depends only on the carbon–carbon spacing in the (001) planes it is assumed to be independent of crystal thickness or the presence of slight impurity. The disadvantage of this standard is that usually only one or at most two rings are measured, the remaining (*hk*0) rings being relatively too weak to allow accurate measurement.

A Thallium Chloride Standard

A vacuum evaporated film of TlCl about 300 A. thick was found to provide a standard specimen satisfying all of the requirements noted above. A typical electron diffraction pattern of such a film is shown in Figure 3 (Plate II). The ring widths of this pattern can be accounted for by a crystal size of 300–400 A plus the finite width of the beam at the photographic plate. No change has been detected in such a specimen left exposed to the air for a number of months. In the work reported here the same TlCl film was used as a standard throughout.

The value used for the lattice constant of the TlCl standard specimen is the precision X-ray value given by Jevins and Karlsons (1939). Taking the wavelength of the Cu $K\alpha_1$ radiation to be 1·5374 A. (in terms of which the lattice constant of rocksalt is 5·628 A.* at 20° C.) they report the lattice constant of TlCl to be 3·834 A. at 20° C. This is the standard value that has been used throughout this work.

MgO as a Secondary Standard

It is convenient to have a secondary standard more quickly prepared for electron diffraction than thallium chloride. Magnesium oxide smoke was found to be a satisfactory secondary standard, although it has the disadvantage that only two of the recorded lines are sharp. The MgO specimens were prepared by holding a formvar-covered $\frac{1}{8}$-inch supporting grid about 10 inches above a short strip of burning magnesium ribbon. Enough MgO should be deposited so that the film is clearly visible.

The lattice constant of the MgO smoke was determined in terms of the TlCl standard. The value obtained for the lattice constant of MgO was 4·202 A. This result is in agreement with the best X-ray determinations on MgO powder.

§ 4. EXPERIMENTAL RESULTS

Alkali Halides (*crystal size greater than* 100 A.)

The lattice constants of six alkali halides were determined for relatively large crystal size. In each case the films were formed by vacuum evaporation and subsequent exposure to the air for a period of several minutes. The chemicals used were the best commercially available grades except for sodium bromide.

---

* Results presented in this paper are expressed in terms of $a_{NaCl}=5{\cdot}628$ A. in order to allow direct comparison with the determinations of previous workers, most of whom used this standard value. It is, however, now recognized that this value for the lattice spacing of NaCl is slightly low.

In this case it appeared that the lattice constant was altered by the small amount of chloride present in the best commercial samples and a specially prepared sample, estimated to contain less than 0·02% chloride, was used.

The results are summarized in Table 1. From two to four determinations of the ratio of the specimen lattice constant to that of the standard were made in each case. The indicated possible errors are the maximum observed deviations. The corresponding x-ray values of the lattice constants are listed. The values for NaBr, LiF and NaF are those given by Jevins, Straumanis and Karlsons (1939) and Jevins and Karlsons (1939). The remaining x-ray values were taken from the 1931 supplement to the *Structurbericht* of the *Zeitschrift für Kristallographie*. The mean crystal sizes as estimated from the ring widths are also listed.

Table 1. Electron Diffraction and x-ray Values of the Lattice Constants of Several Alkali Halides

Substance	Crystal Size (A.)	a (by electrons)	a (by x-rays)
NaCl	150	5·627±0·002	5·628±0·001
KCl	150	6·277±0·003	6·277±0·002
NaF	150	4·625±0·002	4·622±0·001
NaBr	150	5·962±0·002	5·960±0·001
KI	300	7·051±0·002	7·052±0·003
LiF	90	4·015±0·002	4·017±0·001

Alkali Halides (*very small crystals*)

Using the method described previously the lattice constant of a specimen could be determined for a range of crystal sizes from a few Ångström units up to several hundred. This was done for four alkali halides. The precision of the lattice constant determinations decreased as the crystal size decreased and the rings became broader. The probable error in the case of very sharp rings was about 0·05% and this increased to about 0·2% for specimens giving very broad rings. The number of rings measured varied from eight in the sharp patterns to only one or two in the most diffuse patterns. In the following tables the results for each of four alkali halides are given separately. Where the pattern is due to a specimen that has stood in the air, this is indicated in the table. Otherwise the specimen was prepared in the diffraction camera, and the pattern recorded before the specimen was exposed to the air. In most cases successive determinations were made on a specimen as the crystal size was increased by evaporating more material on to the specimen. It should be noted that in each case the lattice constant decreases with crystal size for crystals less than 150 A. across.

Table 2. Variation of the Lattice Constant of NaCl with Crystal Size (x-ray value for $a_{\mathrm{NaCl}}=5{\cdot}628$ A.)

Number of rings measured	a_{NaCl}(A.)	Particle size (A.)	Remarks
2	5·614	48	Exposed to air
4	5·622	75	Exposed to air
5	5·626	80	
2	5·605	40	Same specimen
6	5·620	60	
6	5·630	150	Exposed to air
7	5·624	72	

Table 3. Variation of the Lattice Constant of KCl with Crystal Size
(X-ray value for $a_{\mathrm{KCl}} = 6{\cdot}277$ A.)

Number of rings measured	a_{KCl} (A.)	Particle size (A.)	Remarks
2	6·23(4)	(18)*	Same specimen
2	6·237	20	
2	6·242	30	
4	6·254	42	
4	6·254	42	
8	6·277	150	Exposed to air

* This pattern consisted of a very broad, faint ring superimposed on a relatively high varying background intensity. The line half-width could only be estimated approximately.

Table 4. Variation of the Lattice Constant of NaBr with Crystal Size
(X-ray value for $a_{\mathrm{NaBr}} = 5{\cdot}960$ A.)

Number of rings measured	a_{NaBr}(A.)	Particle size (A.)	Remarks
2	5·913	35	Same specimen
2	5·927	45	
2	5·932	50	
4	5·947	60	
8	5·962	150	Exposed to air

Table 5. Variation of the Lattice Constant of LiF with Crystal Size
(X-ray value for $a_{\mathrm{LiF}} = 4{\cdot}018$ A.)

Number of rings measured	a_{LiF}(A.)	Particle size (A.)	Remarks
2	3·981	32	Same specimen
2	3·999	45	
4	4·010	60	
8	4·016	90	Exposed to air

Gold and Bismuth

Gold was evaporated in the electron diffraction camera and patterns were recorded at various stages during the growth of the film. The maximum crystal size in gold films evaporated slowly (50 A. per minute) was found to be 30–35 A. In order to obtain larger crystals some gold films were evaporated on to silica substrates and subsequently annealed. The maximum temperature at which annealing could be carried out was 250° C., since higher temperatures caused excessive damage to the substrate. After annealing for three hours at 250° C. it was found that the mean crystal size in the gold film had increased to 40 A. A summary of the results for gold films is given in Table 6. It should be noted that the lattice constant is dependent on the crystal size, decreasing as the crystals became smaller.

Evaporated films of Bi showed intense bands extending outward from the inner rings. These bands were most marked in the thinner films, but could be detected in the thicker films as well. On account of these bands, the patterns due to films of very small crystallites could not be measured with sufficient accuracy to be of interest. However, two patterns with different crystal sizes were measured. Results are given in Table 7.

Table 6. Variation of the Lattice Constant of Gold with Crystal Size (x-ray value for $a_{Au} = 4{\cdot}070$ A.)

Number of rings measured	a_{Au} (A.)	Crystal size (A.)	Remarks
1	3·983	14	Same specimen
4	4·059	33	
1	3·991	16	Same specimen
1	3·993	18	
1	3·998	20	
3	4·059	33	Before annealing
4	4·062	40	After annealing

Table 7. Lattice Spacing of Bi for Two Crystal Sizes (x-ray spacing for Bi $d_{1\bar{1}0} = 2{\cdot}268$ A.)

$d_{1\bar{1}0}$ (A.)	2·215	2·254
Crystal size (A.)	35	100

§ 5. DISCUSSION OF RESULTS

In Table 1 it is seen that, for each of the six alkali halides studied, the values of the lattice constants determined by electron diffraction for relatively large crystals are in agreement with the x-ray values within the experimental error of ±0·05%. These results are in agreement with those of Boochs (1939) who determined the lattice constants of NaCl, NaBr and KCl in terms of that of a gold film deposited upon a heated rocksalt substrate. He reported that in each case the results agreed with the x-ray values to within the experimental error of ±0·15%. Finch and Fordham (1936) determined the lattice constants of twelve alkali halides using thinned gold foil and colloidal graphite as standards. They found significant increases over the x-ray values in the case of eight of the alkali halides. This led the authors to suggest an increased spacing in small crystals of the alkali halides. These observations were not confirmed by our work, and the explanation of Finch and Fordham's results is still obscure.

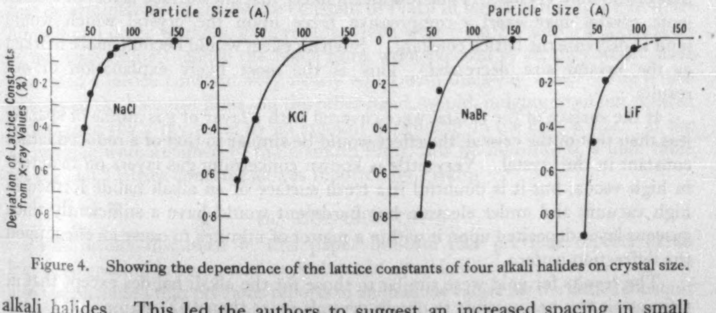

Figure 4. Showing the dependence of the lattice constants of four alkali halides on crystal size.

It is seen from Tables 2 to 5 that for alkali halide crystals less than 100 A. across the lattice constant is less than the x-ray value and decreases with decreasing crystal size. The results are shown graphically in Figure 4. For the smallest crystals obtained, which were 20–30 A. across, the decrease in the lattice constant varied from 0·4 to 0·8% depending on the substance. In each of the four cases studied the lattice constant approached the x-ray value for a crystal size of 100–150 A.

Experimentally, we have observed an outward shift of the peaks of the diffracted intensity in the electron diffraction patterns due to very small crystallites. For crystals less than 100 A. thick the resolution due to the atom rows nearly parallel to the beam will be almost negligible and we should consider whether the crystals are sufficiently thin to be treated as two-dimensional gratings. Von Laue (1926) has treated the case of a random array of cross gratings only one atom layer thick. He found that rings with sharp inner edges, but with intensity falling off more slowly in the outward direction, would be produced. If such an effect were occurring it would lead to a marked asymmetry in the intensity distribution of the rings. Since the intensity appears to fall off uniformly on either side of the peak in our patterns, we may assume that the crystals are giving rise to the normal three-dimensional diffractions. It therefore seems most probable that the shift we have observed in the positions of the peaks of the diffraction rings must have resulted from a change in the lattice spacing.

By means of the classical theory of ionic crystals as outlined by Seitz (1940) it is possible to calculate whether there is a change in the electrostatic binding energy of a lattice ion of an ionic crystal as the crystal size becomes very small. It has been shown by Hojendahl (1938) that the Madelung constant for an NaCl crystal only 30 A. across is the same as that for an infinite crystal to 1 part in 6,000. We may also assume that the repulsive energy of an ion is independent of crystal size since the repulsive forces extend over only one or two atom distances. Thus the attractive and repulsive energies of an ion in an NaCl crystal only 30 A. across are the same as those in an infinite crystal. Therefore, neglecting surface effects, we would not expect any change in the lattice constant of a very small NaCl crystal due to a variation in the binding energy with crystal size.

However, it has been shown by Lennard-Jones and Dent (1928) that an isolated (100) plane of an NaCl crystal would have a lattice constant a few per cent less than that of the bulk crystal. Thus it appears likely that the surface layers of a small ionic crystal may exert a compressive force upon the crystal which would tend to decrease the lattice constant. Such an effect would become more marked as the crystal size decreased. This is the most likely explanation of our results.

If the surface of the crystal were covered with a layer of gas atoms of spacing less than that of the crystal, the effect would be similar to that of a reduced lattice constant in the crystal. Very little is known concerning gas layers on materials in high vacua, but it is doubtful if a fresh surface of an alkali halide formed in high vacuum and under electron bombardment would have a sufficiently thick gaseous layer deposited upon it within a matter of minutes to cause an effect upon the diffraction pattern.

The results for gold were similar to those for the alkali halides except that in this case it was not possible to obtain crystals more than 40 A. across. It is seen from Table 6 that in very thin evaporated gold films, with a crystal size of less than 20 A., the value of the lattice constant is almost 2% less than the X-ray value. The largest crystal size obtained in evaporated gold films was 33 A., and for such films the value of the lattice constant was 0·25% less than the X-ray value. Annealing the film caused the crystal size to increase slightly (to 40 A.), and the lattice constant increased to 4·062 A., 0·2% less than the X-ray value of 4·070 A. It is most probable that the decrease in the spacing with crystal size is due to the compressive force exerted by the surface tension of the small gold particles.

Chia-Si Lu and Malmberg (1943) measured the spacing in a thinned gold foil specimen by electron diffraction (in terms of ZnO smoke) and by x-rays. In both cases these workers found the lattice constant to be 0·3% less than the accepted x-ray value. Our results are in agreement with this report.

It has been mentioned that Finch and Fordham (1936) obtained high values for the lattice constants of a number of alkali halides determined in terms of gold foil and colloidal graphite standards. We have not measured the spacing in colloidal graphite, but the above noted results on gold might have led one to suspect that the gold foil used as a standard by these workers actually possessed a lattice constant less than the x-ray value which they assigned to it. On the other hand, the value they obtained for the length of the basal axis of graphite in terms of their gold standard was in agreement with a later precision x-ray determination of the graphite spacings (see Finch and Wilman 1937). Wilman (1940) used colloidal graphite as a standard in the electron diffraction determination of the lattice constants of silver and NaCl (deposited from solution). The crystal sizes in his specimens were relatively large and he found satisfactory agreement with the x-ray values. He concluded that graphite was a reliable standard for electron diffraction and that the large discrepancies noted by Finch and Fordham were real and connected with the fact that their halide specimens were prepared by condensation from the vapour. Our results do not bear out this conclusion and the results of Finch and Fordham must be regarded as not yet satisfactorily accounted for.

The results for bismuth (Table 7) indicate that in this case also the lattice constant decreases as the crystal size diminishes. For a crystal size of 100 A., the largest obtained in an evaporated film, the spacing of the $(1\bar{1}0)$ planes was 0·6% less than the x-ray value and for a crystal size of 35 A. the decrease amounted to 2%. This result explains a discrepancy noted by Pickup (1936). He reported that determinations of the lattice constant of NaCl in terms of that of Bi, both by himself and other workers, gave results which were from 0·2% to 0·7% in excess of the x-ray value. Since the NaCl films were exposed to air they would have possessed a lattice constant very nearly equal with the x-ray value. The lattice spacing of the bismuth films, on the other hand, would, judging from our results, be less than the x-ray value by an amount depending on the crystal size. If the x-ray value were assigned to the bismuth films, this would result in a high value for the NaCl lattice constant as was reported by Pickup.

§ 6. CONCLUSIONS

The results discussed in this paper indicate that previous reports of an increased spacing in very small crystallites of alkali halides were in error. It may also be concluded that previous reports of anomalous values for the lattice constant of NaCl, determined by electron diffraction in terms of bismuth, were due to the fact that evaporated bismuth films have a lattice spacing less than the x-ray value by an amount dependent on the crystal size.

ACKNOWLEDGMENTS

The above research was carried out under the direction of Professor G. D. Scott, to whom the author is indebted for much helpful advice and discussion. Financial assistance was provided by a Garnett W. McKee–Lachlan Gilchrist Scholarship held during the 1949–50 session.

REFERENCES

Boochs, H., 1939, *Ann. Phys., Lpz.*, **35**, 333.
Burton, E. F., and Kohl, W. H., 1945, *Electron Microscopy*, 2nd Ed. (New York: Reinhold).
Chia-Si Lu, and Malmberg, E. W., 1943, *Rev. Sci. Instrum.*, **14**, 271.
Cosslett, V. E., 1935, *Nature, Lond.*, **136**, 988.
Finch, G. I., and Fordham, S., 1936, *Proc. Phys. Soc.*, **48**, 85.
Finch, G. I., and Wilman, H., 1934, *J. Chem. Soc.*, 751; 1937, *Ergebn. Exakt. Naturw.*, **16**, 353.
Gnan, J., 1934, *Ann. Phys., Lpz.*, **20**, 361.
Hojendahl, K., 1938–39, *K. Danske Vidensk. Selsk., Mat.-fys. Medd.*, **16**, 135.
Jevins, A., and Karlsons, K., 1939, *Z. Phys. Chem.*, **42**, Abt. B, 143.
Jevins, A., Straumanis, M., and Karlsons, K., 1939, *Z. Phys. Chem.*, **40**, Abt. B, 143.
von Laue, M., 1926, *Z. Kristallogr.*, **64**, 115,.
Lennard-Jones, J. E., and Dent, B. M., 1928, *Proc. Roy. Soc.*, **121**, 247.
Pickup, E., 1936, *Nature, Lond.*, **137**, 1072.
Seitz, F., 1940, *Modern Theory of Solids*, 1st Ed. (New York: McGraw-Hill).
Shishacow, N. A., 1937, *Phys. Z. Sowjet*, **12**, 20.
Wilman, H., 1940, *Proc. Phys. Soc.*, **52**, 323.

The Parameters of Simple Excess Semiconductors

By P. T. LANDSBERG, R. W. MACKAY and A. D. McRONALD
Department of Natural Philosophy, University of Aberdeen

Communicated by R. V. Jones; MS. received 27th November 1950

ABSTRACT. Graphical information is given which facilitates the evaluation of the parameters entering into the theory of simple excess semiconductors.

§1. INTRODUCTION

The relations entering into the usual theory of excess semiconductors are simple, but they involve a Fermi–Dirac integral and the position of the Fermi level on some suitable energy scale. Both of these must in general be determined, if a parameter of the semiconductor is to be calculated from given information. A systematic set of graphs is presented here in order to obviate much of the labour involved in such calculations.

§2. MODEL AND NOTATION

In this paper the usual theory of semiconductors (Wilson 1931) is assumed, intrinsic conduction is neglected, and the possibility of surface states and of a continuous range of activation energies of the impurity centres (Gisolf 1947) is excluded. Taking the bottom of the conduction band as the energy zero, energies in the band being positive, let ϵ^* and ϵ' denote the energy of the Fermi level and of the electrons in the impurity levels respectively. The additional parameters which enter into the theory are the temperature T, and n_b and n_f, the volume densities of all available electrons (i.e. of the impurity-bound electrons at $T=0$) and of the conduction electrons respectively. These quantities are related by the equations

$$n_b=[1+\exp(\eta^*-\eta')]n_f, \qquad n_f=n_0F(\eta^*), \qquad \ldots\ldots(1)$$

where

$$n_0 = \frac{4\pi}{\boldsymbol{h}^3}(2m^*\boldsymbol{k}T)^{3/2}, \quad \eta^* = \frac{\epsilon^*}{\boldsymbol{k}T}, \quad \eta' = \frac{\epsilon'}{\boldsymbol{k}T} \quad \text{and} \quad F(\eta^*) = \int_0^\infty \frac{\eta^{1/2}d\eta}{1+\exp(\eta-\eta^*)}. \qquad \ldots\ldots(2)$$

The function $F(\eta^*)$ has been tabulated (McDougall and Stoner 1938). If one wishes to know n_f, given n_b, ϵ' and T, η^*, which is given only implicitly, must be determined. It follows that one has either to make some preliminary guesses of η^* or to sketch the curves of n_b and $F(\eta^*)$ as a function of η^*. This procedure, while cumbersome, is frequently required, and is facilitated by the graphs to be discussed in § 3.

Numerical or graphical information, bearing on those properties of semiconductors which are of interest here, has recently been given by Müser (1950), who used Gisolf's model of a semiconductor, by Putley (1949), who dealt specifically with germanium, and by Woodward (1949), who used certain approximations for the function $F(\eta^*)$ defined above.

§ 3. COMMENTS ON THE FIGURES

To cover a large number of cases, reduced volume densities n/n_0 and energies $\epsilon/\boldsymbol{k}T$ have been plotted. Figures 1 (*a*) and (*b*) enable one to pass from actual values to reduced values, and vice versa. Use has been made of Birge's (1941) values for the constants involved, and the usual electronic mass has been taken for the effective electronic mass. It should be noted that interpolation for intermediate values of $\log(n/n_0)$ and η is extremely simple. For instance, to find the value of ϵ corresponding to $\eta = 0{\cdot}6$ for a certain temperature, the curve marked $\eta = 6$ can be used, provided the value of ϵ which it yields is divided by ten.

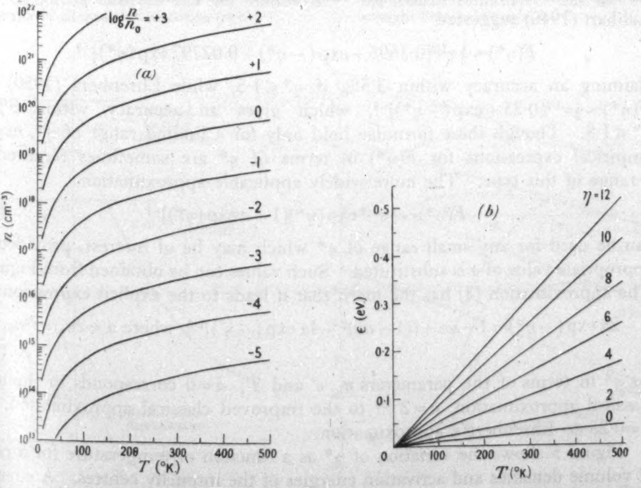

Figure 1, (*a*) and (*b*). **Relation between actual and reduced values for various temperatures.**

ϵ' will in general be fixed, and the choice of η', of which only a few values are considered here, will then be influenced by the approximate temperature for which one desires to calculate the constants of the semiconductor.

The full lines of Figures 2 and 3 are obtained from the equations (1). The curves of Figure 2 have been plotted for various values of η', including one value ($\eta'=2$) which corresponds to impurity levels situated actually in the conduction band. The simplest way of calculating such curves is to chose values of η^*, determine $F(\eta^*)$ from tables, and hence obtain n_f/n_0 and n_b/n_0.

The function $F(\eta^*)$ is for sufficiently negative η^* given by the usual classical approximation $\frac{1}{2}\pi^{1/2}\exp\eta^*$, for which the improved form $\frac{1}{2}\pi^{1/2}\exp\eta^*[1+2^{-3/2}\exp\eta^*]^{-1}$ is proposed here. This result is readily obtained from the well-known expansion

$$F(\eta^*)=\frac{\pi^{1/2}}{2}\exp\,\eta^*\sum_{n=0}^{\infty}(-1)^n\frac{\exp(n\eta^*)}{(1+n)^{3/2}},\qquad \eta^*<0,$$

terms of order $\exp 2\eta^*$ being regarded as negligible compared with unity. For sufficiently large positive η^* (strong degeneration) $F(\eta^*)$ can be approximated by $\frac{2}{3}\eta^{*3/2}[1+\pi^2/8\eta^{*2}]$. The effect of these approximations is also indicated in Figure 3, in order to suggest the magnitude of the error arising from their use.

While the above approximations are obtained theoretically, empirical formulae to represent $F(\eta^*)$ over certain ranges have also been given. Busch and Labhart (1946) suggested

$$F(\eta^*)\sim\tfrac{1}{2}\pi^{1/2}[0{\cdot}3695+\exp(-\eta^*)-0{\cdot}02797\exp(\eta^*)]^{-1},$$

claiming an accuracy within 3·5% if $\eta^*\leqslant 1{\cdot}5$, while Ehrenberg (1950) gave $F(\eta^*)\sim\frac{1}{2}\pi^{1/2}[0{\cdot}25+\exp(-\eta^*)]^{-1}$, which gives an accuracy within 5% if $\eta^*\leqslant 1{\cdot}8$. Though these formulae hold only for a limited range of η^*, explicit empirical expressions for $F(\eta^*)$ in terms of η^* are sometimes required for a range of this type. The more widely applicable approximation

$$F(\eta^*)\sim\tfrac{1}{2}\pi^{1/2}\exp(\eta^*)[1+a\exp(\eta^*)]^{-1} \qquad \ldots\ldots(3)$$

can be used for any small range of η^* which may be of interest, provided the appropriate value of a is substituted. Such values can be obtained from Figure 4. The approximation (3) has the merit that it leads to the explicit expression

$$2\alpha\exp(-\eta^*)=1-a\alpha+[(1-a\alpha)^2+4\alpha\exp(-\eta')]^{1/2},\text{ where }\alpha=2n_b/\pi^{1/2}n_0, \qquad \ldots\ldots(4)$$

for η^* in terms of the parameters n_b, ϵ' and T; $a=0$ corresponds to the usual classical approximation, $a=2^{-3/2}$ to the improved classical approximation, and $a=0{\cdot}25$ to Ehrenberg's approximation.

Figure 5 shows the variation of η^* as a function of temperature for a range of volume densities and activation energies of the impurity centres. A curve of this type was given by Shifrin (1944), and two others were given in tabular form by Putley (1949)†. The corresponding curves of n_f against temperature can be obtained by using Figure 3. It is, however, preferable to show η^* (as in Figure 5), rather than n_f, as a function of temperature, since it is this quantity which enters into the relation (Putley 1949)

$$\sigma=\sigma_0\log(1+\exp\eta^*) \qquad \ldots\ldots(5)$$

---

† Some of Putley's values in his Table 2 are about 1% in error.

for the conductivity of a semiconductor in which the electrons have a mean free path independent of their energy and inversely proportional to the temperature. σ_0 is a constant for the semiconductor. For given ϵ' the relation between any maximum, $\eta_0{}^*$ say, of η^* and the corresponding temperature is known to be

$$\eta_0{}^* = \eta' - \log\left(-\tfrac{2}{3}\eta' - 1\right). \qquad \ldots\ldots(6)$$

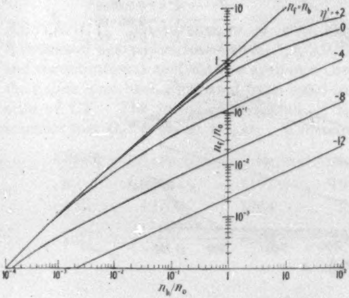

Figure 2. Relation between the volume density of conduction electrons and the volume density of all available electrons (n_b).

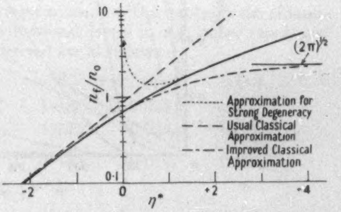

Figure 3. Relation between the volume density of conduction electrons and the position of the reduced Fermi level. The curves are straight lines below $n_f/n_0 = 0{\cdot}1$.

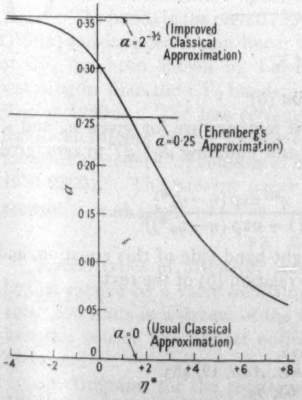

Figure 4. The values of a in equation (3) for various values of η^*.

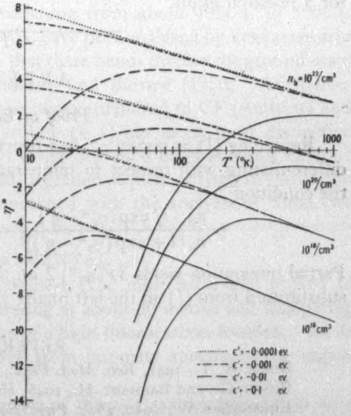

Figure 5. Relation between the reduced Fermi level and the temperature.

If $\epsilon' \geqslant -1{\cdot}5\,\boldsymbol{k}T$ no maximum exists. Equation (6) was obtained by Shifrin (1944) and Putley (1949) by a semi-graphical method, and verified analytically by Ehrenberg (1950) for his empirical expression for $F(\eta^*)$. It is shown in the Appendix that (6) can be obtained rigorously from (1) by the usual analytical methods.

Figure 6 gives the degree of ionization as a function of temperature for various volume densities and activation energies of the impurity centres.

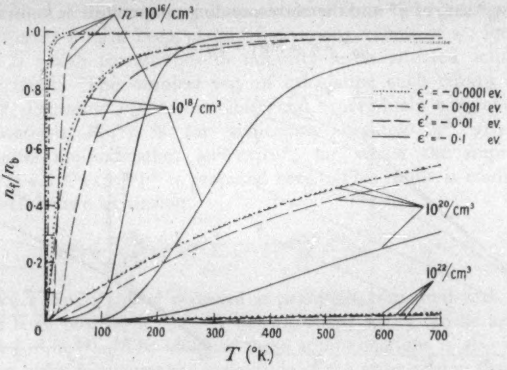

Figure 6. Relation between the degree of ionization and the temperature.

ACKNOWLEDGMENT

Two of us (R. W. M. and A. D. M.) are indebted to the University of Aberdeen for a research grant.

APPENDIX

Proof of Equation (6)

Regarding (1) as giving η^* as a function of temperature for given n_b and ϵ', differentiating with respect to temperature, and equating $d\eta^*/dT$ to zero, gives the condition

$$-\frac{n_b}{n_0}\frac{\eta' \exp(\eta_0{}^*-\eta')}{[1+\exp(\eta_0{}^*-\eta')]^2}=\int_0^\infty \frac{\eta^{3/2}\exp(\eta-\eta_0{}^*)}{[1+\exp(\eta-\eta_0{}^*)]^2}\,d\eta.$$

Partial integration yields $3F(\eta_0{}^*)/2$ on the right-hand side of this equation, and substitution from (1) on the left finally yields relation (6) of the text.

REFERENCES

BIRGE, R. T., 1941, *Rev. Mod. Phys.*, **13**, 233.
BUSCH, G., and LABHART, H., 1946, *Helv. phys. Acta*, **19**, 463.
EHRENBERG, W., 1950, *Proc. Phys. Soc.* A, **63**, 75.
GISOLF, J. H., 1947, *Ann. Phys., Lpz.*, **1**, 1.
MCDOUGALL, J., and STONER, E. C., 1938, *Phil. Trans. Roy. Soc.* A, **237**, 67.
MÜSER, H., 1950, *Z. Naturforsch.*, **5a**, 18.
PUTLEY, E. H., 1949, *Proc. Phys. Soc.* A, **62**, 284.
SHIFRIN, K., 1944, *J. Phys. U.S.S.R.*, **8**, 242.
WILSON, A. H., 1931, *Proc. Roy. Soc.* A, **133**, 458, and **134**, 277.
WOODWARD, P. M., 1949, *T.R.E. Technical Note* No. 22.

The Band-Spectrum of Carbon Monofluoride, CF

BY E. B. ANDREWS AND R. F. BARROW
Physical Chemistry Laboratory, University of Oxford

MS. received 10th October 1950

ABSTRACT. Measurements of two band-systems attributed to CF are reported. A rotational analysis of four bands, 1,0, 0,0, 0,1 and 1,1, of a transition A $^2\Sigma^+$–X $^2\Pi$ is given, and the vibrational analysis of a system B (near case b)–X $^2\Pi$. The rotational constants of the B state have been estimated from band-head separations. X $^2\Pi$ is probably the ground-state of CF. The initial convergence of the vibrational levels in B is rather rapid, and suggests that D_0'' is about $4{\cdot}9_6$ ev. Constants derived are as follows:

State	ν_e	ω_e	$x_e\omega_e$	B_e	α_e	r_e (A.)
B	$49451{\cdot}_8$	$1191{\cdot}_0$	$19{\cdot}_4$*	$1{\cdot}32_0$	0·025	$1{\cdot}31_8$
A $^2\Sigma^+$	42705	1764	2_2	$1{\cdot}727_7$	$0{\cdot}026_0$	$1{\cdot}151_6$
X $^2\Pi$	77 0	$1308{\cdot}_4$	$10{\cdot}8_6$	$1{\cdot}419_0$	$0{\cdot}019_0$	$1{\cdot}270_8$

* $-0{\cdot}_4(v+\frac{1}{2})^3$

---

§ 1. INTRODUCTION

DISCHARGES supported by fluorocarbon vapours have been shown to emit an extensive spectrum stretching from about 1950 A. to 5000 A. The bands in the region 2350–3100 A. have been analysed by Venkateswarlu (1950 a) and assigned to non-linear CF_2: that these bands involve the ground-state of CF_2 has been shown by Laird, Andrews and Barrow (1950). At shorter wavelengths than the CF_2 bands lie two systems attributed to CF (Andrews and Barrow 1950 a). The less refrangible system (A–X) has as its most distinctive feature an intense double double-headed violet-degraded band at about 2240 A.: the other system (B–X) consists of five red-degraded sequences lying in the region 1970–2200 A. The present paper is concerned with the analysis of these two systems.

§ 2. EXPERIMENTAL

Several types of discharge were examined; the most successful proved to be that excited by a valve oscillator operating at about 30 metres and dissipating about 500 watts in a stream of the vapour of a light fluorocarbon fraction. At its best this source was almost entirely free from impurity spectra in the region examined.

Spectrograms for the rotational analysis of the A–X system were taken on a Hilger quartz Littrow instrument (E. 478) on Ilford Process plates. Exposure times were of the order of 1 hour.

Plates for the vibrational analysis of the B–X system were taken on a Hilger Medium quartz instrument ($\lambda > 2000$ A.) and on a small quartz spectrograph for the region 1950–2000 A. Ilford Q1 plates were used.

Arc lines of Fe and Cu were used as standards: wavelengths above 2000 A. were taken from the M.I.T. tables (1939); those below 2000 A. from Shenstone (1936).

§ 3. THE A–X SYSTEM

A spectrogram showing part of the A–X system, and an enlargement of the 1,0 band at 2240 A. are given in the Figure (see Plate*). Only four bands of this system have been observed. On the short wavelength side, the system appears to end rather abruptly with the 1,0 band, while at the long wavelength end, it becomes increasingly overlapped by CF_2 bands. The heads of the 1,1 and 0,0 bands are not very obvious, both because they are overlaid with rotational lines of preceding bands and because they are formed by lines of very low J value. On this account, the vibrational analysis of this system was not considered as certain until a rotational analysis had been completed.

The starting point for the rotational analysis was the long-wavelength sub-band of the 2240 band: the early members of three branches were clearly resolved even with the rather small dispersion used (about 40 cm^{-1}/mm.), and the final analysis of the whole of this band was then accomplished without difficulty. The short-wavelength regions of the 0,0 and 0,1 bands which consist of lines of high J number relatively free from overlapping (see Plate) were next analysed, and extension to the heads, and the analysis of the 1,1 band followed, using standard methods.

The doublet splitting (*c.* 77 cm^{-1}) is found to arise in the lower state. The lower state is then near case-a, and the existence of four branches in each sub-band suggests that one is a satellite branch and that therefore the upper state is near case-b. Investigation of the Λ-type doubling in the lower state shows that it is small, but not negligible: the lower state is therefore $^2\Pi$. The existence of strong Q branches over a wide range of J values rules out the possibility that the upper state is $^2\Pi$ (case–b). Further, no resolution into Λ-doublets can be seen at high J values, so that the upper state cannot be $^2\Delta$ (case–b). The most probable interpretation of the transition is therefore that it is $^2\Sigma - {}^2\Pi$. The spin-splitting in the upper state proves to be very small—too small to be detected with the present measurements—so that the observed eight branches are $^SR_{21}$, $R_1 + {}^RQ_{21}$, $Q_1 + {}^QP_{21}$, P_1, R_2, $Q_2 + {}^QR_{12}$, $P_2 + {}^PQ_{12}$, $^OP_{12}$.

The line-structure is illustrated in the Plate, and the wave numbers and assignments of the lines are given in Tables 1–4.

Table 1. Wave Numbers for the 0,0 Band

J	$^SR_{21}$	R_1	Q_1	P_1	R_2	Q_2	P_2	$^OP_{12}$
0½	42970·7	42964·1	42960·7					
1½	76·8	67·7	60·7	42957·3	42903·4	42892·9	42886·3	42881·0
2½	84·2	70·7	60·7	51·9	08·4	95·9	86·3	78·7
3½	90·9	74·8	60·7		16·9	98·8	86·3	75·4
4½	99·6	79·8	62·4	48·9	21·9	903·4	86·3	72·6
5½	43009·8	84·2	64·1	46·6	31·1	08·4	88·1	
6½	19·3	90·9	66·8	45·7	40·9	13·6	90·5	
7½	28·3	96·4	70·7	45·7	51·9	19·3	92·9	
8½	38·1	43004·2	72·8	45·7	60·7	26·3	95·9	
9½	50·9	11·6	78·1	46·6	70·7	33·2	98·9	
10½	62·6	21·7	84·2	48·9	81·9	40·9	903·4	
11½	74·0	29·8	89·3	51·9	90·9	48·9	08·4	
12½	88·5	40·3	95·2	55·0	43005·5	57·3	13·6	72·6
13½	102·1	50·9	43002·9	58·7	18·4	66·8	19·3	75·4

---

* For Plates see end of issue.

Table 1 (*cont.*)

J	$^{S}R_{21}$	R_1	Q_1	P_1	R_2	Q_2	P_2	$^{O}P_{12}$
14½	43117·7	43062·6	43009·8	42962·4	43031·5	42976·8	42926·3	42878·7
15½	32·2	74·0	19·3	66·8	45·4	87·1	33·2	81·0
16½	47·9	86·5	28·3	72·8	59·4	98·1	40·9	86·3
17½	64·3	99·7	38·1	79·8	74·0	43009·8	48·9	90·5
18½	81·2	113·8	48·4	87·1	89·6	21·7	57·3	95·9
19½	99·5	27·8	59·4	95·2	105·3	34·8	66·8	99·7
20½	218·3	42·9	71·1	43002·9	23·6	48·4	76·8	908·4
21½	35·8	57·9	83·2	11·6	40·3	62·6	87·1	16·9
22½	56·6	75·5	96·2	21·7	57·9	76·7	98·1	21·9
23½		91·7	110·0	31·5	77·5	91·6	43009·8	31·1
24½		209·0	23·6	42·4	96·1	107·4	21·7	40·9
25½		27·2	38·6	53·9	215·7	23·6	34·8	48·9
26½		46·5	54·2	66·3	35·8	40·3	48·4	58·7
27½		65·5	70·1	78·2	56·6	57·9	62·6	70·7
28½		85·5	86·7	91·6	77·9	75·5	76·7	81·9
29½		305·9	204·0	105·3	99·8	94·4	91·6	90·9
30½		28·1	21·9	20·3	322·7	213·6	107·4	43005·6
31½		49·5	40·3	35·4	45·5	33·2	23·6	18·4
32½		71·7	59·6	51·1	69·1	54·0	40·3	31·5
33½		94·9	79·5	67·6	93·3	74·9	57·9	45·4
34½		418·4	99·8	84·7	418·4	96·3	77·5	
35½		42·3	320·9	202·2	44·0	318·7	96·1	
36½		68·2	42·5	21·2	70·0	41·4	215·7	
37½		95·3	64·9	40·3	96·6	64·9	35·8	
38½		520·2	88·0	59·6	523·7	88·0	56·6	
39½		46·4	411·3	79·5	51·9	413·4	77·9	
40½		73·9	34·4	99·8	80·5	38·4	99·8	
41½		602·5	59·1	320·9	609·5	64·4	322·7	
42½		31·0	85·2	42·5	39·6	91·1	45·5	
43½		59·5	511·3	66·5	69·6	517·4	69·1	
44½		89·8	38·6	89·0	700·8	45·3	93·3	
45½		720·5	65·1	413·4	31·8	73·9	418·4	
46½		51·6	92·7	38·4	64·7	602·5	44·0	
47½		83·1	621·2	61·7	95·9	31·0	70·0	
48½		816·0	50·4	89·5	829·1	61·8	96·6	
49½		48·4	79·8	516·6	63·2	92·0	523·7	
50½		81·6	710·1	42·7	97·6	723·3	51·9	
51½		915·7	41·1	68·5	932·8	55·5	80·5	
52½		50·7	72·6	97·9	68·3	87·7	609·5	
53½		86·3	804·7	627·7	44004·3	820·7	39·6	
54½		44022·2	37·5	56·9	41·4	54·1	69·6	
55½		59·5	70·7	86·9	78·9	88·3	700·8	
56½		95·8	905·0	717·7	117·0	923·4	31·8	
57½		133·5	39·2	49·2	55·4	58·6	64·7	
58½		72·0	74·7	81·4	94·8	94·8	97·9	
59½		210·9	44010·6	814·7	234·5	44031·7	830·9	
60½		50·4	47·1	47·3	74·7	68·9	65·6	
61½		90·3	83·9	81·6	315·8	106·8	900·0	
62½		331·0	121·5	915·7	51·4	45·0	35·4	
63½		72·4	60·0	50·7	99·1	84·3	71·6	
64½		414·0	98·7	86·3	441·6	224·0	44007·8	
65½		56·4	238·1	44022·2	84·8	64·0	45·3	
66½		99·1	78·2	60·2	528·6	304·8	83·9	

Table 1 (*cont.*)

J	$^SR_{21}$	R_1	Q_1	P_1	R_2	Q_2	P_2	$^OP_{12}$
67½		44542·2	44318·8	44097·2	44572·0	44346·3	44121·5	
68½			60·0	135·6		88·4	60·0	
69½			401·6	74·4		430·7	99·6	
70½			43·8	213·7		73·6	239·7	
71½			86·6	53·6		517·1	80·4	
72½			529·8	94·3		59·9	320·7	
73½			73·5	335·0			63·3	

Table 2. Wave Numbers for the 0,1 Band

J	$^SR_{21}$	R_1	Q_1	P_1	R_2	Q_2	P_2	$^OP_{12}$
0½	41684·7	41676·2	41674·8					
1½	89·2	78·4	72·4	41668·9				
2½	95·5	81·4	72·4	66·6	41623·1			
3½	703·9	86·7	72·4	63·1	30·9	41611·2		
4½	12·6	93·4	74·8	60·4	39·5	18·4		
5½	22·6	99·3	76·2	60·4	46·8	23·1		
6½	30·5	703·9	81·4	60·4	56·6	27·0		
7½	43·4	10·5	84·7	60·4	66·6	32·6		
8½	53·4	18·5	86·7	60·4	76·2	39·5	41611·2	
9½	64·3	28·4	93·4	60·4	86·7	46·8	14·8	
10½	77·2	35·2	99·3	63·1	99·3	56·6	18·4	
11½	89·9	44·6	703·9	66·6	710·5	66·6	23·1	
12½	806·2	57·7	12·6	68·9	22·6	74·8	30·9	
13½	20·1	68·2	20·6	74·8	35·2	84·7	36·3	
14½	34·1	80·5	28·4	78·4	49·6	95·5	42·5	
15½	50·8	92·9	38·0	84·7	64·7	706·4	51·6	
16½	68·7	806·2	47·5	93·4	77·2	18·5	60·4	
17½	85·2	20·1	57·7	99·3	96·5	30·5	68·9	
18½	902·3	34·1	68·2	706·4	811·9	43·4	76·2	41614·8
19½	20·8	49·5	80·5	16·4	28·6	57·7	86·7	23·1
20½	39·8	65·0	92·9	24·6	46·5	70·9	99·3	30·9
21½	59·4	81·2	806·2	35·2	65·0	86·0	710·5	39·5
22½	80·3	98·4	20·1	44·6	83·1	801·0	22·6	46·8
23½	42000·3	916·2	34·1	57·7	902·3	17·2	35·2	56·6
24½	22·7	34·7	49·5	68·2	21·9	34·1	47·5	66·6
25½	44·8	53·5	65·0	80·5	43·4	50·8	61·8	76·2
26½		73·4	81·2	92·9	62·5	68·7	75·0	86·7
27½		93·5	98·4	806·2	85·7	87·0	89·9	
28½		42014·3	916·2	20·1	42008·4	906·3	806·2	
29½		36·4	34·7	35·7	31·6	25·9	24·0	
30½		58·5	53·5	50·8	55·1	46·5	40·7	
31½		81·7	73·4	68·7	79·0	67·3	58·5	
32½		105·1	93·5	85·2	104·5	88·7	77·9	
33½		29·5	42014·3	902·3	29·5	42011·2	95·6	
34½		54·5	36·4	20·8	54·5	34·0	916·2	
35½		80·4	58·5	39·8	82·9	57·7	34·7	
36½		207·1	81·7	59·4	210·5	81·7	55·8	
37½		33·9	105·1	80·3	38·4	105·6	77·0	
38½		61·7	29·5	42000·3	67·0	31·5	42000·3	
39½		90·1	54·5	22·7	95·7	58·0	22·7	

Table 2 (*cont.*)

J	$^{S}R_{21}$	R_1	Q_1	P_1	R_2	Q_2	P_2	$^{O}P_{12}$
40½		42318·9	42180·4	42045·9	42326·7	42184·9	42045·9	
41½		48·2	206·4	70·2	57·0	212·2	70·2	
42½		78·3	32·8	91·8	88·7	40·1	94·8	
43½		409·3	60·5	115·7	420·6	68·0	118·2	
44½		40·7	88·5	40·8	52·9	97·9	45·3	
45½		73·2	317·8	66·3	86·1	327·5	72·2	
46½		505·3	47·1	92·4	519·6	57·8	99·6	
47½		38·6	76·9	219·4	53·8	88·7	227·4	
48½		72·9	408·2	46·7	88·8	420·6	56·1	
49½		607·1	39·6	75·0	624·2	52·9	85·2	
50½		42·0	71·4	304·2	60·6	86·1	315·0	
51½		78·0	503·7	33·7	97·2	519·6	45·6	
52½		715·4	37·1	63·0	734·6	53·8	76·9	
53½		51·9	71·0	93·9	72·7	88·8	408·2	
54½		89·7	605·2	425·9	811·4	624·2	40·7	
55½		828·2	41·0	57·3	50·5	60·6	73·2	
56½		66·5	76·0	89·9		97·2	506·9	
57½			713·5	522·9		734·6	41·0	
58½			50·7	57·6		72·7	75·8	
59½			88·6	92·4		811·4	611·7	
60½			827·2	627·5		50·5	47·9	
61½			65·6	63·5			84·7	
62½				700·5			722·3	
63½				37·6			60·4	
64½				75·3			99·0	
65½				813·9			838·8	
66½				53·2				

Table 3. Wave Numbers for the 1,0 Band

J	$^{S}R_{21}$	R_1	Q_1	P_1	R_2	Q_2	P_2	$^{O}P_{12}$
0½	44690·7	44685·2	44680·9					
1½	95·1	87·6	79·6	44677·4	44622·3	44612·8	44605·4	44602·0
2½	703·0	90·1	79·6	74·2	28·7	14·9	05·0	598·5
3½	09·8	92·8	79·6	71·3	35·0	18·1	05·0	94·9
4½	17·8	97·7	80·9	68·0	43·1	22·3	05·4	92·7
5½	26·5	703·0	82·3	65·5	50·9	26·7	06·3	89·8
6½	35·4	08·4	85·2	64·3	58·0	31·7	08·0	88·1
7½	44·8	15·2	87·6	64·3	68·0	37·3	10·2	86·3
8½	55·7	21·5	90·7	64·3	77·4	43·1	12·8	86 0
9½	65 9	29·3	95·1	65·5	86·8	49·8	16·0	86·0
10½	77·1	38·1	700·0	68·0	97·7	56·7	19·8	86·0
11½	90·1	45·9	05·4		708·4	64·3	24·0	86·3
12½	802·9	55·7	11·3	71·3	19·6	72·4	28·7	88·1
13½	15·5	65·1	17·8	74·2	32·1	80·9	33·7	89·8
14½	29·4	76·2	24·9	77·4	43·7	90·1	39·6	92·7
15½	43·4	86·6	32·1	82·3	56·5	700·0	45·9	95·1
16½	58·9	98·4	41·0	86·8	70·3	09·8	52·6	98·8
17½	73·7	810·6	50·1	92·8	84·6	20·7	60·0	602·7
18½	90·7	23·6	59·1	97·7	99·1	32·5	68·0	07·0
19½	907·9	36·8	68·9	705·4	814·6	43·7	76·5	12·8

Table 3 (*cont.*)

J	${}^{S}R_{21}$	R_1	Q_1	P_1	R_2	Q_2	P_2	${}^{O}P_{12}$
20½	44924·9	44850·8	44780·1	44712·9	44829·4	44756·5	44685·2	44618·1
21½	43·3	65·3	91·1	20·7	46·2	68·9	95·1	24·0
22½	61·3	80·4	802·9	29·3	62·9	82·3	705·4	31·7
23½	81·1	96·4	15·5	38·1	80·4	96·1	15·2	37·3
24½	99·7	912·6	28·5	48·0	97·8	810·6	26·5	45·9
25½	45020·1	29·6	41·9	58·3	916·2	25·6	37·4	54·1
26½	41·1	47·0	56·2	68·9	35·2	41·3	50·1	63·1
27½		64·8	70·8	80·1	54·0	56·7	63·2	71·3
28½		83·2	86·3	92·0	73·7	73·7	76·2	
29½		45002·7	902·0	804·8	94·6	90·7	90·1	
30½		22·6	18·4	18·2	45015·7	908·6	804·8	
31½		42·8	35·2	31·7	37·3	26·8	19·4	
32½		63·6	53·0	46·2	59·3	45·8	34·8	
33½		85·3	71·1	61·0	81·8	64·8	50·8	
34½		107·1	89·9	76·5	105·4	84·2	67·6	
35½		29·5	45009·2	92·2	29·0	45005·1	85·0	
36½		52·8	29·1	908·6	52·8	25·9	902·0	
37½		76·7	49·3	26·8	77·1	47·6	20·5	
38½			70·2	44·0	201·0	68·7	39·3	
39½			92·1	61·8		92·1	58·8	
40½			114·0	80·5		114·8	78·3	
41½			36·5	99·7		38·2	99·7	
42½			60·2	45020·1		63·1	45020·1	
43½			84·1	41·1		87·3	41·1	
44½				61·7			62·9	

Table 4. Wave Numbers for the 1,1 Band

J	${}^{S}R_{21}$	R_1	Q_1	P_1	R_2	Q_2	P_2	${}^{O}P_{12}$
0½	43402·4	43396·3	43393·3					
1½	10·3	99·7	93·3	43389·0	43335·9	43325·1	43318·7	43315·3
2½	15·4	402·4	93·3	86·3	42·5	28·7	18·7	11·6
3½	24·6	07·1	93·3	83·4	49·5	31·8	18·7	09·1
4½	32·0	11·3	94·9	80·9	57·4	35·9	18·7	05·9
5½	40·5	18·4	96·3	79·8	66·5	41·4	20·9	
6½	49·1	22·7	98·8	79·0	72·8	46·3	22·7	
7½	59·1	29·2	402·4	79·0	83·4	51·5	25·1	01·4
8½	70·3	36·2	05·8	79·0	93·3	57·4	28·7	01·4
9½	81·5	44·0	10·3	79·8	402·4	64·9	31·8	01·4
10½	92·8	52·1	15·4	80·9	13·4	72·3	35·9	01·4
11½	505·6	61·7	21·2	84·2	22·7	80·9	41·4	
12½	20·2	71·9	27·5	87·1	36·2	89·0	45·5	05·9
13½	32·4	81·5	34·4	89·0	49·1	98·8	51·5	09·1
14½	46·4	92·8	42·3	94·9	61·7	407·9	57·4	11·6
15½	61·3	504·3	50·3	99·7	75·4	18·8	64·9	14·5
16½	76·9	16·6	59·1	405·8	89·5	29·2	72·3	18·7
17½	92·7	29·2	68·2	11·3	504·3	40·5	80·9	22·7
18½	609·3	42·7	78·0	18·4	20·8	52·1	89·0	28·1
19½	27·7	56·7	89·5	24·6	35·7	64·4	98·8	35·9

Table 4 (*cont.*)

J	${}^{S}R_{21}$	R_1	Q_1	P_1	R_2	Q_2	P_2	${}^{O}P_{12}$
$20\frac{1}{2}$	43646·0	43571·7	43500·9	43432·0	43551·9	43478·0	43407·9	43340·5
$21\frac{1}{2}$	64·5	86·7	13·1	42·3	68·5	92·8	18·4	46·3
$22\frac{1}{2}$	83·4	602·5	25·7	52·1	86·7	505·6	29·2	54·5
$23\frac{1}{2}$	703·8	19·5	38·6	61·7	604·4	20·2	40·5	62·4
$24\frac{1}{2}$	23·3	36·6	51·9	71·9	23·0	35·7	52·1	72·3
$25\frac{1}{2}$	45·0	54·7	67·1	83·2	42·3	51·9	64·4	
$26\frac{1}{2}$	66·5	72·9	82·3	95·3	61·8	68·5	78·0	
$27\frac{1}{2}$		92·0	97·9	507·6	82·6	85·6	92·8	
$28\frac{1}{2}$		711·3	614·2	20·2	703·8	602·5	505·6	
$29\frac{1}{2}$		31·8	31·0	32·4	24·7	21·2	20·2	
$30\frac{1}{2}$		52·7	48·7	48·5	46·7	39·6	35·7	
$31\frac{1}{2}$		74·1	66·7	63·0	69·7	59·5	51·9	
$32\frac{1}{2}$		95·9	85·4	78·2	93·2	79·8	68·5	
$33\frac{1}{2}$		819·2	704·9	94·4	819·2	700·0	86·7	
$34\frac{1}{2}$		42·0	24·7	611·2	42·0	20·5	604·4	
$35\frac{1}{2}$		65·6	45·0	27·7	65·6	42·5	23·0	
$36\frac{1}{2}$		89·7	66·5	46·0	92·0	64·7	42·3	
$37\frac{1}{2}$						87·7		

The rotational constants B and D were determined by the centre-of-gravity method using averaged values of $\frac{1}{2}\{\Delta_2F_2''(J)+\Delta_2F_1''(J)\}/(J+\frac{1}{2})$ and of $\Delta_2F'(K)/(K+\frac{1}{2})$ for the lower and upper states.

The band-origins ν_0 were calculated from the early members of the Q-branches using the relation (Almy and Horsfall 1937)

$$\nu_0=\tfrac{1}{2}\{Q_1(J)+Q_2(J)\}-(B'-B'')(J+\tfrac{1}{2})^2-B'',$$

which follows from the Hill and Van Vleck expressions (see Herzeberg 1950) for the levels of a ${}^2\Pi$ state, omitting what are here negligibly small terms in D.

The doublet separation A was determined from the Q lines from

$$\{Q_1(J)-Q_2(J)+\Delta_1F'(J-\tfrac{1}{2})\}^2=4B''^2(J+\tfrac{1}{2})^2+A^2-4AB'',$$

which follows under the same conditions from the Hill and Van Vleck equations.

The values of ν_0 and of A are given in Table 5: the other constants are collected in Table 9.

Table 5

(*a*) Deslandres Scheme of Band-Origins

v'	$v''\to 0$		1
1	44643·2	1286·7	43356·5
	1719·5		1719·4
0	42923·7	1286·6	41637·1

(*b*) Values of A

v'	$v''\to 0$	1
1	76·9	76·7
0	77·1	76·5

The Λ-type doubling is not much larger than the random error in the values of $\Delta_1F(J)$, and a precise estimate of it is hardly possible. However, if we assume that the variation of the defect with J is linear, and construct moving averages, we obtain for the best-observed level, $v''=0$, values of ϵ of 0·3 and 0·5 cm^{-1} at

$J=30$ and 65 for one sub-state ($^2\Pi_{3/2}$) and of $-0{\cdot}4$ and $-1{\cdot}0$ cm^{-1} at the same J values in the other sub-state. This fits with the view that the lower state is $^2\Pi_{\rm reg}$, and the sign of the effect shows that the upper state is $^2\Sigma^+$ (Mulliken and Christy 1931, Gaydon 1944).

§4. THE B–X SYSTEM

This system consists of five red-degraded sequences of double double-headed bands (see Plate). The identity of the 0,0 sequence is not obvious from the apparent intensities, for the variation of sensitivity with wavelength is very considerable in this region. However, a picture taken on a 1-m. vacuum spectrograph by Dr. A. R. Downie showed the 1977 A. sequence to be much weaker than the 2025 A. sequence, and the vibrational intervals show that the latter, and not the sequence at 2075 A., is the 0,0 sequence.

For most of the bands three heads have been measured, and in some favourable cases it was possible to observe four heads. The Deslandres scheme in Table 6

Table 6. Deslandres Scheme for the B–X System of CF

v' ↑ / v''→	0		1		2		3		4		5		6
											47515	1190	46324·6
4													*70·7*
													253·9
											1020		
					50158·6				47696·7	1201·9	46494·8		
3					*74·8*				*71·4*		*74·5*		
					50083·8				47624·9	1204·6	46420·3		
									1062·7 1068·1		1060·3 1065·5		
			50357·9				47855·1	1221·1	46634·0	1199·5	45434·5		
2			*76·5*				*74·1*		*77·2*		*79·7*		
			50281·4				47781·0	1224·2	46556·8	1202·0	45354·8		
			1104·6 1103·6				1108·2 1111·1		1104·7 1108·9				
	50536·0	1282·7	49253·3	1263·1	47990·2	1243·3	46746·9	1217·6	45529·3*				
1	*79·4*		*75·5*		*78·8*		*77·0*		*81·4*				
	50456·6	1278·8	49177·8	1266·4	47911·4	1241·5	46669·9	1222·0	45447·9				
	1144·4 1142·2		1148·1 1152·5		1149·5 1150·5		1143·6 1140·6						
	49391·6	1286·4	48105·2	1264·5	46840·7	1237·4	45603·3						
0	*77·2*		*79·9*		*79·8*		*74·0*						
	49314·4	1289·1	48025·3	1264·4	46760·9	1231·6	45529·3*						

gives the wave numbers and vibrational intervals for the inner heads of each doublet. The mean value of the doublet interval is about 77 cm^{-1}, and the mean value of $\Delta G''_{0,1}$ is $1284{\cdot}_3$ cm^{-1}: the corresponding values obtained from the analysis of the $^2\Sigma-{}^2\Pi$ system are 77 and 1286·7 cm^{-1}. The lower states of the two systems are therefore the same, X$\,^2\Pi$; this state is most probably the ground state of CF. The doublet separation in the upper state of the present system B must be very small, so that it is near case-b. Under these conditions the head-forming branches in B–X will be $^SR_{21}$, $R_1+{}^RQ_{21}$, R_2 and $Q_2+{}^QR_{12}$ whether B is $^2\Pi$ (case–b), $^2\Delta$ (case–b) or $^2\Sigma$. The heads in Table 6, and in Table 7, which gives the wavelengths of the strongest heads of the sequences, are labelled accordingly as $^SR_{21}$, R_1, R_2 and Q_2.

Table 7. Wavelengths of Band-Heads of the B–X System

Band-head		λ	Band-head		λ
1,0	$^SR_{21}$	1977·56*	0,1	$^SR_{21}$	2075·73
1,0	R_1	78·79*	0,1	R_1	78·11
1,0	R_2	80·95*	0,1	R_2	80·04
1,0	Q_2	81·90*	0,1	Q_2	81·57
0,0	$^SR_{21}$	2022·14	0,2	R_1	2134·22
0,0	R_1	23·98	0,2	R_2	35·89
0,0	R_2	25·95	0,2	Q_2	37·86
0,0	Q_2	27·17	0,3	R_1	92·14
			0,3	Q_2	95·70

* λ_{vac}: all values above 2000 A. are given as λ_{air}.

Neglecting what are here likely to be small effects arising from Λ-type doubling, spin-splitting, and the influence of D terms, approximate B-values for the upper vibrational levels can be obtained. Treatment of the branch-formulae gives:

$$({}^SR_{21})_{\text{head}}-(R_1)_{\text{head}}=\frac{2B'B_1''}{B_1''-B'}\,; \qquad (R_2)_{\text{head}}-(Q_2)_{\text{head}}=\frac{2B'B_2''}{B_2''-B'},$$

where B_1'' and B_2'' are the effective B-values for the $^2\Pi_{1/2}$ and $^2\Pi_{3/2}$ sub-levels, and

$$B_1''=B_v''(1-A/B_v''), \qquad B_2''=B''_v(1+A/B_v'').$$

The head-separations and the B'-values calculated therefrom are given in Table 8. The values of B' at constant v' agree satisfactorily, and may be considered as confirming the vibrational analysis of the B–X system. It may be noted that the results from the $^SR_{21}$–R_1 separations are all slightly smaller than those got from R_2-Q_2 separations. This effect may be real, and arise from the failure of the

Table 8. Band-Head Separations and Values of B' for the B–X System

v', v''	R_2–Q_2	B'	$^SR_{21}$–R_1	B'	v', v''	R_2–Q_2	B'	$^SR_{21}$–R_1	B'
0, 0	29·2	1·307	44·9	1·304	2, 1	23·3	1·262	30·0	1·251
0, 1	35·4	1·311	55·1	1·302	2, 3	31·1	1·265		
0, 2	43·2	1·311			2, 4	35·9	1·262		
1, 0	24·3	1·284	31·4	1·272	2, 5	46·3	1·264		
1, 1	27·6	1·284			3, 2	19·5	1·221		
1, 2	34·4	1·291			3, 4	27·8	1·236		
1, 3	38·8	1·285			3, 5	31·1	1·232		
1, 4	49·5	1·286			4, 6	24·8	1·191		

Note: the following values of B'' were used: $B_1''=1{\cdot}392_9-0{\cdot}018_4\,(v''+\tfrac{1}{2})$, $B_2''=1{\cdot}445_1-0{\cdot}019_6\,(v''+\tfrac{1}{2})$.

simple expressions involving B_1'' and B_2'' to represent the true course of the rotational levels in X $^2\Pi$, in which the usual transition from case-a to case-b takes place with increasing J. However these discrepancies are barely outside the errors of measurement, and the variation of B' with v has been determined by simple averaging over all the results; this gives $B_v' = 1{\cdot}32_0 - 0{\cdot}02_5(v+\tfrac{1}{2})$.

§ 5. SUMMARY AND DISCUSSION

The constants for the CF molecule are summarized in Table 9.

Table 9

State	ν_e	ω_e	$x_e\omega_e$	B_e	α_e	r_e (A.)	D
B (near case-b)	49452	$1191{\cdot}_0$	$19{\cdot}_4^{(1)}$	$1{\cdot}32_0$	$0{\cdot}02_5$	$1{\cdot}31_8^{(4)}$	—
A $^2\Sigma^+$	42705	$1764^{(2)}$	$22^{(2)}$	$1{\cdot}727_7$	$0{\cdot}026_0$	$1{\cdot}151_6^{(4)}$	$6{\cdot}8\times10^{-6(3)}$
X $^2\Pi_{\text{reg}}$	77 0	$1308{\cdot}_4^{(5)}$	$10{\cdot}8_6$	$1{\cdot}419_0$	$0{\cdot}019_0$	$1{\cdot}270_8^{(4)}$	$6{\cdot}7\times10^{-6(3)}$

Notes :

(1) $-0{\cdot}_4(v+\tfrac{1}{2})^3$.

(2) Since only $\Delta G_{0,\,1}$ is known for A $^2\Sigma^+$, it is not possible to obtain $x_e\omega_e$ for this state directly. The value given here has been estimated from the relation derived by Pekeris on the basis of the Morse function: $x_e\omega_e = (\alpha_e\omega_e + 6B_e^2)^2/36B_e^3$. This expression gives tolerable results for the other two states: thus $x_e\omega_e = 13{\cdot}3$ for X and $19{\cdot}6$ for B.

(3) The experimental values of D are :

X $^2\Pi$: $v=0$, $6{\cdot}6_2\times10^{-6}$: $v=1$, $6{\cdot}7_9\times10^{-6}$
A $^2\Sigma^+$: $6{\cdot}8_4\times10^{-6}$ $6{\cdot}8_6\times10^{-6}$

calculated values from $D_e = 4B_e^3/\omega_e^2$ are : X : $6{\cdot}68\times10^{-6}$, A : $6{\cdot}63\times10^{-6}$.

(4) From $\mu r^2 = 27{\cdot}98_{65}\times10^{-40}/B$, with $\mu = 12{\cdot}212\times10^{-24}$ gm.

(5) A check on the value of ω_e follows from Guggenheimer's relation (1946), which becomes $\omega = 2156(28)^{1/4}\mu_A^{-1/2}r_e^{-1{\cdot}23}$: this gives $\omega_e'' = 1362$, in fair agreement with the observed value.

The lower state X is almost certainly the ground state of CF. Not only is a $^2\Pi$ state expected as the normal state of this molecule, arising, as in the isoelectronic molecules NO and O_2^+, from the configuration . . . $\sigma^2\pi$, but also the magnitude of the doublet splitting is of the order expected [for CH, $A=28$; Howell (1945) predicted 60 for CF]. The fact that the A–X system was not observed in the CF_2 absorption experiments of Laird, Andrews and Barrow (1950) is of course no argument against the view that X is the ground state of CF, but merely indicates that the stationary concentration of CF under these particular conditions was too small for detection. The values of the other ground-state constants are seen to be reasonable in comparison with neighbouring molecules. The internuclear distance 1·27 A. for CF is somewhat shorter than that for CF_4, 1·36 A.: the corresponding figures for BF and BF_3 are 1·26 and 1·29 A. In SiF and SiF_4 with distances of 1·60 and 1·54 A. the order is reversed, but in spite of the fact that the value for SiF appears here to be unexpectedly large, the CF–SiF increment is only 0·33 A., whereas the usual change in going for CX to SiX is about 0·4 A., e.g. for CH, $r_e'' = 1{\cdot}119$ A., SiH, $r_e'' = 1{\cdot}520$ A.

The force-constant, $k_e'' = 7{\cdot}42\times10^5$ dyne/cm., has, as expected, the highest value for a Group IVb halide known. Comparison with the values for BF, AlF and SiF—8·05, 4·36 and $4{\cdot}89\times10^5$—shows, as do the distances, that the ground state of CF is somewhat less stable than would have been predicted.

The new value for the force-constant in CF enables one further comparison to be made between the force-constants of the mono- and tetra-halides of this group (Andrews and Barrow 1950 b). Values are given in Table 10, where $k(\mathrm{MF}_4)\mathrm{i}$ indicates a force-constant calculated with the simple valency force field (Herzberg 1945), and $k(\mathrm{MF}_4)\mathrm{ii}$ values calculated by Heath and Linnett (1948) including the effect of repulsion between non-bonded atoms.

Table 10

	C–F	C–Cl	Si–F
$k_0(\mathrm{MX})$	7·17	3·76	4·79
$k(\mathrm{MX}_4)\mathrm{i}$	9·14	4·38	7·16
$k(\mathrm{MX}_4)\mathrm{ii}$	4·32	1·79	5·7
$k(\mathrm{MX}_4)\mathrm{i}/k(\mathrm{MX})$	1·27	1·16	1·49
$k(\mathrm{MX}_4)\mathrm{ii}/k(\mathrm{MX})$	0·60	0·48	1·19

The value of $k(\mathrm{CF})$ fits in well with the value of $k(\mathrm{CCl})$ (Venkateswarlu 1950 b) and the trend of the ratios suggests somewhat less repulsion in CF_4 than in CCl_4. The earlier comparison led to the conclusion that the lower force-constants (ii) for the later members of the group were to be preferred to those of (i): that the values of $k\mathrm{i}$ may be too high is now supported by the fact that $k(\mathrm{CF}_4)\mathrm{i} > k(\mathrm{CF})$ although $r_0(\mathrm{CF}_4) > r_0(\mathrm{CF})$. The figures of Table 10 suggest, however, that the effect of repulsion in the carbon compounds may have been overestimated. A short extrapolation of a force-constant–distance curve for CF gives $k = 5{\cdot}5$ at $r = 1{\cdot}36$ A., the bond-distance in CF_4. This is 75% of the force-constant in CF and may be a better approximation to the real value in CF_4.

The figures given may also serve to give a rough prediction of ω_e'' for CBr, about whose spectrum there is still doubt (Coleman and Gaydon 1947, Durie and Iredale 1948, Venkateswarlu 1950 b). With $k(\mathrm{CBr}_4)\mathrm{i} = 3{\cdot}36$, and $k\mathrm{i}/k(\mathrm{MBr}) = 1{\cdot}1$, $k(\mathrm{CBr}) = 3{\cdot}05$ and $\omega_e'' \sim 700\ \mathrm{cm}^{-1}$.

Finally, we consider the dissociation energy of CF. The vibrational levels in the B-state appear to converge rather rapidly: with the values in Table 9 we obtain a limit at 61,700 cm^{-1} above $v'' = 0$ of $\mathrm{X}\,{}^2\Pi_{1/2}$. A Birge–Sponer extrapolation of the ground-state levels gives $D_0'' = 39{,}000\ \mathrm{cm}^{-1}$. The difference between these values, 22,700 cm^{-1}, is very close to the separation ${}^1\mathrm{S}_0$ to ${}^3\mathrm{P}$ in C, namely, 21,648 cm^{-1}, and tempts one to conclude that $\mathrm{CF(B)} \rightarrow \mathrm{C}({}^1\mathrm{S}_0) + \mathrm{F}({}^2\mathrm{P})$ at about 61,700 cm^{-1}, giving $D_0'' = 40{,}050\ \mathrm{cm}^{-1}$, or 114 kcal. (4·96 ev.).

If the limit at 61,700 cm^{-1} is real, then there is only one other possibility to be considered, that $\mathrm{CF(B)} \rightarrow \mathrm{C}({}^1\mathrm{D}_2) + \mathrm{F}({}^2\mathrm{P})$: the other excited states of C and of F lie too high to be in question. This would give $D_0'' = 61{,}700 - 10{,}194 = 51{,}500\ \mathrm{cm}^{-1}$, or 147 kcal. (6·38 ev.). If this were the case, the Birge–Sponer extrapolation would have been 12,500 cm^{-1} too *low*, i.e. the value of $x_e''\omega_e''$ would have been too high.

It is sometimes possible to check a value of $x_e''\omega_e''$ by considering the value of $x_e''\mu^{1/2}$, which is often a constant for a group of molecules (Barrow 1947–8), and indeed varies not much from group to group (except for molecular ground states giving a ${}^1\mathrm{S}_0$ atom on dissociation). The early members of groups are sometimes anomalous, however, and the fact that $x_e''\mu^{1/2} = 2{\cdot}90 \times 10^{-14}$ for CF, while the mean value for the other halides of IVb is $2{\cdot}26 \times 10^{-14}$ is not necessarily significant. Comparison might more properly be made with the isoelectronic molecules NO and $\mathrm{O}_2{}^+$, for which the values are 2·68 and $3{\cdot}21 \times 10^{-14}$.

We therefore accept the conclusions that the Birge–Sponer extrapolation gives about the right value for D_0'', and that the state B dissociates into $C(^1S_0)+F(^2P)$: then $D_0''=40{,}050\,cm^{-1}$. If this is correct, then $A\,^2\Sigma^+$ dissociates either into the same products, or into excited $C(^3P)+F(^2P)$ some 38,700 cm^{-1} above $C(^1S_0)+F(^2P)$. In the former case, since $C(^1S_0)_g+F(^2P)_u$ give only a $^2\Sigma^+$ and a $^2\Pi$ state, state B is identified as $^2\Pi$ (case-b).

Although we cannot expect any one-to-one correspondence between force-constants and energies of dissociation, it is interesting to compare the three isoelectronic molecules CF, NO and O_2^+. The figures are given in Table 11.

Table 11

Molecule	CF	NO	O_2^+
Force-constant (dyne/cm.)	$7{\cdot}4\times10^5$	16·0	16·6
Energy of dissociation (ev.)	4·96 or 6·38	5·30 or 6·49	6·48

Note : the values for NO and O_2^+ are from Herzberg (1950).

They lend some support to the lower value for D_0'' of CF, and we must conclude that $4{\cdot}9_6$ ev. is the most probable figure. A fourth state of CF may be responsible for the failure to observe bands of the A–X system with $v'>1$, but heads of the 2,0 band would lie in the 0,2 sequence of the B–X system and may have escaped observation. Predissociation has not therefore been established, though it may occur. Stable states arising from the combination $C(^1D_0)+F(^2P)$ are, however, to be expected and may give rise to band systems in regions covered on our spectrograms by CF_2 bands. These systems may be revealed by excitation under different experimental conditions.

ACKNOWLEDGMENTS

The authors are glad to record their thanks to Messrs. Imperial Chemical Industries (General Chemicals Division) for the fluorocarbon, to the Royal Society for a grant, and to the Directors of Messrs. Peter Spence & Co. Ltd. for a maintenance grant to one of us (E. B. A).

REFERENCES

Almy, G. M., and Horsfall, R. B., 1937, *Phys. Rev.*, **51,** 491.

Andrews, E. B., and Barrow, R. F., 1950 a, *Nature, Lond.*, **165,** 890; 1950 b, *Proc. Phys. Soc.* A, **63,** 185.

Barrow, R. F., 1947–8, *Victor Henri Memorial Volume: Contribution to the Study of Molecular Structure* (Liège : Desoer), p. 201.

Coleman, E. H., and Gaydon, A. G., 1947, *Disc. Faraday Soc.*, No. 2, p. 169.

Durie, R. A., and Iredale, T., 1948, *Trans. Faraday Soc.*, **44,** 806.

Gaydon, A. G., 1944, *Proc. Phys. Soc.*, **56,** 160.

Guggenheimer, K. M., 1946, *Proc. Phys. Soc.*, **58,** 456.

Heath, D. F., and Linnett, J, W., 1948, *Trans. Faraday. Soc.*, **44,** 561.

Herzberg, G., 1945, *Molecular Spectra and Molecular Structure. II: Infra-red and Raman Spectra of Polyatomic Molecules* (New York : Van Nostrand), pp. 167, 182; 1950, *Molecular Spectra and Molecular Structure.—I: .Spectra of Diatomic Molecules* (New York : Van Nostrand).

Howell, H. G., 1945, *Proc. Phys. Soc.*, **57,** 37.

Laird, R. K., Andrews, E. B., and Barrow, R. F., 1950, *Trans. Faraday Soc.*, **46,** 803.

M.I.T.Wavelength Tables, 1939 (London : Chapman and Hall).

Mulliken, R. S., and Christy, A., 1931, *Phys. Rev.*, **38,** 87.

Shenstone, A. G., 1936, *Phil. Trans. Roy. Soc.* A, **235,** 195.

Venkateswarlu, P., 1950 a, *Phys. Rev.*, **77,** 676; 1950 b, *Ibid.*, **77,** 79.

Investigation of the γ-Rays from Polonium

By M. A. GRACE, R. A. ALLEN, D. WEST and H. HALBAN
Clarendon Laboratory, Oxford

MS. received 16*th October* 1950, *and in amended form* 25*th January* 1951

ABSTRACT. A method of standardizing polonium sources by measurement of the number of γ-rays is described. The hard γ-radiation of 0·773 Mev. energy emitted in the decay of ^{210}Po has been found to have an intensity of $1{\cdot}8 \pm 0{\cdot}14 \times 10^{-5}$ quanta per α-particle. The internal conversion of this line to the extent of $6{\cdot}7 \pm 1{\cdot}7\%$ gives rise to K x-radiation of lead. No other soft radiation was detected. The decay scheme of polonium is discussed.

INTRODUCTION

POLONIUM decays by the emission of a 5·3 Mev. α-particle to the stable nucleus ^{206}Pb. Bothe and Becker (1930), Joliot (1931) and de Benedetti and Kerner (1947) have shown that a weak γ-radiation of about 0·8 Mev. accompanies this α-particle emission. Recently Siegbahn and Slätis (1947) have shown that no other component of γ-radiation of energy greater than 150 kev. is present. De Benedetti and Kerner's results gave no indication of a softer component until thin aluminium absorbers were used, when a component of about 11 kev. was detected. This soft radiation is of the same energy as that found by Curie and Joliot (1931) in a careful series of measurements, using an ionization chamber. They attributed it and other soft radiation to the L and M radiation of polonium. In a measurement of the radiations from Ra(D + E) Bramson (1931) found γ-rays which she attributed to the K radiation of ^{210}Po: this has not been confirmed.

These results suggest that above 150 kev. there is only the single 0·773 Mev. line and below about 20 kev. the x-radiation from ^{210}Po, possibly due to ionization by α-particles. The presence of other γ-ray lines found earlier by Webster (1932) and by Bothe (1935) has not been confirmed by later measurements. The existence, however, of weak radiation in the 20–150 kev. range cannot be excluded on the above evidence.

When Chang (1946) reported the existence of a fine structure in the α-particle spectrum of ^{210}Po interest in the γ-rays of this nucleus was revived, and the results were discussed at length by Feather (1946), who suggested that a cascade emission of soft γ-rays by the residual nucleus might be taking place. Although later measurements of Wadey (1948) with equipment similar to that of Chang showed no evidence of fine structure in the α-particle spectrum, it was demonstrated that the form of distribution was influenced by the material of the source backing. Further investigation by Haissinsky *et al.* (1949) showed that an apparent fine structure of α-particles could be introduced by the penetration of polonium into the fine surface structure of the metal foil supporting the source. It was concluded that this phenomenon accounted for Chang's results.

The γ-radiation of ^{210}Po was further investigated by Zajac, Broda and Feather (1948). They showed that although soft radiation to the extent required by Chang's results was not present, soft radiation of about 80 kev. energy was emitted with an intensity comparable with that of the hard line. Critical absorption measurements indicated that this radiation lay between the absorption edges of lead and gold and could not be the K radiation of polonium, lead or bismuth. It was therefore necessary to assume that it was nuclear in origin and the suggestion made that it acted as a 'feeder' for the 0·773 MeV. line, being excited to the extent of about 1 quantum per 10^5 disintegrations by an α-particle of shorter range. The possibility that the radiation was delayed and corresponded with the x-ray excited levels of 1·6 minute period of Waldman and Collins (1940) was excluded by experiments in which delays between a few milliseconds and about 10 minutes should have been detected. These delay measurements also exclude the possibility that this 84 kev. line gives rise through high internal conversion to the L and M x-rays of Curie and Joliot: the spin change required to give such high internal conversion would have involved measurable delays in emission.

We were interested in a quantitative determination of the intensity of the hard γ-radiation as a means of providing a simple method of standardizing polonium. At the same time we investigated the soft radiation found by Zajac *et al.* Whilst our result for the intensity of the hard radiation is in agreement with the estimate of Zajac *et al.* we have found evidence that the soft radiation is the K radiation of lead.

The following experiments were carried out:

1. Measurement of the source strength by counting α-particles.
2. Measurement of the intensity of the hard γ-rays.
3. Search for γ-rays excited by α-particle bombardment of certain elements.
4. Critical absorption measurements on the soft radiation using a scintillation counter.
5. Search for coincidences between soft and hard γ-rays.
6. Critical absorption measurements on the soft γ-rays using a proportional counter.
7. Intensity of electron radiation.

§ 1. STRENGTH OF POLONIUM SOURCE

The polonium source was prepared by Mr. Lambie of the Radiochemical Centre by the electrolytic deposition of about 200 mc. of ^{210}Po from a RaD solution on one side of a platinum foil: this foil was 1 cm. square and about 30 mg/cm^2 thick. The ^{210}Po had previously been extracted twice by electrochemical deposition on silver so as to remove as much of the RaD and RaE as possible. The strength of the RaE content was found from later measurements to be less than $7 \pm 7 \times 10^{-3}$ μc.

The strength of the source was determined by counting the α particles with an air-filled ionization chamber shown in Figure 1. It consists of a long brass tube holding the source at one end with a small window at the other. This tube could be evacuated and its length extended up to 4 metres by the addition of extra sections. It was fitted with diaphragms down its length so as to reduce the effect of scattering at the walls. It is of interest to note that, except with the shortest tube (1 metre), when these diaphragms were not fitted the counter bias curve showed no plateau.

The ionization chamber was mounted directly behind the entry window and was displaced relative to the hole so that no α-particles should strike the central wire. This was connected to a head amplifier and main amplifier in the normal manner and the time constants adjusted for a collection time of about 50 μsec. Figure 2 shows that over a wide range of discriminator setting the counting rate was constant.

If $N'(x)$ was the actual counting rate at a distance x cm. it was found that

$$N'(100{\cdot}2\text{ cm.}) = 27938 \pm 100/\text{min.},$$
$$N'(203{\cdot}0\text{ cm.}) = 7040 \pm 40/\text{min.},$$
$$N'(301{\cdot}4\text{ cm.}) = 3260 \pm 30/\text{min.}$$

Because of the finite resolving time τ of the system it was necessary to make a counting loss correction of the form $N'(x) = N(x)\{1 - \tau N(x)\}$, where $N(x)$ is the true counting rate at distance x. The value of τ was found to be 120 μsec. from the above values of $N'(x)$ and this is in good agreement with the differentiation time constant of the circuits (approximately 100 μsec.). The strength of the source corrected in this way was $213{\cdot}2 \pm 3{\cdot}5$ mc., where 1 mc. $= 3{\cdot}6 \times 10^7$ disintegrations/sec. The gross error of 1·6% in this figure is made up of 1% error in determining the area of the hole, 0·1% error in assessment of the counting loss and 0·5% error in determining $N'(x)$.

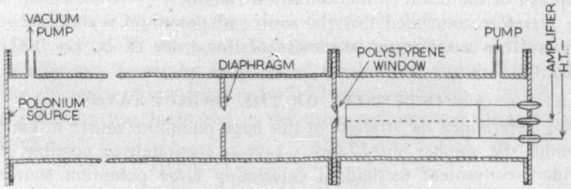

Figure 1. Low geometry α-particle counter.

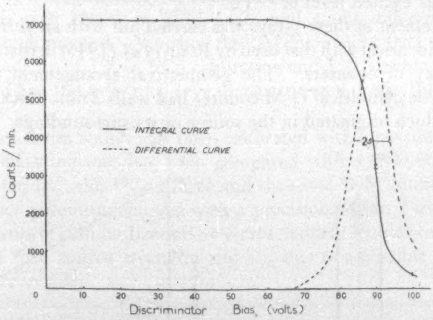

Figure 2. Integral bias curve for polonium α-particles.

Source Thickness

By analogy with the straggling in range of α-particles there will be a distribution in pulse height due to the fluctuation in the number of ionizing collisions; this has been calculated by Fano (1947) to be of the order of 8 kev. In addition to this there will be a spread of pulse height due to: (i) the thickness of the source, (ii) non-uniformity of the window, (iii) the spread of the beam in the ionization chamber which causes the induced effect by the positive ions to vary. A measure of the magnitude of these effects can be obtained by determining the standard deviation of the pulse height distribution (Figure 2). This gives $s=\frac{1}{2}\times 10=5$ volts for a differential counting rate 60·7% of maximum. The voltage scale of the discriminator bias was calibrated by interposing a foil of known stopping power and observing the change in position of the foot of the curve. This calibration gave: 90 volts = 2·0 cm. air equivalent = 3·4 MeV.

Therefore s is equivalent to 0·11 cm. air = 190 kev. Later measurements with α-particles from ThC suggest that this spread of pulse height is principally due to the spread of the beam in the ionization chamber.

It is therefore concluded that the source of polonium is of $213 \cdot 2 \pm 3 \cdot 4$ mc. strength and has a maximum thickness of the order of $2s$, i.e. 0·22 cm. air equivalent.

§ 2. INTENSITY OF THE HARD γ-RAYS

Having determined the strength of this large polonium source it was decided to determine the number of 0·77 MeV. γ-rays as accurately as possible, (i) so as to provide a convenient method of calibrating large polonium sources, and (ii) because the result is of value in itself in constructing the decay scheme of ^{210}Po, particularly for a calculation of the change in angular momentum involved in the transition to this excited level of ^{206}Pb.

The measurement of these γ-rays was carried out with an aluminium counter of construction identical with that used by Bradt *et al.* (1946) in their measurements on the efficiency of counters. The geometrical arrangement is indicated in Figure 3 (*a*). The cylindrical G-M counter had walls 2 mm. thick which stopped any electrons which originated in the source or its surroundings.

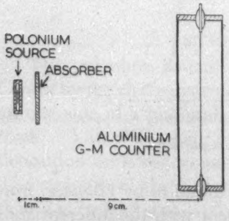

Figure 3 (*a*).

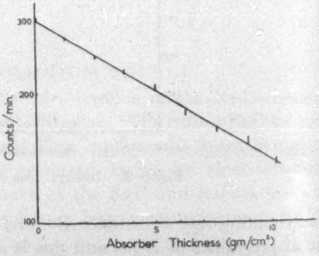

Figure 3 (*b*). Absorption of hard γ-rays in lead.

The source on its platinum backing was mounted in a copper box 1 mm. thick with less than $\frac{1}{4}$ mm. of air between the source and the box: it had been established in separate measurements that the intensity of γ-rays (of energies greater than 200 kev.) excited by α-particle bombardment of these materials would contribute less than 0·6% to the total γ-ray intensity. This is made up of less than 0·25% platinum, less than 0·14% copper and about 0·2% air.

So as to ensure that little or no soft radiation was being detected, an absorption curve in lead was plotted for absorbers of thickness $\frac{1}{2}$ to 10 gm/cm^2. This is shown in Figure 3 (*b*) and gives no indication of a soft component to the extent of more than 3%. No claim can be made for the accuracy of the mass absorption coefficient obtained from this measurement ($0{\cdot}073 \pm 0{\cdot}003$ cm^2/gm.) because the geometrical arrangement was poor. It is lower than that obtained by de Benedetti and Kerner ($0{\cdot}081$ cm^2/gm.) and the difference can probably be attributed to the detection of radiation scattered by the absorbing foil.

The efficiency of the counter to 1·2 MeV. γ-rays from a ^{60}Co source was found by putting the source 10 cm. from the counter wire; this source had been calibrated (± 3%) by β–γ coincidences. The efficiency of the counter was found to be $\eta(1{\cdot}2\,\text{MeV.}) = 7{\cdot}26 \times 10^{-3}$, compared with $\eta(1{\cdot}2\,\text{MeV.}) = 7{\cdot}57 \times 10^{-3}$ found by Bradt *et al.*

This difference of 4½% lies within the combined errors of the calibration of the ^{60}Co source (± 3%) and that due to possible differences in the counter dimensions (± 3%). It was justifiable, therefore, to make use of the *ratio* of the values of efficiency found by Bradt *et al.* for 1·2 MeV. and 0·77 MeV. γ-rays to obtain the efficiency of our counter for 0·77 MeV. γ-radiation.

The polonium was measured in the same position and the γ-ray intensity found from

$$N(\mathrm{Po}) = \left(\frac{n(\mathrm{Po})}{n(\mathrm{Co})} \times \frac{\eta(\mathrm{Co})}{\eta(\mathrm{Po})}\right) N(\mathrm{Co}),$$

where $N(x)$ is the disintegration rate of source x, $n(x)$ is the counting rate due to source x and $\eta(x)$ is the efficiency of counting γ-rays from source x using Bradt's values. In this way errors in solid angle and slight differences in counter construction are eliminated. We thus find $N(\mathrm{Po}) = 13{\cdot}9 \pm 0{\cdot}83 \times 10^4$/sec. This gross error is made up of 3% in ^{60}Co calibration and 3% possible soft component contribution. Thus the ratio of γ-rays to α-particles is $1{\cdot}80 \underset{\pm}{\times} 0{\cdot}14 \times 10^{-5}$ quanta per α-particle.

Since the polonium source has been calibrated with a possible error of 1·6% and the γ-ray counting rate has been compared with a ^{60}Co standard with an error smaller than 1%, this ^{60}Co source and the same G-M counter may be used to calibrate other polonium sources with a precision within 2·6%. In this way the principal errors of standardization by γ-rays, namely 3% due to the uncertainty in the absolute ^{60}Co source strength, and 3% due to a possible soft component contribution, are avoided.

§ 3. EXCITATION OF γ-RAYS BY POLONIUM α-PARTICLES

When standardizing polonium sources by measurement of the γ-rays, it is important to know that the materials forming the surroundings of the source do not contribute an appreciable number of γ-rays under α-particle bombardment. A number of materials were tested for this purpose and an upper limit to their γ-ray yield obtained.*

A scintillation counter fitted with a naphthalene crystal (activated with anthracene) was used to detect the γ-rays. It has been ascertained that with the particular value of discriminator setting employed the counter would not detect the soft γ-radiation from polonium and therefore was insensitive to any X-radiation emitted by these materials. On the other hand it had also been shown that the counter detected γ-rays of 200 kev. Thus the threshold of the counter lay between 80 and 200 kev. and any significant effect must be attributed to γ-rays of energy greater than this.

---

* Horton (1949) had suggested that the inelastic scattering of α-particles might take place in elements of medium atomic weight with a cross section sufficiently large to permit the detection of γ-rays. These measurements were made to test this suggestion. Later, however, Horton reported that an error had occurred in the calculations which when corrected indicated that the effect might be too small to be detected by the present method.

Measurements were made alternately with the source covered by a standard foil and by the foil under examination. The standard foil was of silver. It was found that all the elements tested for which Z was greater than 13 gave no significant effect compared with the standard. Since it is unlikely that all these materials give equal effects it was concluded that within the limits of experimental error each gives zero effect. The results for the materials tested are shown in Table 1.

Table 1

Z	Element	Element count	Silver count	Quanta per 10^9 α-particles
3	Lithium	6725 ± 15	6276 ± 15	402 ± 19
7	Air	6032 ± 15	5914 ± 15	112 ± 20
7	NH_4NO_3	6071 ± 15	5914 ± 15	98 ± 20
13	Aluminium	6656 ± 13	6302 ± 13	307 ± 16
	Cl, Ca, V, Fe, Co, Ni, Cu, Zn, Se, Rb, Sr, Zr, Mo, Pa, Cd, In, Sn, I, Ba, Ta, W, Ir, Pt, Au, Tl, Pb.			Less than 30

§ 4. CRITICAL ABSORPTION MEASUREMENTS ON THE SOFT RADIATION

A scintillation counter fitted with a NaI(Tl) crystal was used as a detector for investigating the absorption of the soft γ-rays. The high detection efficiency of this material for soft γ-radiation enabled good statistical precision to be obtained in the presence of the 0·77 Mev. component.

The polonium source was enclosed in a 'Perspex' box 1 mm. thick, chosen because the absorption coefficient of this material for the soft γ-radiation is small. The α-particles from the source were stopped in a silver foil (25 mg/cm^2) so as to avoid damage to the box. The number of γ-rays arising from the α-particle bombardment of the silver was negligible (less than 10^{-8} per α-particle).

The γ-radiation was absorbed in foils of lead, gold and tungsten in the geometrical arrangement shown in Figure 4(*a*). Figure 4(*b*) shows the absorption curves. The contribution to the total counting rate at each point by the hard radiation was estimated by extrapolating the linear section of the absorption curve obtained for large thicknesses, back to zero thickness. Table 2 gives the values for the mass absorption coefficient μ/ρ obtained from these curves.

Table 2

	(μ/ρ) meas.	(μ/ρ) Zajac *et al.*	(μ/ρ) 84 kev.	(μ/ρ) lead K radiation
Lead	2·5	2·2	2·2	3·0
Gold	2·7	6·1	~8	2·7
Tungsten	4·4	5·7	~7	~9

Also shown in the Table are the values for μ/ρ obtained by Zajac *et al.* and those for 84·5 kev. and for the K radiation of lead (75 kev.).

It is clear from these values that a discrepancy exists between our figures and those of Zajac *et al.* Whereas the latter's figures suggest that the principal component of the γ-radiation lies between the absorption edges of lead

(88·2 kev.) and gold (80·9 kev.), the present measurements suggest that it lies between those of gold and tungsten (69·6 kev.). It is possible, therefore, that this radiation is the K radiation of lead (75 kev.) or polonium (79·8 kev.).

The influence of the platinum backing to the source has been shown to introduce a negligible intensity ($<10^{-7}$ quanta per α-particle) of γ-radiation of energy greater than 200 kev. Later measurements with the proportional counter give no indication of the presence of platinum K radiation ($<10^{-7}$ quanta per disintegration). The value of μ/ρ for tungsten will, however, tend to be low due to the detection of K X-rays from this material emitted in the process of photoelectric absorption. The absorption coefficient of these absorbers is principally, 95%, due to the photoelectric effect in this energy region. In gold and lead the absorption is due to the L and M shells and therefore the X-radiation is L and M radiation. The critical absorption curves show no significant indication of the L and M radiation from polonium which Curie and Joliot have shown to be present to the extent of 4×10^{-4} and $1{\cdot}5 \times 10^{-3}$ quanta per disintegration: it is therefore assumed that these energies lie below the threshold of the counter and further that no secondary X-radiation from the lead and gold absorbers will be detected. On the other hand in tungsten the absorption is due to the K shell; since the K radiation of tungsten is 59·4 kev. it seems probable that this would be detected by the counter and therefore the measured value of μ/ρ for tungsten will be less than that obtained with good geometry.

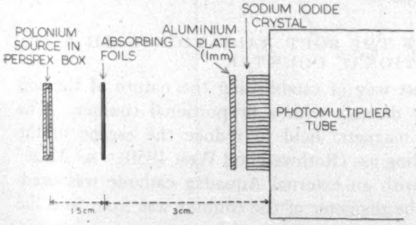

Figure 4 (*a*).

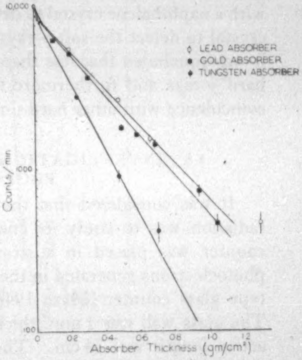

Figure 4 (*b*). Absorption of soft γ-rays.

Although these effects would tend to mask the difference between gold and tungsten absorption, the results could not be simulated by a mixture of radiations and it is concluded that part at least of the radiation lies between 69·6 and 80·9 kev.

An upper limit to the intensity of this radiation can be obtained from the efficiency of the G-M counter using the figures of Bradt *et al.* (1946). Since the number of counts due to these soft quanta is less than 3% of that due to the hard radiation and the efficiency of the G-M counter for this soft radiation is one-fifth of that for the hard, the upper limit to their intensity is 15% of the hard γ-rays, i.e. approximately 3×10^{-6} quanta per α-particle.

The efficiency of NaI(Tl) crystal to x-rays is unknown and therefore it is not possible to obtain a better estimate of the intensity of this soft radiation by this method.(see, however, § 6).

§ 5. SEARCH FOR COINCIDENCES BETWEEN SOFT AND HARD RADIATION

If this soft γ-radiation were nuclear in origin it could arise either from (*a*) a level of about 80 kev. above the ground state of lead being excited either by the 0·773 Mev. γ-ray or directly by α-particle excitation, or (*b*) a level 80 kev. above the 0·773 Mev. level and acting as a 'feeder' for it (as suggested by Zajac *et al.*). Process (*a*) is improbable, for if the angular momentum of the level were small ($J<6$) the level should be excited to the extent of about 10^{-1} quanta per α-particle, using Gamow's one-body theory of the nucleus: high angular momentum of this level can be excluded by the results of the delay experiments of Zajac *et al.* Process (*b*) was investigated by looking for coincidences between soft and hard γ-rays. A pair of scintillation counters were fitted respectively with a naphthalene crystal to detect the hard γ-rays and an activated sodium iodide crystal to detect the soft γ-rays. No significant coincidence rate was found and it was concluded that less than 13% of the soft γ-rays were in coincidence with hard γ-rays and furthermore that less than 8% of the hard γ-radiation was in coincidence with other hard γ-radiation.

§ 6. INVESTIGATION OF THE SOFT RADIATION WITH A PROPORTIONAL COUNTER

It was considered that the best way of establishing the nature of the soft radiation was to study its energy directly with a proportional counter. The counter was placed in a strong magnetic field to reduce the escape of the photoelectrons generated in the filling gas (Rothwell and West 1950). A 'Maze' type glass counter (Maze 1946) with an external Aquadag cathode was used. The glass wall was 1 mm. thick, the diameter of the counter was 5 cm. and the active length was 34 cm. The counter was filled with a mixture of krypton (64·2 cm. Hg pressure) and carbon dioxide (4·6 cm. Hg pressure). The polonium source, covered with a silver foil 25 mg/cm^2 thick to absorb the α-particles, and a Tufnol sheet 0·2 cm. thick to remove β-particles, was placed in contact with the wall of the counter. The counter was connected to a linear simplifier through a head amplifier unit and the amplified pulses were fed into a four-channel pulse analyser (Cooke-Yarborough, Bradwell, Florida and Howells 1950).

Figure 5 shows the pulse size distribution measured with the counter placed in an axial magnetic field of 7000 gauss. In a krypton-filled counter, a monochromatic x- or γ-radiation of energy greater than the K electron binding energy of krypton gives rise to two peaks of about equal intensity (West and Rothwell 1950). The peaks occur at energies (i) equal to the total energy of the radiation, and (ii) equal to the total energy minus the energy of the K x-rays of krypton (12·7 kev.) The lower energy peak (the 'escape' peak) arises when the vacancy in the K shell of a krypton atom, caused by the photoelectric absorption of the incident radiation, is filled by the emission of a K x-ray which escapes from the counter. The higher energy peak arises when the vacancy in the K shell is filled with the emission of Auger electrons, or when a K x-ray is reabsorbed in the counter. It is apparent from Figure 5 that an intense radiation (peak A and in escape peak B), together with a weak radiation of higher energy (peak C), is present. The 'escape' peak corresponding to the higher energy radiation is masked by the lower energy radiation. This type of distribution is strong evidence that K x-radiation is present, the weak, higher energy radiation being the Kβ radiation and the strong, lower energy, radiation the Kα.

The energy of the radiations was determined by calibrating the counter with 50·8 kev. characteristic x-rays from a ^{169}Yb source which decays by K capture. Errors due to lack of linearity in the amplifier were eliminated by referring all pulse sizes to the output of a standard pulse generator in the way described by Hanna, Kirkwood and Pontecorvo (1949). Calibration runs were made immediately before and after runs with the polonium source to eliminate errors due to drift in the apparatus. Values of 72 kev. and 82 kev. were obtained for the energies of the strong and weak radiations respectively. A second run gave values of 74 kev. and 84 kev. The mean values, 73 kev. and 83 kev., are close to the energies of the Kα and Kβ radiations of thallium and lead as can be seen from Table 3.

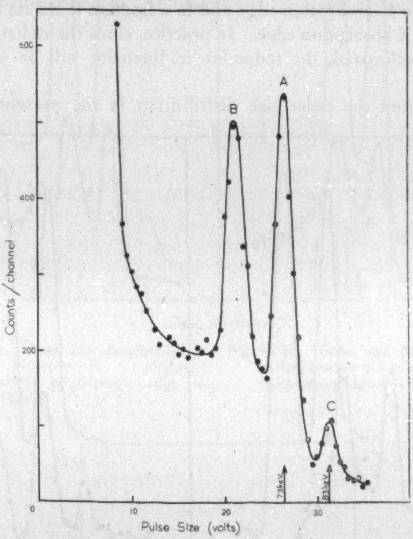

Figure 5. Pulse size distribution due to the soft radiation from polonium.

Table 3

	Kα_2	Kα_1	Kβ
Energy of Tl$_{81}$ x-rays (kev.)	71·0	73·0	82·6
Energy of Pb$_{82}$ x-rays (kev.)	72·9	75·0	84·8
Energy of Bi$_{83}$ x-rays (kev.)	75·0	77·3	87·3
Energy of Po$_{84}$ x-rays (extrapolated) (kev.)	77·3	79·8	89·9
Relative intensity	50	100	25

The accuracy of this energy measurement is not sufficiently great to determine whether the radiation is that of thallium, lead or bismuth. The use of critical absorbers in conjunction with pulse size distribution measurements however should enable the radiation to be characterized unambiguously. The absorbers were placed in contact with the counter, immediately in front of the polonium source. It was unnecessary to take precautions to avoid counting fluorescence x-rays excited in the absorbers. These differ in energy from the primary radiation and can easily be distinguished in the pulse size distributions. Absorbers of thickness 0·005 inch were used. A radiation passing normally through these absorbers will be reduced to a fraction 0·55 of its initial intensity if its energy lies below that of the K absorption edge and to a fraction 0·1 if its energy is greater than that of the K absorption edge. In practice, since the radiation falling on the absorber is uncollimated, the reduction in intensity will be somewhat greater than this.

Figure 6 shows the pulse size distribution in the presence of a tungsten absorber whose absorption edge is at 69·6 kev. It is apparent that the radiation is strongly absorbed. This is in agreement with the scintillation counter measurements and sets the energy above 69·6 kev. The two peaks in the distribution under tungsten are due to the K x-radiation of tungsten excited by the absorption of the incident radiation in the K shell of tungsten.

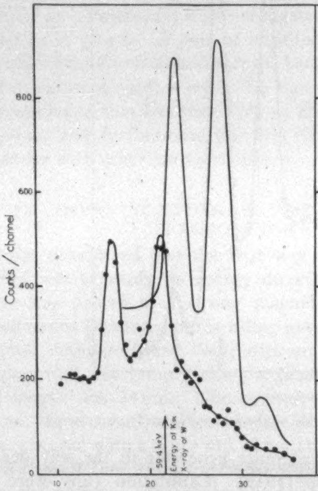

Figure 6. Pulse size distribution in the presence of a tungsten absorber (absorption edge at 69·6 kev.).

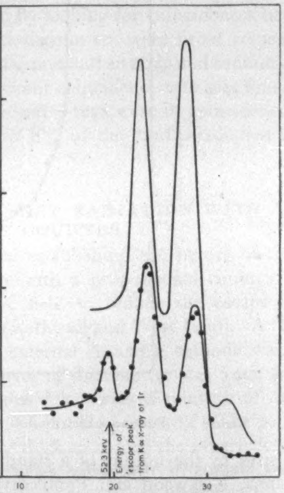

Figure 7. Pulse size distribution in the presence of an iridium absorber (absorption edge at 76·5 kev.).

Figure 7 shows the distribution in the presence of an iridium absorber whose absorption edge is at 76·5 kev. The majority of the radiation is not strongly absorbed in this case, so its energy lies below 76·5 kev. Part of the radiation must however have an energy greater than 76·5 kev. since there is some excitation of the K radiation of iridium (the small, low energy peak in the distribution in Figure 7 corresponds to the 'escape' peak due to the K x-radiation of iridium).

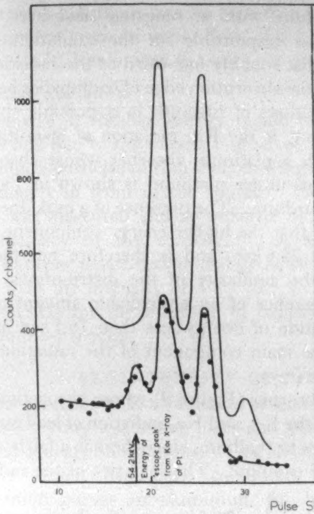

Figure 8. Pulse size distribution in the presence of a platinum absorber (absorption edge at 78·6 kev.).

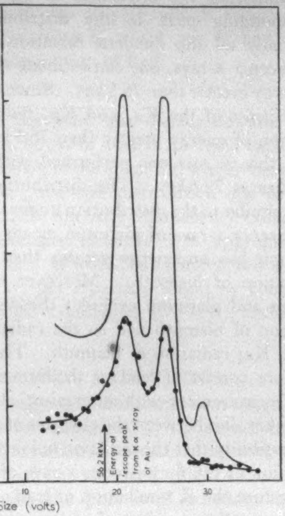

Figure 10. Pulse size distribution in the presence of a gold absorber (absorption edge at 80·9 kev.).

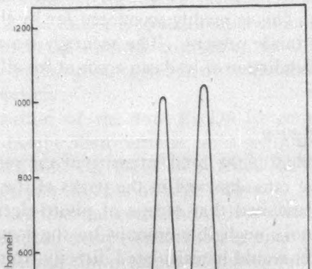

Figure 9. Pulse size distribution in the presence of an osmium absorber (absorption edge at 73·9 kev.)

By comparing the intensities of the peak due to iridium K x-rays and the corresponding peak in the distribution with a tungsten absorber, where essentially all the incident radiation is responsible for the excitation of the fluorescence x-rays, one can estimate that roughly one-third of the radiation has an energy greater than 76·5 kev. Since the absorption edge of iridium lies between the energies of the $K\alpha_1$ and $K\alpha_2$ radiations of bismuth it is possible that the radiation of energy greater than 76·5 kev. is the $K\alpha_1$ radiation of bismuth. To check this, a run was performed with a platinum absorber whose absorption edge lies at 78·6 kev. The distribution under platinum is shown in Figure 8 and is similar to the distribution under iridium. The presence of a peak due to the fluorescence x-rays of platinum means that the higher energy component of the radiation has an energy greater than 78·6 kev. and is therefore not the $K\alpha_1$ x-radiation of bismuth. Moreover the similarity of the distributions under iridium and platinum excludes the presence of an appreciable amount of $K\alpha_1$ radiation of bismuth and so the radiation of energy less than 76·5 kev. cannot be the $K\alpha_2$ radiation of bismuth. The main component of the radiation must therefore consist of lead or thallium x-rays.

A measurement with an osmium absorber (Figure 9) whose absorption edge at 73·9 kev. lies between the energies of the $K\alpha_1$ and $K\alpha_2$ radiation of lead excludes the possibility that the radiation belongs to thallium, since there is a fairly strong excitation of the fluorescence x-rays of osmium. The majority of the radiation is therefore the K x-radiation of lead.

The small component of energy greater than 76·5 kev. was further investigated using a gold absorber (Figure 10) whose absorption edge lies at an energy of 80·9 kev. In this case a peak due to the fluorescence x-rays of gold is not resolved. There is, however, a broadening of the distribution in the region where this peak would lie, which indicates the presence of a certain amount of radiation of energy greater than 80·9 kev. This is readily accounted for by the $K\beta$ radiation of lead (84·8 kev.) which is certainly present. The accuracy is not sufficient however to decide whether the $K\beta$ radiation of lead can account for all the radiation of energy greater than 76·5 kev.

Intensity of the X-Radiation

An approximate value of the total intensity of the radiation can be deduced from the total counting rate observed in the peaks of the pulse size distribution in Figure 5. It was assumed that escape of photo-electrons generated in the krypton was reduced to a negligible amount by the magnetic field so that the efficiency of the counter would be calculated directly from the geometry and the known absorption coefficient of krypton for the radiation. The overall efficiency of the counter was calculated to be 1·3%, which gives a figure of $1{\cdot}5 \times 10^{-6}$ x-rays per α-particle. This estimate is probably subject to an uncertainty of about 30% due to approximations made in calculating the counter efficiency and in integrating the pulse size distribution in Figure 5. This figure is not in disagreement with the estimate made from scintillation counter measurements (§ 4).

The measurements with the proportional counter do not exclude the presence of a weak component of polonium K x-radiation, reported by Bramson (1931). This may arise during the decay of RaE present as contamination. This possibility was examined by measuring the pulse size distribution from a source of Ra(D + E) in equilibrium. A strong peak due to the 47 kev. radiation from RaD was present but there was no sign of a peak due to polonium K x-rays. The measurement gives an upper limit of 0·1 polonium K x-rays per 47 kev. γ-ray, that is, 3×10^{-3} polonium K x-rays per disintegration of RaE.

Secondary Radiations

The rise in the low energy region of the pulse size distribution shown in Figure 5 is due to the presence of silver K x-rays of energy 22·2 kev. excited by polonium α-particles during their slowing down in the silver foil which was placed immediately in front of the source. The pulse size distribution due to these x-rays was measured and an estimate of their intensity obtained by calculating the efficiency of the counter. The intensity obtained was approximately 10^{-5} x-rays per α-particle stopped in the silver. As would be expected, this is much lower than the intensity of $1{\cdot}8 \times 10^{-3}$ x-rays per α-particle found by Curie and Joliot (1931) for the intensity of copper K x-radiation (8·1 kev.) excited by polonium α-particles.

§ 7. INTENSITY OF ELECTRON RADIATION

The presence of K x-radiation of lead suggests that internal conversion of the 0·773 Mev. γ-ray was taking place and this was confirmed by the detection of the internal conversion electrons. This electron radiation was measured with a G-M counter which had been calibrated with a standard Ra(D + E) source. Absorption curves in aluminium for both the polonium radiation and the β-radiation from Ra(D + E) were obtained so that correction could be made for the protective covering of the polonium source. This measurement showed that the intensity of the internal conversion electrons from polonium (strength 140 mc.) was $6 \pm 1{\cdot}4 \times 10^3$/sec., which is equivalent to $1{\cdot}2 \pm 0{\cdot}28 \times 10^{-6}$ electrons per α-particle. Observation of the decay of this radiation over a period of two months showed that the RaD + E contamination amounted to $7 \pm 7 \times 10^{-3}$ μc. This modifies the number of internal conversion to $1{\cdot}2 \pm 0{\cdot}3 \times 10^{-6}$ electrons per α-particle, which is in good agreement with the numbers of x-rays: $1{\cdot}5 \pm 0{\cdot}5 \times 10^{-6}$ per α-particle.

Qualitative confirmation of the low Ra(D + E) content was obtained by comparing the pulse height distributions on a scintillation counter for the radiation from polonium and the β-radiation from Ra(D + E). The electrons from polonium gave a greater number of large pulses.

Further evidence that internal conversion gives rise to these electrons was obtained by detecting electron–x-ray coincidences in a pair of scintillation counters. The low coincidence rate and the presence of background did not permit good precision but the order of magnitude of the coincidence rate was correct.

§ 8. DISCUSSION

It is concluded from the measurements described above that:

(i) The intensity of the 0·773 Mev. γ-radiation is $1{\cdot}8 \pm 0{\cdot}14 \times 10^{-5}$ quanta per disintegration.

(ii) The soft radiation in the 80 kev. region consists of the K x-radiation of lead (more than 85%).

(iii) The total soft radiation is present to the extent of about $1{\cdot}5 \pm 0{\cdot}5 \times 10^{-6}$ quanta per disintegration.

(iv) The electrons have an intensity of $1{\cdot}2 \pm 0{\cdot}3 \times 10^{-6}$ electrons per disintegration.

(v) There is approximate agreement between the number of X-rays ($1\cdot5 \pm 0\cdot5 \times 10^{-6}$ per α-particle) and the number of electrons ($1\cdot2 \pm 0\cdot3 \times 10^{-6}$ per α-particle). This suggests that these arise from the internal conversion of the 0·773 MeV. γ-rays. Taking the figure for the number of electrons where the precision is better, an internal conversion coefficient of $6\cdot7 \pm 1\cdot7\%$ is obtained.

From this value of the internal conversion coefficient for the 0·773 MeV. line the multipole character of the transition can be estimated from the figures of Rose *et al.* (1949) as shown in Table 4.

Table 4

Type of Multipole	ΔJ	Change of parity	I.C.C. (%)
Electric quadrupole	2	No	0·9
Electric octupole	3	Yes	2·1
Magnetic dipole	1	No	3·8
Electric 16 pole	4	No	4·4
Magnetic quadrupole	2	Yes	7·8
Electric 32 pole	5	Yes	9·5

This suggests that the transition is magnetic quadrupole which requires the excited level of lead to have an angular momentum of 2 units, since that of the ground state is presumably zero.

On the basis of Gamow's one-body theory of α-radioactivity it is possible to determine the relative penetrabilities of the potential barrier for α-particles with energies E and $E-\Delta E$ when the latter carries away angular momentum j. Using Birge's figures for the values of the constants, the relative penetrabilities $P(E-\Delta E, j)/P(E)$ are 5·5, 4·7, 3·2, 1·8, 1·0 and $0\cdot37 \times 10^{-5}$ for $j = 0, 1, 2, 3, 4, 5$. Gamow does not claim that this theory accurately represents the process of α-particle emission, but on the other hand the values of internal conversion coefficients can be calculated more rigorously. The comparison, therefore, of Table 4 with these values combined with our result suggests that the application of Gamow's one-body theory of the nucleus to the calculation of relative emission probabilities is not in error by a factor of more than two.

It is to be hoped that further knowledge of the decay scheme of polonium may be found by determination of the ratio of K to L internal conversion coefficients and by a better determination of the internal conversion coefficients.

ACKNOWLEDGMENTS

We are indebted to Professor Feather and Miss Zajac for interesting discussions and to Mr. Lambie of the Radiochemical Centre for the preparation of the source. Our thanks are due to Lord Cherwell for his interest in this work. Part of this work was carried out at the Atomic Energy Research Establishment, Harwell, and acknowledgment is made to the Director for permission to publish. One of us (R. A. A.) is grateful to the Department of Scientific and Industrial Research for a research grant.

Note added in proof. The results of Alburger and Friedlander (*Phys. Rev.*, 1951, **81,** 523), published while the present article was in the press, confirm the existence of internal conversion electrons from the 0·77 MeV. γ-rays, for which an internal conversion coefficient of between 1% and 5% is given.

REFERENCES

de Benedetti, S., Kerner, E. H., 1947, *Phys. Rev.*, **71,** 122.
Bothe, W., 1935, *Z. Phys.*, **96,** 607; *Ibid.*, 1936, **100,** 273.
Bothe, W., and Becker, H., *Z. Phys.*, **66,** 307.

Bradt, H., Gugelot, P. C., Huber, O., Medicus, H., Preiswerk, P., and Scherrer, P., 1946, *Helv. phys. Acta*, **19,** 77.

Bramson, S., 1931, *Z. Phys.*, **66,** 721.

Chang, W. Y., 1946, *Phys. Rev.*, **69,** 60.

Cooke-Yarborough, E. H., Bradwell, J., Florida, C. D., and Howells, G. A., *Proc. Inst. Elect. Engrs.*, Part III, **97,** 108.

Curie, I., and Joliot, F., 1931, *J. Phys. Radium*, **2,** 20 : See also Bothe, W., and Franz, 1928, *Z. Phys.* **52,** 466.

Fano, U., 1947, *Phys. Rev.*, **72,** 26.

Feather, N. 1946, *Phys. Rev.*, **70,** 88.

Gamow, G., and Critchfield, C. L., 1949, *Atomic Nucleus and Nuclear Energy Sources* (Oxford : University Press).

Haissinsky, M., Faraggi, H., Coche, A., and Avignon, P., 1949, *Phys. Rev.*, **75,** 1963.

Horton, G. K., 1949, *Thesis*, Birmingham.

Hanna, G. C., Kirkwood, D. H. W., and Pontecorvo, B., 1949, *Phys. Rev.*, **75,** 985.

Joliot, F., 1931, *C.R. Acad. Sci., Paris*, **193,** 1415.

Maze, R., 1946, *J. Phys. Radium*, **6,** 164.

Rose, M. E., Goertzel, G. H., Spinrad, B. I., Harr, J., and Strang, P., 1949, *Phys. Rev.*, **76,** 1883.

Rothwell, P., and West, D., 1950, *Proc. Phys. Soc.* A, **63,** 539.

Siegbahn, K., and Slätis, H., 1947, *Ark. Mat. Astr. Fys.*, **34A,** 15.

Wadey, W. G., 1948, *Phys. Rev.*, **74,** 1846.

Waldman, B., and Collins, G. B., 1940, *Phys. Rev.*, **57,** 338.

Webster, H. C., 1932, *Proc. Roy. Soc.* A, **136,** 428.

West, D., and Rothwell, P., 1950, *Phil. Mag.*, **41,** 873.

Zajac, B., Broda, E., and Feather, N., 1948, *Proc. Phys. Soc.*, **60,** 501.

LETTERS TO THE EDITOR

Spin-Lattice Relaxation in Diluted Paramagnetic Salts

In experiments to measure the specific heats of various paramagnetic salts diluted with non-magnetic materials (Benzie and Cooke, to be published) it has been found that such dilution in all cases resulted in an increase of the spin-lattice paramagnetic relaxation time. The Waller (1932) mechanism of spin–lattice relaxation, depending on direct spin interaction, has been found to be quite inadequate to explain the shortness of paramagnetic relaxation times found experimentally, and it now appears to be firmly established that the predominant mechanism is that put forward by Kronig (1939) and Van Vleck (1940), in which spin transitions are a result of thermal modulation of the electric field of the crystalline lattice acting on the spins through spin–orbit coupling. On this picture there would be no direct dependence of relaxation times on dilution. On the other hand, some distortion of the crystalline lattice would occur on dilution and would be expected to affect the relaxation time. Temperley (1939) has suggested an additional mechanism of spin–lattice relaxation in which he supposes spin transitions to occur in groups, thereby causing the relaxation time to be reduced.

Measurements have been made on the effect of dilution on relaxation time, particularly for hydrated manganese ammonium sulphate at 4·22° K. Dilution consisted in replacing some Mn^{++} ions by non-magnetic Zn^{++} ions by growing mixed crystals from a solution of manganese and zinc ammonium sulphates. Measurements of relaxation times were made as described by Benzie and Cooke (1950). As they point out, there is difficulty in comparing relaxation times, as a normal salt requires a ' mixture ' of relaxation times to describe its behaviour; thus the result of measurement is an apparent relaxation time τ_a which depends on the measuring frequency ν. Relaxation times are assumed to be comparable when they refer to the same value of $\nu\tau_a$. For manganese ammonium sulphate τ_a (here taken at $\nu\tau_a = 1/\pi$) is little dependent on ν, so that no great error results even if this is not quite correct.

In the Figure $1/\tau_a$ is plotted against concentration of manganese salt for a field of 508 gauss. The quantity $1/\tau_a$ is used in the presentation as it is a kind of ' mean spin transition probability' and thus its significance may be appreciated more readily than that of a relaxation time. The graphs for 339 and 678 gauss would be similar, as the field dependence of τ_a is within experimental error independent of dilution (compared with values for 508 gauss, τ_a is 10% less for 339 gauss, 13% greater for 678 gauss). A remarkable feature is the rapid initial fall-off of $1/\tau_a$ with dilution, starting with the pure salt. When the diluting ions were Mg^{++} instead of Zn^{++} the effect was little different (see Figure).

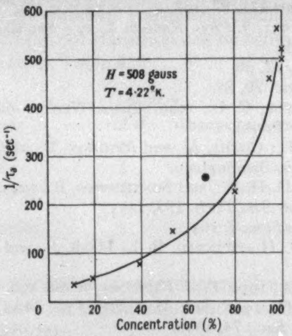

Dependence of $1/\tau_a$ on concentration of manganese ammonium sulphate in a mixed crystal of manganese and zinc ammonium sulphate (×), manganese and magnesium ammonium sulphate (●).

Quantitative results are lacking for other cases, but the increase in relaxation time on dilution was very great in the case of iron ammonium alum and caesium titanium alum (diluted with the corresponding aluminium alums) and cobalt ammonium sulphate, but small in the case of the double sulphates of copper and ammonium potassium and rubidium. (The double sulphates were diluted with the corresponding zinc salts.)

Reference to the Table will show that the magnitude of the effect corresponds to some extent to the difference of the ionic volumes associated with the paramagnetic ion and the diluting ion. This suggests that the effect might arise from distortion of the crystal lattice by the dilution. On the other hand it is hard to believe that the slight distortions involved could have such a large effect and, further, cobalt ammonium sulphate shows a very great increase in relaxation time (at least 5 times for approximately 50% dilution), although the ionic volumes of cobalt and zinc ammonium sulphates are practically identical. The Temperley effect would always result in an increase of relaxation time on dilution but it is not clear how this would vary with dilution or from one salt to another. Before coming to a definite conclusion further experiments on cobalt ammonium sulphate with both Mg^{++} and Zn^{++} as diluting ions would be necessary, but the present experiments suggest that either the Temperley effect is much more powerful than has been supposed or there is some undiscovered relaxation mechanism.

Iron ammonium alum	280			Aluminium ammonium alum	276
		Hydrated double sulphates			
Manganese ammonium	214	Cobalt ammonium	208	Zinc potassium	198
Magnesium ammonium	209·5	Copper ammonium	208	Copper rubidium	208
Zinc ammonium	208	Copper potassium	198	Zinc rubidium	207

Figures give gram-ionic volumes.

Department of Physics,
University College of the South West,*
Exeter, Devon.
17th February 1951.

R. J. Benzie.

Benzie, R. J., and Cooke, A. H., 1950, *Proc. Phys. Soc.* A, **63**, 201.
Kronig, R. de L., 1939, *Physics*, **6**, 33.
Temperley, H. N. V., 1939, *Proc. Camb. Phil. Soc.*, **35**, 256.
Van Vleck, J. H., 1940, *Phys. Rev.*, **57**, 426.
Waller, I., 1932, *Z. Phys.*, **79**, 370.

* The work reported here was carried out at the Clarendon Laboratory, Oxford.

Extension of Line Series in the Arc Spectrum of Indium: Ultra-Violet Absorption Bands probably due to InH and GaH

A programme of studies of line and band absorption spectra, with special reference to the vacuum ultra-violet, is in progress here. First results have been briefly reported in several cases (Garton 1950 a, b, c). In these experiments the absorption vessel has the form of a King type carbon-tube furnace, capable of operating at temperatures up to 2,300° C., with a heated zone of 2–3 inches length. In studying line spectra, an atmosphere of purified helium is usually maintained within the furnace chamber. In a note on new intense absorption lines in indium vapour occurring in the Schumann region (Garton 1950 a) it was stated that a considerable extension of the sharp and diffuse series of this element had been obtained under low dispersion. Photographs have since been obtained on a 'medium quartz' spectrograph, with the result that the members of the $5\,^2\mathrm{P}^0_{1/2}$–$m\,^2\mathrm{D}_{3/2}$ and $5\,^2\mathrm{P}^0_{1/2}$–$m\,^2\mathrm{S}_{1/2}$ series have been observed resolved up to $m=24$. Further series lines in which the sharp and diffuse members blend can be followed up to $m=30$. Details of measurements will be published later.

While engaged in these experiments in the quartz ultra-violet a trial was made of replacing the helium atmosphere within the furnace by one of hydrogen. This resulted in the appearance of open-band structure in the region 2330–2500 A. and extending faintly to considerably longer wavelengths. The strongest part of this structure, which exhibits no prominent heads, is intermixed with atomic lines converging to the $5\,^2\mathrm{P}^0_{3/2}$ limit.

A similar result was obtained with gallium vapour in a hydrogen atmosphere, the open-structure bands being prominent in the 2160–2400 A. range, again extending faintly to longer wavelengths.

These bands are provisionally ascribed to the hydrides of In and Ga. In the case of InH, emission bands extending from the green to the infra-red were reported by Grundström (1938, 1939), who stated that he was attempting to obtain bands of GaH. No report seems to have appeared to date, and this is believed to be the first observation of a spectrum which can be ascribed to this molecule. It is regretted that at the time of the experiments arrangements were not convenient for investigating whether Grundström's InH bands were obtainable in absorption.

In order to make a proper study of the bands reported further exposures will be necessary, using a longer absorbing column and higher dispersion. Steps in these directions are being taken.

Department of Physics,
Imperial College, London S.W.7.
15th February 1951.
W. R. S. Garton.

Garton, W. R. S., 1950 a, *Nature, Lond.*, **166**, 150; 1950 b, *Ibid.*, **166**, 317; 1950 c, *Ibid.*, **166**, 690.
Grundström, B., 1938, *Nature, Lond.*, **141**, 555; 1939, *Z. Phys.*, **113**, 721.

A Correction Factor to Gray's Theory of Ionization[*]

It seems necessary to modify Gray's equation (1928, 1949) for the energy absorption in an attempt to correct for the disagreement between theory and experiment (Mayneord 1930, Clarkson 1939, 1941, Wilson 1939, Aly and Wilson 1949, Ibrahim and Wilson (unpublished)), especially for long wavelengths and materials of high atomic number.

According to Gray, the ionization J in ion pair/cm³ sec., in a cavity very small compared with the range of the secondary electron in air, is given by $J=E/W\rho$, where W is the average energy expended per ion pair formed in air, ρ is the stopping power[†] of the medium relative to that of air and E is the energy absorbed in the medium in ev/cm³ sec. But $E=n_{\mathrm{I}}({}_{\mathrm{e}}\sigma_{\mathrm{a}}+{}_{\mathrm{e}}\tau)I$, where I is the flux of γ-ray or X-ray energy, n_{I} is the electron density of the particular material, ${}_{\mathrm{e}}\tau$ and ${}_{\mathrm{e}}\sigma_{\mathrm{a}}$ are the photoelectric and true scattering absorption coefficients respectively.

---

[*] This letter is a part of material contained in a thesis for the degree of Ph.D. in the University of London. It is published with the permission of the University.

[†] $\rho=n_{\mathrm{I}}S_{\mathrm{I}}/n_{\mathrm{a}}S_{\mathrm{a}}$, where S_{I} and S_{a} are the electronic stopping powers of the material and air and n_{a} is the electron density of air.

Since $I=nh\nu$, where n is the number of incident quanta per second per unit area perpendicular to the beam, h is Planck's constant and ν is the effective frequency of the radiation. Then

$$E=n_1 n[{}_e\sigma_a h\nu+{}^e\tau h\nu]. \qquad \ldots\ldots(1)$$

No energy is removed for the ejection of recoil electrons because they are free electrons, but in the case of photoelectrons a certain energy, generally $h\nu_K$ or $h\nu_L$ (where ν_K and ν_L are the critical frequencies of the K and L shells respectively), is removed, due to the binding energy of the electron in the atom. Therefore

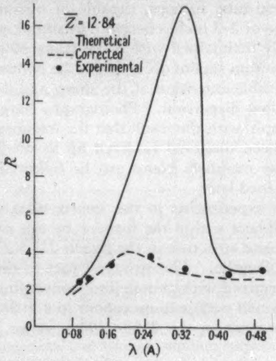

$$E=n_1 nh\nu[{}_e\sigma_a+{}_e\tau(\nu-\nu_K)/\nu].^* \qquad \ldots\ldots(2)$$

In the case of elements of low atomic number using hard X-rays and γ-rays as sources of radiation, i.e. the limit within which Gray's theory agrees with experiment, ν_K is very small (actually tending to zero) and equation (2) tends to equation (1).

Therefore the ratio R of the ionization currents in two chambers, one of high atomic number and the other with atomic number as for air, will be

$$R=\frac{{}_e\sigma_a+{}_e\tau_1(\nu-\nu_K)/\nu}{{}_e\sigma_a+{}_e\tau_a}\,\frac{S_a}{S_1},$$

when no reduction of intensity due to absorption in the walls of the chambers takes place.

From the Figure we see that for a cerium mixture for which $\overline{Z}=12{\cdot}84$ the experimental results of Ibrahim and Wilson [in measuring these values an attempt has been made to eliminate the effect of chamber volume and absorption of radiation in chamber walls] agree approximately with the modified theoretical values, although there is a considerable deviation from Gray's theoretical values. The discrepancy is of course due to the fact that the K electron of cerium ($Z=58$) has a critical potential of about 40 kev., which is accounted for in our modified equation.

The author is greatly indebted and wishes to express gratitude to Dr. C. W. Wilson of the Westminster Hospital for valuable discussions.

Physics Department,
Westminster Hospital,
London, S.W.1.
24th January 1951.

ALI A. K. IBRAHIM.

ALY, M. S., and WILSON, C. W., 1949, *Brit. J. Radiol.*, **22,** 243
CLARKSON, J. R., 1939, *Brit. J. Radiol.*, **12,** 135; 1941, *Phil. Mag.*, **31,** 437.
GRAY, L. H., 1928, *Proc. Roy. Soc.* A, **122,** 648; 1949, *Brit. J. Radiol.*, **22,** 364.
MAYNEORD, W. V., 1930, *Proc. Roy. Soc.* A, **130,** 63.
WILSON, C. W., 1939, *Brit. J. Radiol.*, **12,** 231.

* It is either ν_K or ν_L, according to the sufficient energy of the incident quanta to eject either electron from the K or L orbit.

Deterioration of Anthracene under α-Particle Irradiation

It has been reported previously (Birks 1950 a) that intense α-particle irradiation of anthracene causes a major decrease in its scintillation efficiency. This effect has now been studied quantitatively. The top surface of a small flat crystal of anthracene was irradiated for 50 hours by a flux of $1{\cdot}1 \times 10^9$ α-particles/cm²/minute from a rectangular Po source, 2·5 cm. × 0·25 cm., mounted centrally 0·7 cm. above the crystal. Periodically during the irradiation the crystal was removed for test and mounted in a fixed position on a type 5311 photomultiplier 1·4 cm. below a small weak Po source. Integral pulse-size distributions were taken in the usual manner with a linear amplifier, discriminator and scaler. It was found that, allowing for the Po decay, the irradiation caused no decrease in the number of scintillations from the crystal, but that their relative amplitude I/I_0 obtained from the mean pulse size decreased as

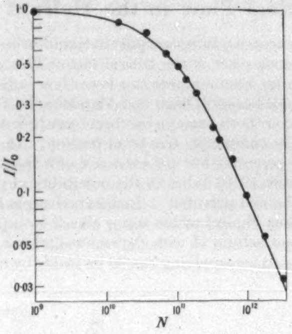

$$I/I_0 = 1/(1+AN), \qquad \ldots\ldots (1)$$

where N is the total number of α-particles/cm² striking the crystal, and $A = 10^{-11}$. The observations and the curve corresponding to (1) are plotted in the Figure.

No recovery of fluorescent efficiency was observed during a fortnight after the irradiation. The brown discoloration of the irradiated surface layer of the crystal indicates that the effect is due to permanent molecular damage caused by the intense ionization. After irradiation the crystal was reversed and the scintillations from the lower non-irradiated surface were observed through the discoloured layer and were found to be reduced in amplitube to $0{\cdot}7 I_0$. The decrease due to optical absorption in the irradiated layer is, therefore, small compared with the total decrease in I/I_0, which must be accounted for by some other mechanism.

The exciton theory used previously for mixed organic crystals (Birks 1950 b) suggests a possible 'quenching' process. If q_0 is the original number of molecules of anthracene/cm² in the irradiated volume, and each α-particle damages p molecules, then the concentration of damaged molecules after N α-particles/cm² have struck the crystal will be $x = \exp(pN/q_0) - 1$ molecules per undamaged molecule of anthracene. If a damaged molecule has an exciton capture probability k relative to an anthracene molecule, the relative amplitude of the fluorescent anthracene radiation will be

$$\frac{I}{I_0} = \frac{1}{1+kx} = \frac{1}{1+kpN/q_0} \qquad \text{(for } pN/q_0 \text{ small).} \qquad \ldots\ldots (2)$$

Taking $p/q_0 \sim 10^{-14}$, which is the order of magnitude of the molecular area in cm², we find, on comparison of (1) and (2), $k \sim 1{,}000$. This high value of k is consistent with the low fluorescent efficiency of anthracene under α-particle excitation (Birks 1950 a), which is attributable to local quenching by the molecules damaged by the incident α-particle.

The decrease in I/I_0 for higher values of N is now being investigated for anthracene and other organic crystals.

Department of Natural Philosophy,
The University, Glasgow.
26th February 1951.

J. B. Birks.
F. A. Black.

Birks, J. B., 1950 a, *Proc. Phys. Soc.* A, **63**, 1294; 1950 b, *Ibid.*, **63**, 1044.

Sub-critical Flow in the Helium II Film

In practically all experiments on film transport in liquid helium II the observations have been made while the flow took place at the critical rate. This is a maximum rate of mass transport to which the transfer from a higher to a lower level adjusts itself. Exceptions are the experiments with a double beaker (Daunt and Mendelssohn 1946 a) and with an oscillating film (Atkins 1950), and in both cases it has been concluded that film flow at less than the critical rate appears to be completely free from friction. In these experiments the flow occurred in a gravitational potential, but the existence of a thermo-mechanical effect in the film (Daunt and Mendelssohn 1950) indicates the possibility of producing film flow at sub-critical rates also under a thermal potential. Such experiments have now been carried out.

A small Dewar vessel (see Figure) whose top is closed by an optically flat glass cover is suspended in a bath of liquid helium II with the rim well above the bath level. Film flow into the vessel can be produced by supplying heat to its inside by means of a resistance. The apparatus is similar to those used by Atkins (1948) and by Brown and Mendelssohn (1950) for the observation of high flow rates except that the influx of stray heat was cut down to approximately 10^{-6} watt/sec. Under these conditions the spurious inflow of helium was too small to be observable, and rates of one-fifth of the critical could still be measured with fair accuracy.

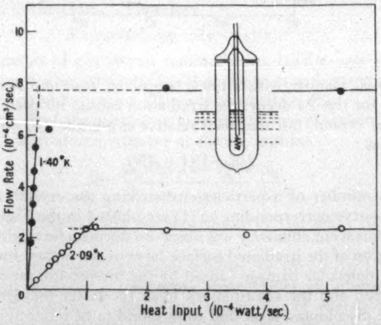

Film flow under thermal potential.

The results for two of a number of temperatures (see Figure) show that the flow rate is strictly proportional to the rate at which heat is supplied until a critical value is reached. For heat inputs higher than this critical one the rate of film flow remains virtually unchanged. While there is a sharp break at the critical velocity in the curve for 2·09° K., the transition is more continuous at 1·4° K. This latter feature is probably of a non-fundamental character and can be explained by the geometry of the apparatus used (Brown and Mendelssohn 1950).

In contradistinction to the existence of a critical rate of frictionless transport in liquid helium II as postulated by one of us (Mendelssohn 1945), it has been suggested (Gorter and Mellink 1949) that friction in superflow might make its appearance more gradually, increasing with the third power of the velocity. This suggestion is based on observations in wide channels (Mellink 1947), which can indeed be interpreted in this manner. The present results, however, seem to leave no doubt that in pure superflow, as occurring in film transfer, friction is completely absent for a wide range of sub-critical velocities. The strictly linear increase, followed by the break, makes it quite impossible to admit a process in which friction increases with the third power of the flow rate.

It may, nevertheless, be possible to reconcile our results with those obtained in wide channels by considering that in the latter the 'normal component' of the liquid can move relative to the walls, while it is probably stationary in the film. Retaining the two-fluid model for liquid helium, one must then distinguish between friction of the superfluid against the wall and against the normal component, the latter being possibly proportional to the third power of the relative velocity but becoming very small at low temperatures. Moreover, since there are reasons to believe that the critical velocity may vary inversely with the diameter of the flow channel (Daunt and Mendelssohn 1946 b), it may become very small for wide channels, where it would be completely overshadowed by super-critical flow. Thus, because of the small critical velocity, friction between the two components would make its appearance almost immediately in flow through wide channels, giving rise to the observed third-power law. In thin films, on the other hand, frictionless flow would persist up to a high critical velocity, to be followed by the appearance of very strong friction. Recent observations on channels of 1–2 μ width (Bowers and Mendelssohn 1950) seem indeed to favour such a mechanism, but a final decision has clearly to be left to further experiments.

The strict proportionality of the flow rate with heat input in the present experiments shows that the entropy of the helium transferred by the film is independent of the velocity. Comparison of the heat input with the measured specific heat of the bulk liquid (Keesom and Keesom 1935) indicates further that the value of this entropy is *zero*. A discussion of this aspect of the experiments has to be left to a more detailed communication.

The Clarendon Laboratory,
Oxford.
2nd March 1951.

B. S. Chandrasekhar.
K. Mendelssohn.

Atkins, K. R., 1948, *Nature, Lond.*, **161,** 925; 1950, *Proc. Roy. Soc.* A, **203,** 119, 240.
Bowers, R., and Mendelssohn, K., 1950, *Proc. Phys. Soc.* A, **63,** 178.
Brown, J. B., and Mendelssohn, K., 1950, *Proc. Phys. Soc.* A, **63,** 1312.
Daunt, J. G., and Mendelssohn, K., 1946 a, *Nature, Lond.*, **157,** 839; 1946 b, *Phys. Rev.*, **69,** 126; 1950, *Proc. Phys. Soc.* A, **63,** 1305.
Gorter, C. J., and Mellink, J. H., 1949, *Physica,* **15,** 285.
Keesom, W. H., and Keesom, A. P., 1935, *Physica,* **2,** 557.
Mellink, J. H., 1947, *Physica,* **13,** 180.
Mendelssohn, K., 1945, *Proc. Phys. Soc.*, **57,** 371.

REVIEWS OF BOOKS

Giant Brains or Machines That Think, by E. C. Berkeley. Pp. xvi + 270, 1st Edition. (New York: John Wiley and Sons; London: Chapman and Hall, 1949.) 32*s*.

This book is primarily concerned with large-scale calculating machines. It includes detailed information about IBM punched card machines (usually called Hollerith in this country after the originator), the Rockefeller differential analyser at M.I.T., the Automatic Sequence Controlled Calculator at Harvard University, the ENIAC built at the Moore School of Electrical Engineering, University of Pennsylvania, and machines using telephone relays built by the Bell Telephone Laboratories. With the exception of the IBM machines, which are widely used for commercial accounting, all these machines are the result of pioneer development work, and only one example of each (two in the case of the BTL machine) has been constructed.

In the first chapter the author is concerned with supporting the implication contained in the title that calculating machines can 'think'. Many people, however, will consider that he stretches the meaning of the word unduly. An automatic calculating machine can store numbers and perform a prearranged series of arithmetical operations on them. It is not, however, justifiable to say that such a machine can think, even though at certain stages the nature of the operation performed may depend in some way on the result of previous operations (e.g. on the sign of a number previously calculated) and may, therefore, be unknown to the operator. It is true that the sequences of operations performed by automatic calculating machines are much more complex in structure than the simple cycles performed by machines hitherto familiar—such as automatic lathes—and that they have suggested to those concerned lines of thought which may help to elucidate some aspects of animal behaviour. But the author, with his insistence on the statement that existing calculating machines can think, obscures rather than clarifies these important issues.

The book is intended for anyone who has a general interest in scientific matters. It calls for some readiness to follow involved arguments and descriptions. In places the treatment is somewhat condensed, and anyone unfamiliar with the subject would find consecutive reading rather exhausting; the author, however, advises his readers not to do this, but to read what interests them, taking a bit here, and a bit there. Some sections would have been made easier to follow if technical terms had been introduced and defined only when they were essential for the later discussion. The style is informal but for the most part concise.

About one-third of the book is taken up with detailed descriptions of the machines mentioned above. Each machine is dealt with under the following headings : origin and development, general organization, physical devices used, input and output of information and the handling of it inside the machine. This is undoubtedly the most useful section of the book, and the author has brought together much information which was hitherto obtainable only from scattered papers. The book also contains some discussion of machines for performing the processes of symbolic logic, and some remarks on the social implications of the subject. A good feature is a bibliography of 20 pages.

The author has rightly dealt at greatest length with those machines which were completed and working at the time he was writing. It is, nevertheless, a pity that he did not say more about the EDVAC and machines like it. Although none of these machines were in operation until just before the book was published, the ideas on which they are based are original and even revolutionary ; moreover, a discussion of them would have brought out very clearly how, and within what limits, a machine can perform the highly complex sequences of operations which the author chooses to call 'thinking'.

M. V. WILKES.

Atomic Energy, edited by J. L. CRAMMER and R. E. PEIERLS. Pp. 200. (Harmondsworth, Middlesex : Penguin Books, 1950.) 1*s.* 6*d.*

This excellent little work consists partly of a reprint of the Penguin *Science News II*, which was devoted to atomic energy and has been out of print for some years. Although written in a semi-popular style and directed to a non-specialist public, the names of the authors of the various articles—Peierls, Bethe, Morrison, Frisch, etc.—provide a guarantee of the accuracy of the statements made.

Four entirely new articles have been written for the present edition. Sir John Cockcroft discusses the factors influencing the design of nuclear reactors and appears fairly confident that the technical difficulties holding up the design of reactors for the efficient production of atomic power will eventually be overcome, but points out that we cannot be definite about this until experience is gained of the operation of pilot plants. He estimates that this stage may occupy the next ten years. After that the developments depend 'on our experience, on availability of materials, and on the world political situation'.

Professor C. E. Tilley discusses the distribution of world resources of uranium and thorium, while W. J. Arrol and K. Fearnside give a fascinating account of the applications of radioactive isotopes in biology and industry. J. L. Crammer adds a short article on health hazards connected with the handling of radioactive materials.

The 24 plates illustrate the spectacular progress that has been made at Harwell since the appearance of the first edition of this work.

Altogether the book represents a notable addition to the semi-popular literature on atomic energy and its applications. E. H. S. B.

Vorlesungen über theoretische Physik, by A. SOMMERFELD. Band I, Mechanik. Pp. xii + 276. 4th Edition, 1948. Band II, Mechanik der deformierbaren Medien. Pp. xv + 375. 2nd Edition, 1946. Band III, Electrodynamik. Pp. xvi + 367. 1st Edition, 1948. Band VI, Partielle Differentialgleichungen der Physik. Pp. xiii + 332. 1st Edition, 1947. (Wiesbaden: Dieterich'sche Verlagsbuchhandlung.) 18 DM. each.

The publication of Sommerfeld's lectures on theoretical physics will be hailed not only by those who have been privileged to attend them, but generally by all teachers and students of this important aspect of physics. In fact, this series of books will remain for all time among the great classics of science. Sommerfeld's fame as a teacher equals his reputation as a successful investigator. He belongs to that brilliant succession of inspiring teachers who built up the German school of theoretical physics. Their way of looking at theoretical problems, their conception of the relation between mathematical methods and physical ideas present peculiar features which, in spite of the universal character of science, quite distinctly differentiate the German tradition from the French or the English one. This circumstance should enhance the interest of Sommerfeld's lectures for the English reader, who cannot fail to derive ample profit from an appreciation of such differences in outlook and from familiarity with the youthful and vigorous approach of the German school. In this study, he could certainly find no better guide than Sommerfeld; this series of his lectures, published at the end of a long and eventful career, embodies his best and most mature thought. It covers the traditional ground of classical physics subdivided, in accordance with the German custom, into six sections, which correspond to as many 'semesters' of three-hour lectures (so that the entire cycle covers three years of University study). The successive sections, each embodied in a separate volume, are the following: (I) Mechanics, (II) Hydrodynamics and elasticity, (III) Electricity and magnetism, (IV) Optics, (V) Thermodynamics and statistics, (VI) Differential equations of theoretical physics.* To get a full record of Sommerfeld's teaching activity, one should, of course, add to this collection his famous *Atombau und Spektrallinien*, whose successive editions present such an impressive picture of the rapid development of atomic and quantum theory.

A particularly attractive feature of Sommerfeld's style, apart from its admirable lucidity and precision, is its liveliness. This he achieves by two apparently opposite, but in fact perfectly consonant, means: on the one hand, he discreetly but aptly calls the attention of the student to the historical development of the subject; on the other, he is careful to acquaint him with its most modern and topical aspects. For instance, the volume on hydrodynamics includes a brief discussion of the latest work on turbulence, which has the double advantage of introducing the student to a major trend of current research and of firmly linking the new ideas with the fundamental principles of the theory. Besides, he always lays the emphasis on the physical rather than on the mathematical side of the problems, and chooses his illustrations from problems of practical interest. In the volume on mechanics, one looks in vain for motions of insects contained in hollow thin cylinders rolling on rough inclined planes†, but one does find interesting accounts of the application of the gyroscope to the stabilization of ships, and of the theory of billiards.

This healthy physical attitude by no means entails any neglect of the necessary rigour of the mathematics. On the contrary, it is a delight to find at the appropriate places those brilliant pieces of mathematical analysis of physical phenomena, in which Sommerfeld is such a *virtuoso*. Most interesting from the didactic point of view is the sixth volume, entirely devoted to the mathematical methods and setting, so to speak, the crown on the whole course. Only when the student has learnt how to handle the tool of mathematics in the most varied circumstances is he able to appreciate its wonderful flexibility and to acquire correct views on the significance of mathematical 'analogies' between different branches of physics and the use of 'models' in the analysis of phenomena.

L. ROSENFELD.

---

* Volumes IV and V are not yet ready, but are due to appear, the first very soon and the other by next year.

† E. T. Whittaker, *Analytical Dynamics*, Ch. VI, Miscellaneous Example 14.

Structure of Molecules and the Chemical Bond, by Y. K. SYRKIN and M. E. DYATKINA; translated from the Russian by M. A. PARTRIDGE and D. O. JORDAN. Pp. ix+509. 1st Edition. (London: Butterworth's Scientific Publications, 1950.) 63*s*.

In 1946 Syrkin and Dyatkina published this book in Russia, and we all hoped that an English translation would soon be made available, for although we knew that a lively school of theoretical chemistry was developing over there, we knew relatively little of what progress it had made, and of how 'permeable' the iron curtain had proved to ideas from the West. The translation that we wanted is now before us, revised and (quite obviously) improved in the process.

First of all, the scope of the book is roughly that of Pauling's classic *Nature of the Chemical Bond*, with the addition of rather more mathematics and a chapter on the method of molecular orbitals. The text is extremely readable, and the standard of difficulty considerably below that of the *Quantum Chemistry* of Eyring, Walter and Kimball. There is an immense and valuable compilation of numerical data of all kinds—more complete even than Pauling's—though it is a pity that references to origin are so scanty as not to allow an easy assessment of their present reliability.

Next, there is a good deal of interesting new material in the book, though the specifically Russian contribution is rather less than one might have anticipated: up to the time of writing this book no significant new idea appears to have originated in Russia. Some examples of the new material are a good chapter on the Boron Hydrides (quite properly, too, since the authors have made useful contributions to this problem), an excellent set of numerical values for the excitation of atoms (particularly complex atoms with d-electrons) to the valence state, and a considerable emphasis on what are called 'transitional structures'. An example will show what is meant by these latter. In the conventional treatment of ionic-covalent resonance it is usual to write

$$\Psi = c_1\psi_{\text{cov}} + c_2\psi_{\text{ion}},$$

where ψ_{cov} and ψ_{ion} are covalent and ionic wave functions and c_1, c_2 are constants. This composite wave function Ψ is generally interpreted as a superposition of covalent and ionic structures in the ratio $c_1^2 : c_2^2$, but Syrkin and Dyatkina introduce covalent, ionic and transitional structures in the ratio $c_1^2 : c_2^2 : 2c_1c_2$. As a result the simple pictorial character of covalent and ionic weighting in the form introduced by Pauling is largely lost, and properties such as the dipole moment receive contributions, whose relative magnitudes are not always easy to see at once, from all three types of structure. This new treatment is presumably more accurate, but also more unwieldy.

There are certain notable omissions. It seems a great pity never to use the concept of an electronegativity scale, other than in the completely trivial sense that nitrogen is less electronegative than oxygen. Even though this concept is proving a little ambiguous in recent English theoretical analysis, there is surely a strong case for introducing Pauling's and, even more, for defining Mulliken's absolute electronegativities. It seems a pity also that no mention is made of Penney's pioneer work on the greater stability of C_6H_6 than C_4H_4 or C_8H_8 as being dominated by the σ-electrons; or of the equally pioneer work of Van Vleck on the stereochemistry of tetrahedral and related molecules. These omissions result from a failure to appreciate the deep chemical significance of the 'approximation of perfect pairing'.

All this leads us to ask: is the account properly balanced? Here let it be said at once that in so far as the relative contributions of East and West are concerned, no exception to the treatment here presented can be made. But it is hard to avoid three other extremely serious criticisms—criticisms which to the present writer appear to vitiate much of the undoubted value of the book.

In the first place the outlook is surprisingly naïve, seeing that the subject of theoretical chemistry, in its wave-mechanical form, is more than twenty years old. It is surely inadequate to give (p. 83) details of the reaction between ozone and benzene as proof that the latter molecule is plane hexagonal. Why is there no mention of the absolutely clear-cut and convincing evidence from vibrational analysis? And why (p. 2), when referring to the failure of the Sommerfeld–Bohr theory to deal with any molecular problem, is it thought fit to add: "*more recently*, defects have become apparent in the application of this theory to atomic spectra"? 'More recently' is somewhat of an under-statement, for the defects were apparent as soon as an attempt was made to explain the spectrum of atomic helium some years before the work of Pauli and Niessen on H_2^+. There are plenty of other examples of this kind. Thus (p. 47) it is claimed that for the hydrogen molecule ion "the value for the energy cannot be regarded as exact". In one sense this is true, but since it can be shown to be correct to about 1 part in 10^6, which is vastly better than is yet provided by experiment, the comment is at least naïve. There is a similiar naïveté in the treatment (p. 408) of the three-electron problem with spin degeneracy. How does it come about that practically the whole of a chapter of 27 pages is needed to prove the final formula, when it can be done quite adequately in two or three paragraphs, and could perfectly well be obtained from the more general four-electron formula by deleting certain terms? A student who ploughs through this sort of stuff will have a completely false idea of the mathematical aspect of the subject.

In the second place there are far too many rank mistakes, several of them extremely serious. It is horrible, for example, to think of the confusion that will be caused by the description (p. 100) of Pauling's postulate of the arithmetic mean $[E_{AB}=\frac{1}{2}(E_{AA}+E_{BB})]$ for the energy of a covalent bond. "According to the method of Pauling, one half of the energy of the bond is apportioned to each electron, and each electron of the atoms A and B contributes the same energy to the molecule AB as to the molecules AA and BB." This is sheer nonsense. So also is the comment on ring strain (p. 253) in molecules like cyclopropane C_3H_6; and the wave-mechanical formulations of Pauli's Exclusion Principle (p. 63) and of the variation method (p. 47) are not satisfactory. The 'derivation' of the wave equation (p. 4) treats ψ as a displacement, and thereby greatly confuses the subsequent probability interpretation. These, and others, are pretty serious errors in a book costing three guineas; they would certainly mislead the student.

Finally, we may enquire whether the book contains any judgment or criticism of the present techniques, any reflection on the validity of the explanations provided, or any indications of some of the deep (yet intrinsically simple) unsolved difficulties in the subject. There are none at all. The account proceeds with a bustling efficiency just as if almost "everything in the garden was lovely", when, as a recent Discussion at the Royal Society showed very clearly, this is really far from being the case. Surely the time has come when in a book of this size we may look for a critique as well as a dogma! C. A. COULSON.

Contribution a l'Étude des Réactions Mutuelles des Cristaux dans la Déformation des Métaux Polycristallins, par ROGER MICHAUD. Pp. xvi + 98. 1st Edition, (Paris: Publications Scientifiques et Techniques du Ministère de L'Air. 1950.) 500 fr.

In this little book the author describes an investigation he has made of the plastic deformation of polycrystalline metals. There is no attempt made to review the subject in a wider aspect, and the author has obviously intended that the book should be regarded purely as a research paper. His experiments were performed on specimens of aluminium consisting of single crystals, bicrystals and coarse polycrystals, and the modes of deformation within the crystals and near the crystal boundaries were studied by means of x-rays, using both the Laue method and a divergent beam method of the kind developed by Guinier. The main conclusion from the work is that the boundary between adjoining crystals does not exert a direct influence of its own upon their mode of deformation: it is to be regarded instead as a frontier across which the crystals interfere with each other.

The title of the book is well justified, and those who are interested in the deformation of polycrystals will value M. Michaud's contribution to this subject. A. H. COTTRELL.

Ionization Chambers and Counters, by D. H. WILKINSON. Pp. ix + 266. Cambridge: Monographs on Physics. 1st Edition. (Cambridge: University Press, 1950.) 25*s*.

The subject of electrical counting is very extensive if it is taken to include the many applications and associated circuits. It is necessary therefore that the scope of a monograph should be severely limited, if more than a sketchy account is to be presented. The author has chosen to deal with the principles of operation of chambers and counters and the relevant theory; particular problems are only mentioned as illustrative examples and no electronics is included.

Among the subjects treated in the introductory chapters are: energy range relation, straggling, ion and electron mobilities, electron capture and recombination. An excellent chapter is devoted to the electrostatics of pulse formation; it includes a discussion of the shape of the pulses from the various detectors, the effect of differentiation, and the use of 'gridded' and thin wire chambers. Ionization chambers, proportional counters, and Geiger counters are dealt with in separate chapters. Each chapter is comprehensive, and the factors limiting the performance under various conditions are assessed. The book concludes with a useful chapter on the speed and statistics of counting.

In view of the title of this book, and the aim of this series of monographs, it is to be regretted that the material is closely confined to chambers, proportional counters, and self-quenching Geiger counters, and that there is no discussion of crystal and scintillation counters or of electron multipliers. Further, the important work of Nawijn on permanent gas counters is omitted, and the very brief discussion of these counters contains a misleading and partly incorrect account of the quenching mechanism.

It is stated that the intention of the book is to provide the necessary theoretical background to enable new counters and chambers to be designed and used effectively. The material selected is treated in a scholarly manner and the book will undoubtedly be of considerable assistance to serious users of these instruments. In addition, a great deal of practical information is included, and the book contains a good bibliography.

B. COLLINGE.

CONTENTS FOR SECTION B

PAGE

Dr. P. B. HIRSCH and the late Mr. J. N. KELLAR. An X-Ray Micro-Beam Technique: I—Collimation 369

Mr. P. GAY, Dr. P. B. HIRSCH, Dr. J. S. THORP and the late Mr. J. N. KELLAR. An X-Ray Micro-Beam Technique: II—A High Intensity X-Ray Generator . 374

Prof. E. A. OWEN and Dr. Y. H. LIU. Recovery and Recrystallization in Highly Stressed Pure Aluminium 386

Prof. F. LLEWELLYN JONES and Dr. D. E. DAVIES. Influence of Cathode Surface Layers on Minimum Sparking Potential of Air and Hydrogen 397

Dr. R. FÜRTH. Space-Charge Distribution, Characteristic, and Current Fluctuations in 'Double Diodes' 404

Mr. H. BARRELL and Miss P. TEASDALE-BUCKELL. The Correction for Dispersion of Phase Change in Fabry–Perot Interferometers 413

Mr. O. S. HEAVENS. Measurement of the Thickness of Thin Films by Multiple-Beam Interferometry 419

Letters to the Editor:

- Prof. K. G. EMELÉUS and Mr. G. A. SMITH. Production of Recombination Spectra 426
- Mr. D. H. PEIRSON. The Background Counting Rate in a Geiger–Müller Counter 427

Reviews of Books 428

Contents for Section A 446

Abstracts for Section A 447

ABSTRACTS FOR SECTION B

An X-Ray Micro-Beam Technique: I—Collimation, by P. B. Hirsch and the late J. N. Kellar.

ABSTRACT. An x-ray micro-beam technique is described which depends on the use of x-ray beams, down to approximately 1 μ diameter, obtained by means of lead glass capillaries. The micro-beam precision camera incorporates collimator holders for aligning the capillaries, and enables simultaneous transmission and back-reflection photographs to be taken. The effect of the divergence of the x-ray beam on the photographs is considered, and a formula is derived for the mean value of the divergence at the specimen. The optimum collimating conditions are discussed in relation to maximum resolution and minimum exposure. The use of totally reflecting glass collimators is considered. An example is given of the application of the micro-beam technique to the study of cold-worked metals. It is found that, using a high intensity generator, single reflections can be obtained from crystals of diameter of the order of 2 μ in about 10 hours.

An X-Ray Micro-Beam Technique: II—A High Intensity X-Ray Generator, by P. Gay, P. B. Hirsch, J. S. Thorp and the late J. N. Kellar.

ABSTRACT. A high intensity x-ray generator has been constructed which combines the use of small foci and a rotating anode. Improvements in target loading per unit area of about fifty times compared with ordinary stationary target tubes* have been obtained. Any width of focus between about 1 mm. and 50 μ can be produced by means of an adjustable, biased electron gun. A detailed experimental investigation of the focusing properties of the high voltage gun has been made; the conditions for obtaining small foci and maximum current are derived. The magnitude of the negative bias is found to be the most important factor controlling the focusing action of the electron gun. The effect of bias on focal structure is discussed for several types of filament, and is explained on the basis of suppression of emission from different parts of the filaments.

Recovery and Recrystallization in Highly Stressed Pure Aluminium, by E. A. Owen and Y. H. Liu.

ABSTRACT. The paper contains an account of an x-ray study of the phenomena observed when polycrystalline pure aluminium is subjected to heavy compressional stresses. The rate of recovery to the metastable state under various conditions has been examined in some detail.

During recovery recrystallization occurs; the crystals grow rapidly at first, but afterwards the rate of growth decreases until finally, after the metastable state has been reached, there are no further changes in crystal sizes. The recovery phenomenon and recrystallization are two different processes but they are not independent of each other. Crystals grow when the value of the stress varies from point to point in the material; when the stresses become evenly distributed, as is found to be the case in the metastable state, the crystals stop growing.

The change from the state immediately following plastic deformation to the equilibrium crystalline state takes place in two stages, one brought about by strain energy and the other by thermal energy. The results are considered in the light of the dislocation theory.

Influence of Cathode Surface Layers on Minimum Sparking Potential of Air and Hydrogen, by F. Llewellyn Jones and D. E. Davies.

ABSTRACT. Oxide layers on the cathode produced marked irregularities in the Paschen curves for air and hydrogen, especially in the neighbourhood of the minimum V_m. V_m in hydrogen was measured at different stages during the removal of oxide layers from the cathode, and also during the deposition of one metal on another as base. Removal of the oxide layer produced smooth Paschen curves, while a thin film of one metal on a different metal as base gave values of V_m which were not characteristic of either metal in bulk. The deposition of thin metallic films had considerable effect on cathode emission owing to the alteration of the work function.

---

* Commercially available x-ray tubes with loading of 0·1 kw/mm².

Space-Charge Distribution, Characteristic, and Current Fluctuations in 'Double Diodes', by R. FÜRTH.

ABSTRACT. The distribution of space charge and potential in thermionic tubes with two hot electrodes ('double diodes') is derived by the method of statistical mechanics for plane parallel electrodes, first for tubes in true thermodynamic equilibrium, and then, approximately, for tubes with applied external voltage or with electrodes at slightly different temperatures. The dependence of current on voltage in the first case (characteristic), and on temperature difference in the second case is calculated. Finally a general expression for the current fluctuations ('noise') in double diodes is given and discussed. The application of this formula to other types of conductors is also indicated.

The Correction for Dispersion of Phase Change in Fabry–Perot Interferometers, by H. BARRELL and P. TEASDALE-BUCKELL.

ABSTRACT. A technique based on well-known interferometric procedures is described for determining the corrections for phase-change dispersion at reflection in Fabry–Perot interferometers. Results obtained during precise determinations of mercury-198 wavelengths are quoted to illustrate its application. A marked difference is found between the dispersion corrections for the silvered and aluminized mirrors actually used, and it is established that the latter have negligible corrections in the region 4047 A. to 6438 A.

Measurement of the Thickness of Thin Films by Multiple-Beam Interferometry, by O. S. HEAVENS.

ABSTRACT. The method of measuring the thickness of thin films by multiple-beam Fizeau fringes has been studied in order to assess the accuracy attainable. In this connection the small-scale irregularities on the surfaces of optical flats and other optically worked glass have been studied by multiple-beam methods. The effect of these irregularities on the accuracy of the thickness measurements is shown and the conditions for optimum accuracy are discussed.

Thickness measurements have been made on films of silver and of lithium fluoride with several different metals as reflecting layers. The measurements cover the range 120 A. to 1500 A. The results for the different reflecting layers show agreement to within the observational error provided that measurements are made within a short time of the preparation of the films. With silver as the reflecting layer an accuracy of ±10 A. can be expected if suitable precautions are taken.

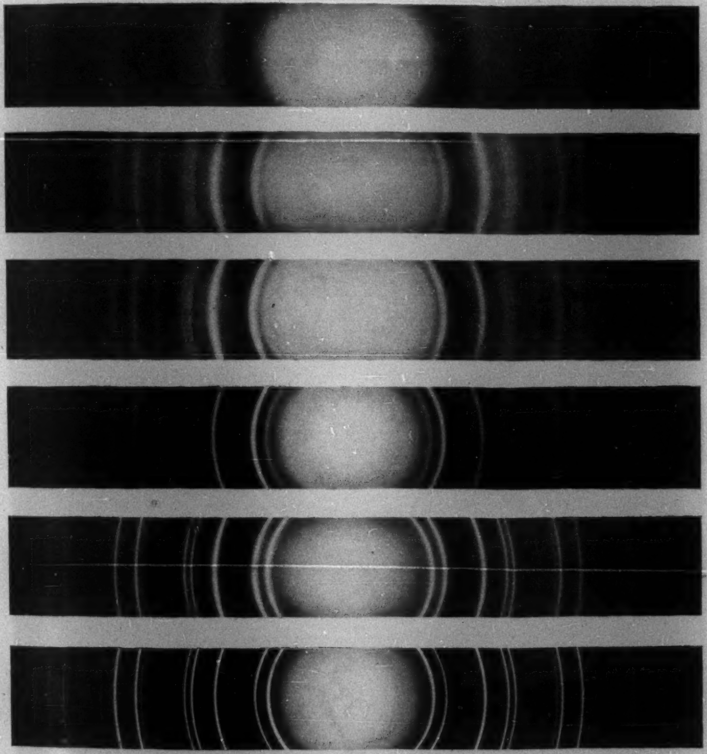

Figure 2. Series of diffraction patterns photographed at successive stages during the growth of an NaBr film in the diffraction camera. Note that the mean crystal size increased and the rings became sharper as more material was evaporated on to the film. The lower pattern was photographed after the film had been exposed to the air.

PLATE I.

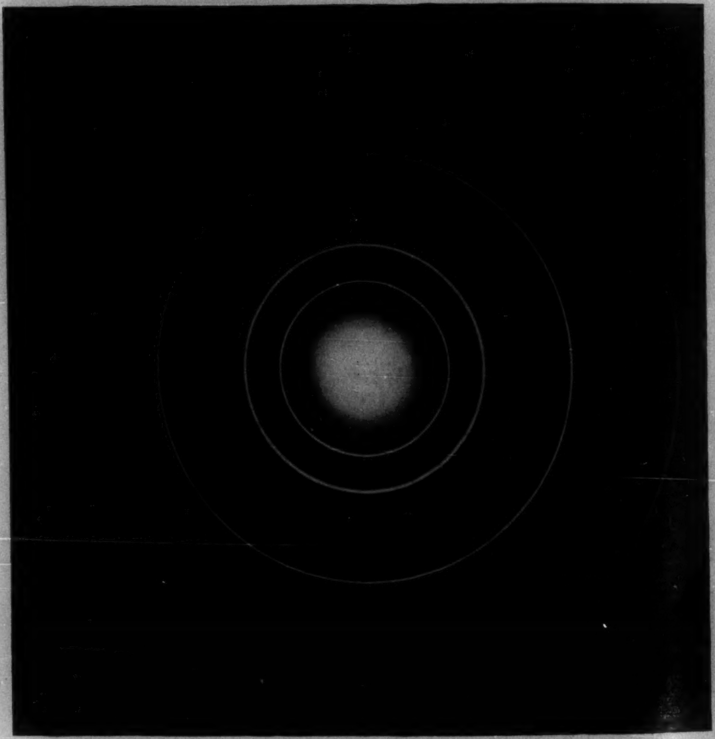

Figure 3. A typical diffraction pattern from a TlCl film about 300 A. thick.

PLATE II.

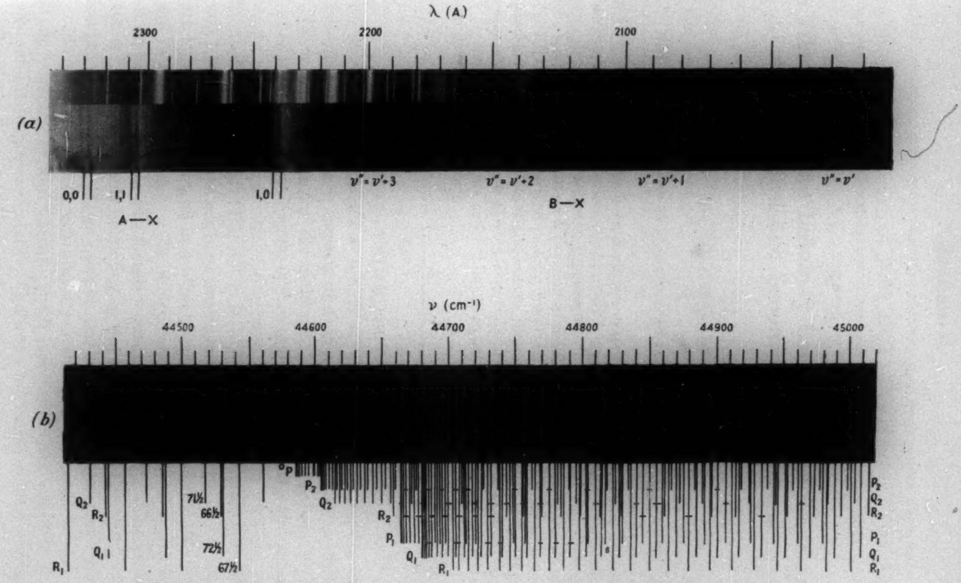

(*a*) Bands of the A–X and B–X systems of CF, photographed on Hilger medium quartz spectrograph: Cu arc comparison specimen. (*b*) The 1,0 band of the A–X system: the lines to the left of the ^{O}P head belong to the 0,0 band.